CHARACTERISATION OF NOVEL THERAPIES TO MITIGATE INFLAMMATION IN RETINAL DEGENERATIONS

KARTIK SAXENA

October 2015

A thesis submitted for the degree of Doctor of Philosophy of
The Australian National University.

CANDIDATE STATEMENT

This declaration certifies that the following work entitled '**Characterisation of novel therapies to mitigate inflammation in retinal degenerations**' is the authors own original work, complies with The Australian National University Research Award Rules and has not been previously accepted for award of a degree or diploma to any other university or institution of higher learning.

Signed: _____

Date: _____

ACKNOWLEDGMENTS

First and foremost thanks goes to my supervisors Professor Jan Provis, Dr Riccardo Natoli and Associate Professor Krisztina Valter-Kocsi. This thesis would not have been possible without their support, dedication and selflessness. Thanks to Jan for her persistence and attention to detail and Krisztina for being a constant source of motivation and enthusiasm. A special thanks to Dr Riccardo Natoli for being a constant source of inspiration at every step of the way (especially during the hardest of times) in my journey through the world of science and life in general. I have learnt a great deal about science and all things worldly while working with him.

Thanks also to all my fellow lab members past and present including Matt Rutar, Zabrina Abdool, Risza Albarracin, HieRin Lee, Mandy Ma, Nilisha Fernando, Helen Jiao, Tanja Racic, Joshua Chu-Tan, Angel lu for their scientific support and unconditional friendship. Thanks for making this a fun and wonderful experience, it has definitely helped me develop (for the better) as a person.

I would also like to thank my friends Amrita, Revantha, Neha, Nimeka, Suvendu, Varun, Poulomi, Animesh, Anjum, Abhishiek, Mahesh, Aseem, Nav, Srishti, Neel, Eli, Ashish for always being there at times of need, especially during the thesis preparation phase. Thank you all for keeping me focused and away from insanity over the years.

And to my beloved wife, Divya, thank you for being a constant source of strength and encouragement. I would not have been able to achieve any of this without your neverending love, support and invaluable advice in all matters big and small.

Finally I would like to thank my parents (Tripti and Sudhir), my brother (Udit) and aunt (Bharati) for their continuous love and support which has been instrumental in getting me through the past 4 years. Special thanks to my mother:

This thesis is dedicated to her and her love for science which we now share.

“*Absence of evidence is **not** evidence of absence!*”

- Carl Sagan

TABLE OF CONTENTS

ABBREVIATIONS

°C	degrees centigrade
µl	microlitres
µm	micrometer
µM	microMolar
ACRF	Australian Cancer Research Foundation
AEEC	Animal Experimental Ethics Committee
AMD	Age related Macular Degeneration
ANOVA	analysis of variance
ANU	The Australian National University
AP	Alkaline phosphatase
APF	Australian Phenomics Facility
ARVO	Association for Research in Vision and Opthalmology
ATP	Adenosine triphosphate
BM	Bruch's membrane
bp	base pairs
BRB	Blood retina barrier
BSA	bovine serum albumin
C1s	complement component 1, s subcomponent
C2	complement component 2
C3	complement component 3
C4b	complement component 4b
C5r1	complement component 5a receptor 1
CA	California
Ca^{2+}	Calcium ion
CCL2	chemokine (C-C motif) ligand 2
CCL3	chemokine (C-C motif) ligand 3
CCL4	chemokine (C-C motif) ligand 4
CCL7	chemokine (C-C motif) ligand 7
CCO	cytochrome oxidase
cDNA	complementary DNA
CEBPα	CCAAT/enhancer binding protein, alpha
CFB	complement factor B
CFD	Complement factor D
CFH	Complement Factor H
CHST2	Carbohydrate (N-Acetylglucosamine-6-O) Sulfotransferase 2
CNS	Central Nervous System
Ct	cycle threshold
Cu	copper
CX3CL1	chemokine (C-X3-C motif) ligand 1
CXCL1	chemokine (C-X-C motif) ligand 1
CXCL10	chemokine (C-X-C motif) ligand 10

CXCL11	chemokine (C-X-C motif) ligand 11
d	days
DAVID	Database for Annotation, Visualization and Integrated Discovery
DHA	Docosahexaenoic acid
DMEM	Dulbeco's Modified Eagle's Medium
DNA	deoxyribonucleic acid
DNAse	deoxyribonuclease
dNTPs	deoxyribonucleotide triphosphate
DPX	Distyrene, plasticizer, xylene
DTT	Dithiothreitol
dUTP	deoxyuridine-triphosphatase
E	efficiency of amplification
EDTA	Ethylene diamine tetraacetic acid
FFPE	Formalin fixed parafin embedded
FGF-2	fibroblast growth factor 2
g	grams
GA	Geographic atrophy
GABA	γ-Aminobutyric acid
GAPDH	glyceraldehyde-3-phosphate dehydrogenase
GCL	ganglion cell
GFAP	glial fibrillary acidic protein
GO	gene ontology
GWAS	Gene wide association studies
H&E	haematoxylin and eosin
H_2O_2	hydrogen peroxide
ID	identification
IDH2	isocitrate dehydrogenase 2
IFN	interferon
IL 1β	Interleukin 1 beta
IL6	interleukin 6
IL8	interleukin 8
ILM	inner limiting membrane
INL	inner nuclear layer
IPL	inner plexiform layer
IS	photoreceptor inner segments
JCSMR	John Curtin school of Medical Research
JNK	c-Jun NH_2-terminal kinase
kb	kilobase
L/M OPSIN	Long / medium wavethength opsin
LD	light damage
LED	light emmitting diode
LHON	Leber's hereditary optic neuropathy
LLLT	low level light therapy

LNA	Locked nucleic acid
LPS	Lipopolysaccharide
mA	milli Amps
MAC	membrane attack complex
max	maximum
MCP-3	monocyte chemoatractant protein 3
miRNA	micro ribonucleic acid
ml	millilitres
mM	milli Molar
mm	milli metre
mRNA	messenger Ribonucleic acid
Na/Ca,K	Sodium/Calcium, Potassium
Na^+	Sodium ion
NASA	National Aeronautics space administration
NBF	neutral buffered formalin
NC	no change
NFL	nerve fibre layer
ng	nanograms
nM	nano molar
NO	nitric oxide
NSW	New South Wales
NY	New York
O_2	oxygen
OCT	optimum cutting temperature
OD	Optic disc
ONL	outer nuclear layer
OPL	outer plexiform layer
OS	outer segments
P	Post Natal
PBM	Photobiomodulation
PBS	phosphate buffered saline
PBS-T	Phosphate buffered saline with tween 20
PCR	polymerase chain reaction
pg	picogram
qPCR	quantitative polymersase chain reaction
R/NIR	red-near infrared
RHO	Rhodopsin
RIN	RNA integrity number
RISC	RNA induced silencing complex
RNA	ribonucleic acid
RNAse	Ribonuclease
ROS	reactive oxygen species
RP	Retinitis Pigmentosa

RPE	Retinal Pigment Epithelium
RT	reverse transcriptase
SD	Sprague Dawley
SHIP	phosphatidylinositol-3,4,5-trisphosphate 5-phosphatase 1
SNP	single nucleotide polymorphism
SOCS	suppressor of cytokine signalling 1
SOD	Superoxide Dismutase
SSC	saline sodium citrate
TBE	tris borate EDTA
TdT	terminal deoxynucleotidyl transferase (buffer)
TLR	Toll like receptor
TNF	tumor necrosis factor
TUNEL	Terminal deoxynucleotidyl Transferase Nick End Labelling
U	Units
USA	United States of America
UTR	untranslated region
UV	ultra violet
V	volts
VEGF	Vascular Endothelium Growth Factor
vs	versus
w	weight
w/v	weight per volume

LIST OF FIGURES

CHAPTER 1

CHAPTER 3

CHAPTER 4

CHAPTER 5

LIST OF TABLES

CHAPTER 1

CHAPTER 2

CHAPTER 3

CHAPTER 4

CHAPTER 5

ABSTRACT

Inflammation is established as a key factor in mediating the progression of a number of retinal degenerations, including both wet and dry age-related macular degeneration (AMD) [1-3]. MicroRNAs (miRNAs) are a class of endogenously occurring non-coding RNA (ncRNA) molecules that are gaining momentum as therapeutic targets for treating a number of human conditions [4-6] and have been identified to modulate inflammation [7]. The purpose of this study is to investigate the modulation of miRNAs in a model of retinal degeneration, the light damage model. MiRNA and their potential roles in mitigating retinal inflammation will also be investigated in animals treated with 670nm red light therapy.

Albino rats raised in dim cyclic light conditions (5lux; 12hr on, 12hr off; controls) were exposed to bright continuous light (1000lux) for 24 hours and returned to dim light conditions for 0, 3 or 7 days. At each timepoint animals were culled and their eyes removed and processed either for histological analyses or RNA based analyses. For histology eyes were fixed in 4% paraformaldehyde, cryoprotected and sectioned to determine the photoreceptor cell death using TUNEL or perform immunohistochemistry experiments using Vimentin and IBA1 or *in situ* hybridisation for Ccl2 and miR-124-3p. RNA was extracted from dissected retinas, reverse transcribed and used for low density array and qPCR analysis to determine the expression changes of genes and miRNAs. Immortalised cell lines were also used for performing cell transfections and similar RNA based analyses as above.

Intense light exposure for 24 hours led to differential expression of a number of miRNAs, 37 of which were significantly modulated by 2-fold or more. Of those, 19 may potentially regulate the inflammatory immune response observed in the model. MicroRNAs -125-3p, -155, -207, -

347, -449a, -351, and -542-3p are all upregulated at 24 hours of exposure along with peak photoreceptor cell death. The miRNAs -542-3p and -351 reached maximum expression at 7 days after exposure, while -125-3p, -155, -207, -347, and -449 reached a peak expression at 3 days. MiR-124-3p expression showed significant downregulation post intense (1000lux) light induced damage to the rat retina. Its expression was localized predominantly to the Müller glia and showed co-localisation with expression of a target gene, Ccl2 (which is a potent chemoattractant molecule responsible for targeted monocyte recruitment in the retina). Luciferase assays in MIO-M1 and HeLa cells confirmed direct binding between miR-124-3p and the CCL2-3'UTR. Additionally, *in vitro* overexpression of miR-124-3p in Müller cells using miRNA mimics significantly inhibited CCL2 upregulation post stimulation with inflammatory cues. Post mortem human tissue showed a similar expression profile for miR-124-3p in the retina. Changes is miRNA expression were also seen in 670nm light treated retinas with or without bright light induced damage, along with the modulation of chemokine gene expression in the pre-treated retinas. Differential expression of miR-351 and miR-155 was confirmed using qPCR, both of which are predicted to target inflammation related genes.

The data indicate that miRNAs are involved in modulating the inflammatory immune response elicited during retinal degeneration. Indeed we found a number of potential candidates, including miR-124-3p, which could prove to be novel therapeutic interventions in mitigating retinal inflammation and the consequent photoreceptor death. 670nm light therapy mitigated retinal inflammation including the modulation of specific miRNAs in the retina.

CHAPTER 1: INTRODUCTION

1.1 GENERAL INTRODUCTION

Sight is one of the primary senses in humans that plays a major role in our ability to perceive and interact with the surroundings and the world we live in. This makes it an essential sense which has a major impact on our quality of life. The retina is a neuronal tissue present at the posterior end of the eye which is responsible for converting light entering the eye to electrical signals which are interpreted by the brain as vision. Age-related macular degeneration (AMD) is a degenerative disorder of the retina which is the leading cause of irreversible blindness in those aged over 60 in the western world. It is a progressive retinopathy that affects the photoreceptors, retina pigment epithelium (RPE), Bruch's membrane and the choroid predominantly in the central macular region, which is the region of the retina that mediates our high acuity and colour vision. AMD is a multifactorial disorder, involving complex interactions between environmental and genetic factors. Although, evidence accruing over the past decade has firmly bolstered the association of inflammatory dysregulation with the pathogenesis of AMD. There are currently no effective treatments targeting the inflammatory immune response implicated in AMD pathophysiology.

MicroRNAs (miRNAs) are a new class of endogenously occurring molecules that have strong therapeutic potential for diseases such as AMD. They are abundant in the central nervous system (CNS) and may be key in modulating inflammation and as a result progression of retinal degenerations. Red-near infrared (R/NIR) light therapy is another novel form of therapy which has been gaining momentum with respect to potentially mitigating inflammation associated with retinal degenerations.

In this chapter I will provide general information about the anatomical structures and function of the retina and the importance of inflammation in AMD pathogenesis, followed by a literature review encompassing the current knowledge of the role of miRNA in modulating inflammation and the beneficial effects of 670nm light therapy in the retina.

1.2 THE RETINA

The retina is a laminated sensory tissue of the CNS that lines the posterior chamber of the eye and converts light to electrical signals through a process known as phototransduction. These signals are then sent to the visual centres of the brain via the optic nerve for further processing.

The retina is considered part of the CNS as it essentially originates as an outgrowth of the developing brain during embryonic development. However true retinal development begins with the establishment of the optic vesicles which gives rise to the neural retina, optic stalk and the RPE. The neural retina contains the retinal progenitor cells (RPCs) which are responsible for the development of all seven retinal cell types. Each of the seven cell types exhibit a staggered differentiation cycle from the RPCs, with ganglion cells being the first to be produced while Müller cells being the last [8]. Each layer and cell type of the retina has a specific functional role (Figure 1.1). The mammalian retina has three distinct layers of neuronal cell bodies ('nuclear layers') and two layers of synapses ('plexiform layers'). Photoreceptor cell bodies are located in the outer nuclear layer (ONL) with their light-receptive outer segments (OS) located deep to the ONL. The inner nuclear layer (INL) and ganglion cell layer (GCL) comprise second and third order neurons respectively. In the INL, horizontal, amacrine and bipolar cells modulate signals generated by the photoreceptors, while the ganglion cells (in the GCL) transmit these signals via the long axons of the optic nerve, to the brain. In addition, there are non-neuronal cell types associated with the retina including the macroglia (Müller cells and astrocytes) and microglia, which are the resident immunocompetent cells. The retinal pigmented epithelium (RPE) comprises phagocytic cells that are functionally integrated with the photoreceptors, and form a barrier between the CNS environment of the retina and the non-neural environment of the adjacent choroid (Figure 1.1A, B).

Photoreceptors are the light-sensing cells of the retina. Retinal degenerations commonly manifest through photoreceptor and RPE cell death, followed by remodelling in the inner layers

of the retina. There are 2 different types of photoreceptors - rods and cones, originally identified by the shape of their outer segments. While the basic structures of cone and rod photoreceptors are similar (Figure 1.1C), they can be distinguished by the shape of their outer segments, the type of photopigment expressed, the light sensitivity level and retinal distribution. Rod photoreceptors make up ~95% of the entire photoreceptor population in human retina and 97% in mice [9]. In both photoreceptor types the discs containing the light-sensitive opsins are organised inside the cytoplasm of the OS. In the rod outer segments the discs are not continuous with the cell membrane [10] and the photopigment they contain (rhodopsin) is highly sensitive, and mediates vision in low light conditions (scotopic/nocturnal). Cones have flattened discs which are continuous with the cell membrane [11] and include photopigments that mediate vision in daylight (photopic/diurnal) and colour perception. While rods are more sensitive to light, cones have faster photoresponses and adaptative properties [12].

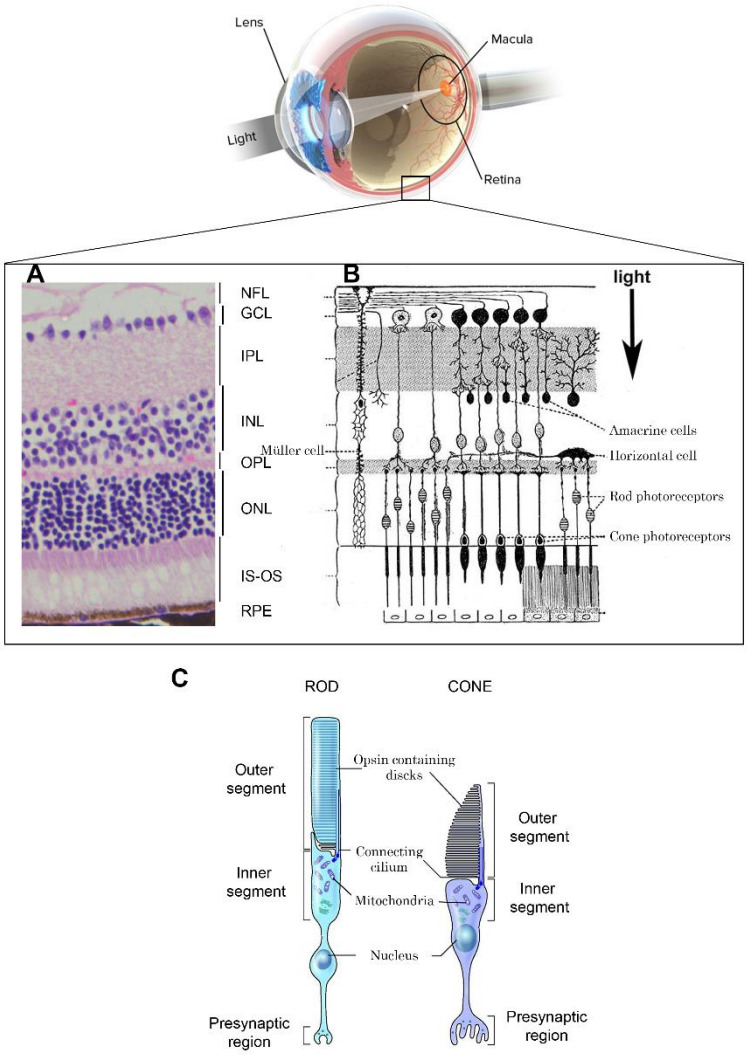

Figure 1. 1 Basic structure of the retina and photoreceptors

Retina is the light sensing tissue lining the back of the eye. (A) Histological section of the mammalian retina stained with hematoxylin and eosin dyes, showing the cell nuclei (purple) and cytoplasm (pink). (B) A schematic diagram showing the interactions between the different layers and cell types of the retina. (C) Schematic diagram of the mammalian rod and cone photoreceptor indicating the structural differences. NFL; nerve fibre layer. GCL; ganglion cell layer. IPL; inner plexiform layer. INL; inner nuclear layer. OPL; outer plexiform layer. ONL; outer nuclear layer. IS; inner segment. OS; outer segment. RPE; retinal pigment epithelium.

Images adapted from:

A. http://www.eperimentica.com/services/tissue-processing/mouse-retina-he.
B. Gray, H, *Anatomy of the human body*, *20th edition* (1918). *Lea and Febiger*.
C. Veleri, S, Lazar C.H, Chang, B, Seiving P.A, Banin, E and Swaroop, A. **Biology and therapy of inherited retinal degenerative disease: insights from mouse models** (2015). *Disease models & mechanisms*.

Phototransduction (i.e. the chemical cascade responsible for conversion of light to electrical signal) takes place in the outer segments, where the light absorbing opsins are located. Membranes infused with photopigments and arranged as stacked discs [13, 14] span the entire length of the outer segment, to maximize the probability of capturing a photon. The outer segments are devoid of cellular protein synthesis machinery. Therefore metabolites, proteins and lipids must pass from the inner segments through the cilium, to reach the outer segment. The inner segment is an extension of the photoreceptor soma and is arranged into two sections, the mitochondria-rich *ellipsoid* and the *myloid* containing the other subcellular organelles, including the Golgi apparatus, smooth endoplasmic reticulum, microtubules and the other subcellular organelles. Outer plexiform layer is comprised of the axon terminals of the photoreceptors (a.k.a cone 'pedicles' or rod 'spherules') where they form synapses with the horizontal and bipolar cells. Hence, the electrical signals generated due to photon detection by the photoreceptors travel passively through the photoreceptor to the pedicle/spherules, and regulate glutamate release from the axon terminals.

In the overall anatomy of the retina, rod photoreceptors are in abundance and far outnumber the presence of cone photoreceptors. However, in humans and primates, the retina contains a specialization known as the *macula lutea,* which is located to the temporal side of the optic nerve (Figure 1.2A). The macula contains a yellow pigment and acts as a filter of potentially damaging short wavelength light [15]. The highly specialized *fovea centralis* (or fovea) is central in the macula, and is characterised by having a peak density of cone photoreceptors and no rod photoreceptors or cones that are sensitive to short wavelength light (Figure 1.2B). The fovea is the primary contributor to our colour perception and high visual acuity.

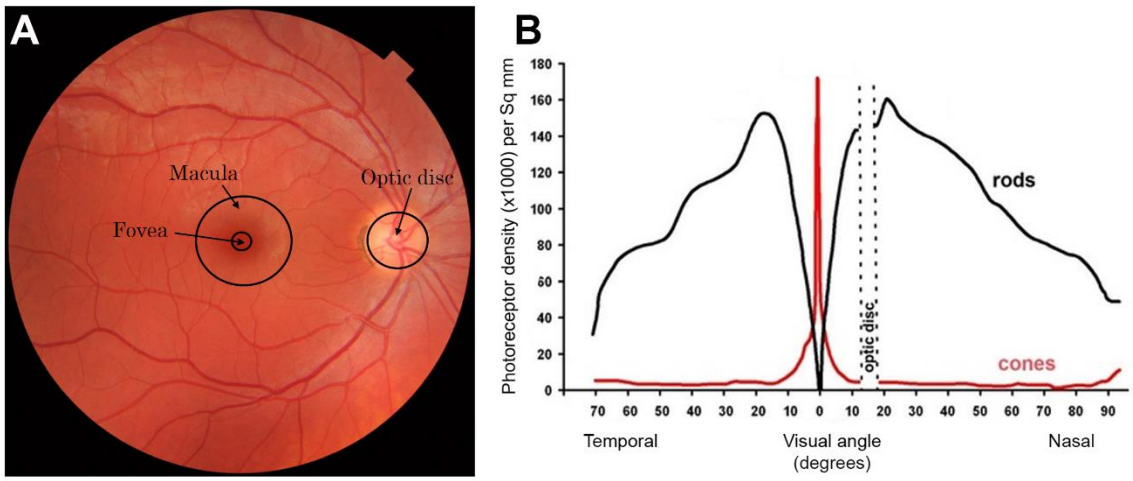

Figure 1. 2 Distribution of rods and cones in the human retina

Representative fundoscopic image of the human retina showing the localisation of the highly specialised macular, foveal region as well as the optic disc (blind spot) (A). Distribution of rod and cone cell densities along the horizontal meridian (B). In humans, Rod population dominates in the overall retina, but they are mainly distributed in the periphery, while cones are highly abundant in the central macular and foveal region.

Images adapted from:

A. Mikael, H. *Medical gallery of Mikael Häggström* (2014). *Wikiversity Journal of Medicine*.
B. Osterberg, G, **Topography of the layer of rods and cones in the human retina** (1935). *Acta Ophthalmologica* (Suppl.) 6, 1-103.

1.2.1 IMMUNE PRIVILEGE

Like the brain, the retina enjoys a degree of 'immune privilege' which to some extent protects CNS tissues from immune attack. It has been argued that this evolutionary adaptation provides useful protection to CNS tissues, which have minimal regenerative potential [16]. In the retina the CNS microenvironment is maintained by the blood retinal barriers (BRB) [17] which minimize both the passive and active movement of cells, proteins and ions into the tissue, to preserve the extracellular milieu needed for efficient neuronal activity [18]. While the BRBs acts as a physical barrier against incessant recruitment of circulating leukocytes capable of causing more harm than good, it does not exclude the normal immune surveillance of the retina essential for maintaining regular neuronal function [19].

Structurally there are two different BRB that exist in the neural retina: Inner and Outer [20-22]. The inner barrier is located at the edge of the inner retina, formed between the endothelial cells of the retinal vasculature and a sheath of glial cell processes including astrocytes, Müller cells and microglia. The outer barrier is formed by the retinal pigment epithelium (RPE) monolayer. Both barriers comprise tight intercellular junctions present between adjacent endothelial / epithelial which restrict paracellular transport of proteins, ions and cells, as well as endocytotic cellular mechanisms that restrict transcellular transport [17]. Under non-inflamed conditions, activated leukocytes from the circulation are capable of inducing local, transient breakdown of the BRB, to achieve extravasation into the neural tissue [23, 24]. However, in numerous retinal pathologies (including uveoretinitis, diabetic retinopathy, light-induced retinopathy and AMD) there is significant, widespread breakdown of the BRBs, leading to altered permeability, changes in the retinal microenvironment, malfunction of neurons, and major tissue damage [17, 25, 26].

1.2.2 AGE-RELATED MACULAR DEGENERATION

AMD is the leading cause of blindness and vision loss among those aged over 60 years in developed nations [27]. It is an age-related retinopathy that leads to progressive focal degeneration of photoreceptors, RPE and Bruch's membrane in the macular region of the retina. The disease is broadly categorised in two forms, known as 'dry' and 'wet'.

'Wet' or Neovascular AMD is associated with serious and acute vision loss, and is characterized by breach of the outer BRB by new blood vessels originating from the underlying choroid [28, 29]. These vessels penetrate Bruch's membrane and can either proliferate and leak outside the RPE ('occult' neovascularization), or penetrate the RPE, proliferate and exude/leak into the retina. Giving this form of the disease its 'wet' annotation [30, 31] (Figure 1.3D). While the emergence of neovascular AMD is seen in only 10% of AMD cases, this form accounts for approximately 90% of severe vision loss. Current treatments for 'wet' AMD only include anti-angiogenic (anti-VEGF) drug based strategies. None of which provide long term relief from disease progression.

The more common dry form of disease is characterized by formation of drusen (basal deposits) and RPE abnormalities including pigment changes and atrophy [28, 32] (Figure 1.3B). The significance of drusen in the pathogenesis of AMD remains unclear, although recently the association of drusen with 'ghost vessels' (i.e. remnants of previously healthy capillaries) in the choroid has been described [33, 34]. Advanced dry AMD is commonly referred to as geographic atrophy (GA) which, as the name suggests, is characterised by the widespread atrophy of photoreceptors and RPE at the macular region [35, 36], and causes moderate to severe vision loss [37, 38]. It is associated with reduced choroidal blood flow and choroidal degeneration [39]. GA is marked by a gradual expansion of the atrophic lesion resulting in progressive RPE atrophy, photoreceptor death and choroidal damage [40-42] (Figure 1.3C). While cones show signs of degeneration/damage earlier than rods, rods undergo cell death

more readily and are particularly vulnerable, with their deterioration contributing to the widening of the atrophic area [40, 43, 44]. The underlying mechanisms responsible for the expansion/progression of the lesion are largely unknown and currently no effective treatments are available to avoid the onset and limit progression [45]. While the aetiology of AMD in unclear, early events that feature in the pathology of outer retina include oxidative damage, inflammation and apoptosis [46].

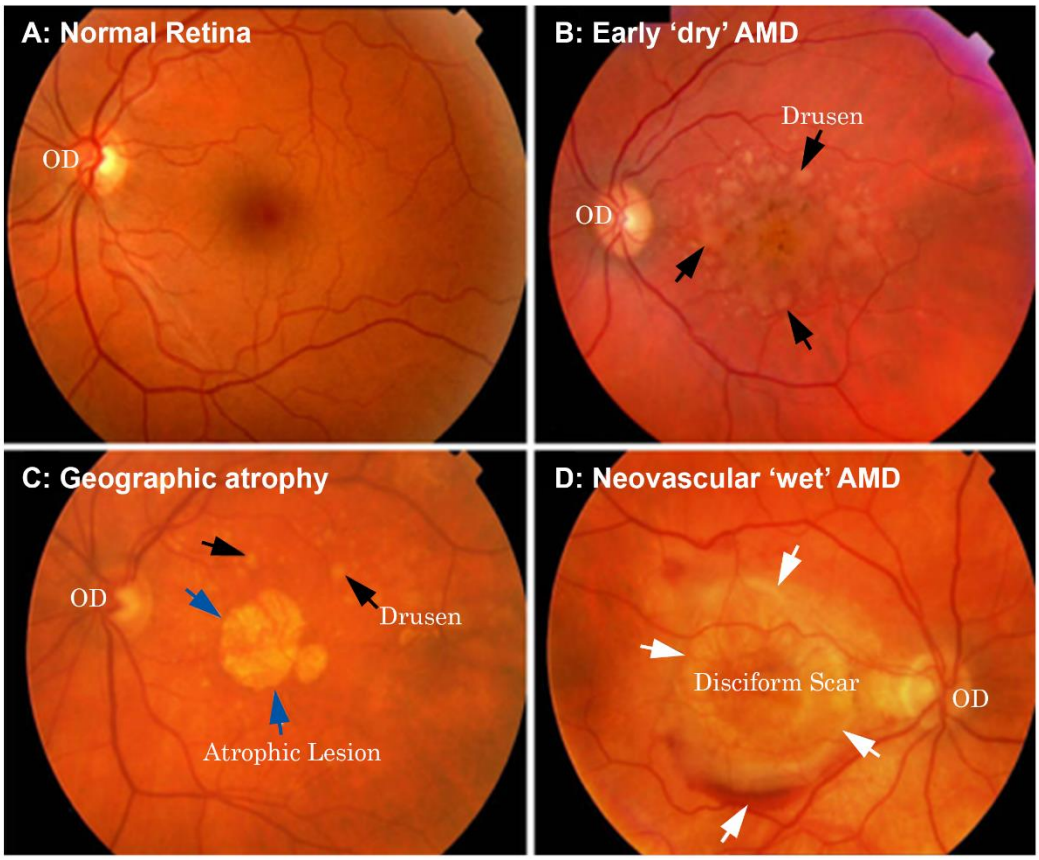

Figure 1. 3 Major pathological features of AMD viewed by fundoscopy

Representative fundoscopic images showing the major pathological aspects of AMD. (A) Normal, unaffected retina with no obvious anatomical changes. (B) Clusters of hard and soft drusen predominantly in the macular region, typically seen in early 'dry' form of the disease. (C) Development of a zone of severe atrophy in the macula leading to damage of RPE and photoreceptors is characteristic of atrophic AMD. (D) Formation of a prominent disciform scar due to proliferating vascular growth into the retina marks the end-stage or neovascular form to AMD. OD; Optic disc.

Image adapted from:

"**Pinpointing the Earliest Defects in Age-Related Macular Degeneration.**" *PLoS Medicine* 3.1 (2006): e38. *PMC*. Web. 22 Sept. 2015.

1.2.2.1 INFLAMMATION IN AMD PATHOGENESIS

The involvement of inflammatory processes and immunity in AMD have been looked at since the early 1900s [21, 47-50]. Several histological studies have identified the aggregation of leukocytes infiltrating through the choroid around disciform lesions in the macula [29, 51], while some studies using electron microscopy techniques have implicated the macrophages, lymphocytes and mast cells in breakdown of the Bruch's membrane and RPE atrophy [47, 48]. Investigations using *post mortem* retinas has identified the close association of macrophages and other leukocytes in and around neovascular membranes, characteristic of wet AMD [49, 52, 53]. Macrophages and giant multinucleated cells have also been identified in close proximity to atrophic AMD lesions [49, 54]. Additionally, histological studies of advanced AMD have demonstrated the increased presence of activated microglial cells in the ONL and subretinal spaces, slowly phagocytosing dead photoreceptor cells in the degenerating retina [55, 56].

Macrophage involvement has been investigated extensively in experimental animal models of AMD. Models using laser to induce choroidal neovascularization in mice have shown that systemic depletion of macrophages is associated with smaller retinal lesions and lower levels of VEGF expression [57, 58]. This suggests that macrophages are actively involved in photoreceptor degeneration and induction of neovascularization. This view is further supported by the demonstration of angiogenic activity of macrophages in culture [59].

Recruitment of inflammatory cells during activation of the innate immune system occurs in almost all CNS pathologies [60, 61], including human retinal pathologies such as age-related macular degeneration (AMD) [54, 56, 62, 63], retinitis pigmentosa [56], late-onset retinal degeneration [56], retinal detachment [64], glaucoma [65-67], and diabetic retinopathy [66, 68]. Similar features are expressed in experimental models of retinal degeneration, thus the results of animal studies in this area are particularly useful and informative [69].

Animal studies indicate that recruitment of inflammatory cells, particularly microglia and monocytes, may be useful in retinal defense [70]. However, it is also clear that widespread recruitment and activation of microglia damages neurons [71-74], most likely due to secretion of pro-inflammatory mediators and cytotoxic factors, including tumor necrosis factor (TNF)-α, interleukin (IL)-1β [60, 75, 76], and release of nitric oxide [71, 77]. Moreover, microglial activation is directly implicated in models of neovascular AMD [78], diabetic retinopathy [79, 80], glaucoma [81, 82], chronic photoreceptor degeneration in *rds* (retinal degeneration slow) mice [83], light-induced damage [74, 84-86] and photoreceptor apoptosis *in vitro* [74]. Although the exact mechanism underlying this targeted recruitment is unclear, a family of chemotactic molecules, the chemokines, have been implicated.

1.2.2.2 CHEMOKINES

Chemokines are a large family of molecules with potent chemoattractant properties in the CNS [87-90]. They are small molecules grouped according to the relative position of their first N-terminal cysteine residues, into C (γ chemokines), CC (β chemokines), CXC (α chemokines), and CX3C (δ chemokines) families [87, 91]. Chemokine expression generates chemical ligand gradients that serve as directional cues for guidance of specific receptor-bearing leukocytes to sites of injury, and are also thought to aid in extravasation of those cells into tissues [92]. Chemokines exert their biological activity by acting as ligands for specialized cell surface receptors, part of the superfamily of seven transmembrane domain receptors consisting of C, CC, CXC, and CX3C receptor subclasses. Chemokine-receptor binding exhibits a high degree of redundancy in their interactions [87].

Increased expression of both α and β chemokines have been characterized in CNS disorders such as MS, AD, ischemia and brain trauma reviewed in [87, 90]. Recent gene expression studies of AMD donor eyes have shown upregulation of CCL2, CXCL1 and CXCL10 in both forms of the disease [93]. A number of studies using laser-induced CNV in mice and light-

induced degeneration in albino rat have suggested a key role of CCL2 in both maintenance of retinal homeostasis as well as enhancing the severity during the degenerative process [59, 94-98]. A recent report by Rutar and colleagues 2015 [99] showed the tissue localization of a number of chemokines with potential involvement in retinal pathogenesis, in the retina and adjacent tissues.

1.2.2.3 ANIMAL MODEL OF RETINAL DEGENERATION – LIGHT INDUCED DAMAGE

In the past decade, light-induced damage in albino rats has emerged as a well-established model to study retinal degeneration because of its high reproducibility, ease of use, rapid non-invasive induction and flexibility [100, 101]. The ability of bright light to induce retinal degeneration has been known for almost half a century. Noell (1966) first described the effect of sufficiently high intensity light on the rat retina. His study demonstrated that intense light exposure induces 'photochemical' damage, inducing photoreceptor cell death and RPE dystrophy leading to vision loss [102]. Since this landmark study, light induced retinal degeneration has been extensively studied and its functional/histological effects investigated (reviewed in [96, 100, 103-105]). It is well established that bright light exposure leads to photoreceptor cell death by apoptosis through oxidative damage generated by bleaching of the rhodopsin chromophore and the subsequent lipid peroxidation of DHA in their OS [106-108].

Several studies indicate that light damage model of retinal degeneration has features in common with progressive dry AMD. These include:

1. Susceptibility to photoreceptor death, RPE atrophy and choroidal changes in a specific location in temporo-superior retina [109-112], at the *area centralis*. This retinal specialisations is analogous to the *macula lutea* of the human retina, the region of targeted damage in AMD [113-115]. Interestingly, even though the *area centralis* in

the rat retina possesses more cones and ganglion cells, it is still substantially less than the fovea/macula of primate retina.

2. Progressive photoreceptor cell death and RPE loss expanding outward from the site of initial acute damage for a prolonged period [105], resembling the increasing lesion size seen in advanced dry AMD [38].
3. Primary involvement of oxidative stress potentially leading to initial photoreceptor cell death and initiation of the inflammatory immune response, similar to that observed in AMD donor tissue [107, 116, 117].
4. Involvement of inflammatory processes, including excessive leukocyte activation/recruitment [86, 118] and complement activation [119, 120], both of which have been implicated in AMD pathogenesis [49, 63, 121].

Gene association studies identified a significant link between the Y402H sequence variant of complement factor H (CFH), a key inhibitor of the alternative complement pathway, and AMD susceptibility [122], along with other risk variants in complement components, including complement component 2 (C2) [123], complement factor B (CFB) [124] and complement component 3 (C3) [125, 126]. Among these C3, which is a vital component capable of driving the activation of all three complement pathways (refer to Figure 1.4), shows robust long-term upregulation in the light damage model where it is expressed by activated microglia/macrophages and deposited in the photoreceptor layer at the site of damage [119]. C3 is also a crucial mediator of the membrane attack complex (MAC), which has been reported in drusen deposits from donor eyes, making photoreceptors around the C3 expressing microglia/macrophages susceptible to cytotoxic damage [121, 127, 128]. Additionally, ablation of the complement factor D (CFD), an alternative pathway gene, has been shown to attenuate

photoreceptor death in the light damage model [120], suggesting involvement of alternative pathway activation similar to AMD.

As a result of these overlapping features the LD model has become an effective model to study AMD and potentially a good system to investigate the efficacy of potential therapies for dry AMD.

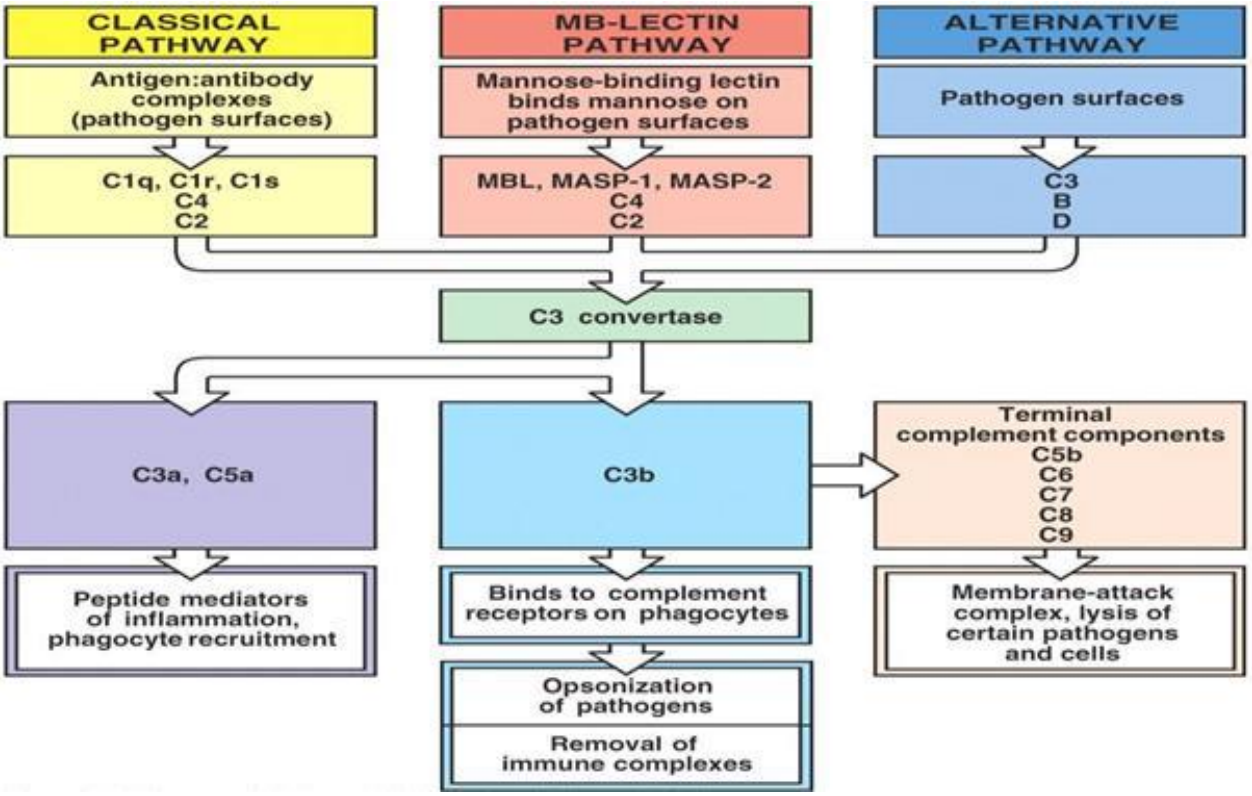

Figure 1. 4 Overview of complement activation pathways

Diagrammatic representation of the three complement activation pathways – classical, mannose binding lectin (MBL), and alternative. All of these converge in the proteolytic cleavage of complement component 3 (C3).

Image taken from:

Janeway et al, Immunology: *The immune system in Health and Disease*, (2005). *Garland Science.*

1.3 MICRO-RNA

1.3.1 ORIGIN

MicroRNAs are small non-coding RNA molecules present in both plants and animals [129]. They are typically ~19-24 nucleotide transcripts encoded by the genome, and are heavily conserved across many different species. Lin-4 was the first miRNA identified in animals in 1993 during a screening of developmental mutants in *C. elegans*. It was observed that mutations in lin-4 lead to developmental defects in *C. elegans* due to a repeated L1 division during the later larval stages [130]. This work marked the beginning of miRNA research, which at first was considered to be an idiosyncrasy of the regulatory mechanism. This view changed in 2000 when another developmentally critical gene in *C.elegans*, let-7, was shown by two collaborating groups to encode a miRNA [131, 132]. Soon after, homologs of let-7 were found in flies and humans further bolstering the existence and importance of these novel regulatory molecules [133].

To date thousands of miRNAs have been identified and characterised and documented in an open access online portal – www.miRbase.com.

1.3.2 BIOGENESIS

MiRNA genes are scattered in different regions across the genome. They can be present in the intron regions of protein coding genes, hence sharing the promoters of certain genes or regions far from the previously annotated genes. And in these regions, they can either exist as clusters yielding polycistronic transcripts or independently yielding monocistronic ones [134-138]. Moreover, with advent of highly sensitive next generation sequencing technologies it has been shown that there are a lot of miRNA redundancies in the genome, in that multiple copies of the same miRNA can be found in many different genomic locations.

A majority, if not all, miRNAs are transcribed by RNA polymerase II in the nucleus where they are initially processed as long primary transcripts (pri-miRNA) averaging ~1000 nucleotides in length [139] (Figure 1.5). The pri-miRNA undergoes two consecutive cleavage events to generate the active, or mature form of the miRNA. The first cleavage takes place inside the nucleus, by an RNase III endonuclease called Drosha, which liberates an intermediate stem loop structure of about 60-100 nucleotides known as the precursor miRNA (pre-miRNA) [140-142]. Drosha cleaves both strands of the RNA duplex near the base of the primary stem loop in a RNase III typical staggered manner resulting in a 5' Phosphate and ~2 nt overhang at the 3' end [143]. These pre-miRNAs are then actively exported to the cytoplasm by Exportin-5 where they undergo a second endonucleolytic cleavage event [144]. Dicer, also a RNase III endonuclease, first identifies the double-stranded portion of the precursor stem loop, potentially by the 5' phosphate and the 3' overhang, and then cleaves off the hairpin loop, typically two helical turns away, releasing a mature miRNA duplex with a 5' phosphate and 3' overhang on either end [135]. This processing by Drosha and Dicer helps distinguish these RNA strands from other breakdown RNAs [145-147]. From this mature miRNA:miRNA duplex, one strand (the lead strand) gets incorporated in the RNA induced silencing complex (RISC) [148], and is responsible for guiding the whole silencing machinery to the prospective mRNA targets (Figure 1.5).

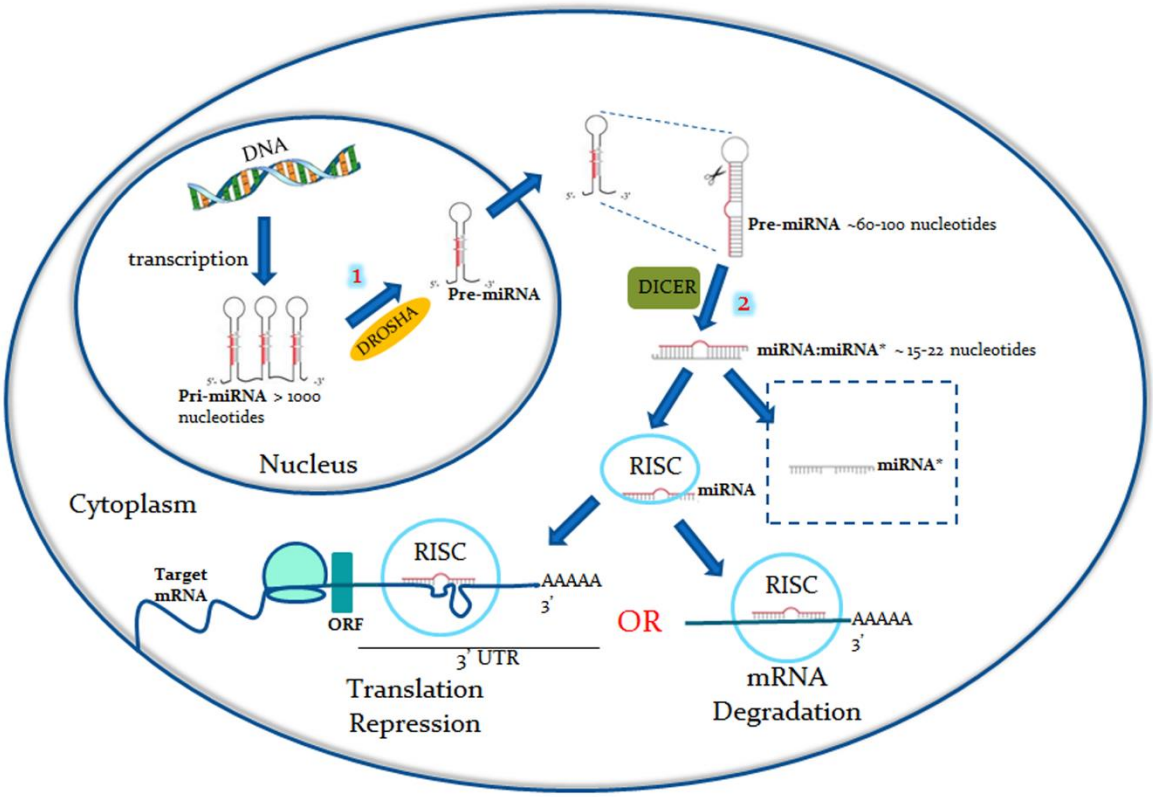

Figure 1. 5 MicroRNA biogenesis and mode of action

Schematic diagram showing the biogenesis and mode of action of mature microRNA (miRNA) sequences inside the cell. This canonical maturation of miRNAs includes two cleavage events (marked '1' and '2'), catalysed by *Drosha* and *Dicer* respectively, resulting in the conversion of the long primary transcripts (Pri-miRNA) in the nucleus to small mature miRNA duplexes in the cytoplasm. Each strand of the mature duplex can then incorporate into the RNA induced silencing complex (RISC) and lead to gene regulation by either translational repression or messengerRNA (mRNA) degradation.

1.3.3 MODE OF ACTION

The miRNAs inside the RISC complex interact with their target mRNAs by complementary base pairing, predominantly in the 3'UTR region of the target gene [142, 147, 149-151]. They direct downregulation of gene expression by one of two mechanisms: mRNA degradation, or translational repression. The choice of mechanism is determined by the degree of complementarity between the miRNA and its target mRNA [147]. Where perfect or near perfect complementarity occurs, the miRNA leads to mRNA cleavage/degradation (more commonly found in plants). However, imperfect complementarity results in translational repression, and is more commonly seen in animals [130, 131, 135] (Figure 1.5). In the case of mRNA cleavage, the miRNA-RISC remains intact after degradation, and is capable of recognising and destroying additional mRNA targets [152]. However, during translation repression the miRNA-RISC remains bound to its mRNA target and can either inhibit translation, resulting in no polypeptide formation, or hinder translation, resulting in a stunted/non-functional polypeptide formation which gets selectively degraded.

1.3.4 BIOLOGICAL RELEVANCE

MicroRNAs play crucial roles in regulation of diverse biological processes including organ development and homeostasis [131], cell proliferation, differentiation, apoptosis, and immune function [153, 154]. These micromanagers of gene expression regulate the mRNA expression profile post transcription, thereby providing the system an efficient way of coping with aberrant gene expression.

Changes in miRNA abundance have been studied in disease since their discovery [155, 156]. To date miRNA deregulation and/or dysfunction has been implicated in almost every disease pathology including autoimmunity, viral infections, neurodegeneration, inflammation, cancer, cardiovascular, or neurological diseases [157-161].

MiRNAs are highly enriched in the CNS and have been shown to play different roles during its development, normal functioning and disease, with several miRNAs showing expression specifically in the CNS tissue/cells [162-165]. For instance, miRNAs -124, -9 and let-7b have been shown to play a role in modulating neurogenesis and neural differentiation [166, 167]. While downregulation of miR-124 has been linked to traumatic spinal cord injury [168]. Additionally, miR-9, -125b, -146a, -29a, -29b-1 have been implicated in Alzheimer's disease [169, 170]; MiR-133b, -7 implicated in Parkinson's disease [171, 172]; and miR-124, -132, -9 implicated in Huntington's disease [173, 174]. Being an extension of the CNS the retina serves as a good model system for characterising and validating miRNA gene regulation as:

1. Its cellular architecture and cellular functions are well known. Hence, phenotypic changes as a consequence of specific miRNA manipulation can be clearly observed/demonstrated.
2. It is easy to access and responsive to experimental, genetic manipulation. Hence, miRNA manipulations using modified oligonucleotide sequences can be achieved locally.
3. Genetic manipulations leading to disruptions of the visual circuitry do not exhibit developmentally lethal effects. Hence, retina specific miRNA manipulations can be performed at different developmental stages to understand their specialised roles in neuronal cell biology.

1.3.5 MIRNA AND INNATE IMMUNITY

The innate immune response is the evolutionarily older of the two immune systems ('innate' *vs* 'adaptive') and constitutes the first line of defence against invading pathogens. The innate response is cell-mediated, involving monocytes, macrophages and dendritic cells and instigates the inflammatory response [175]. MiRNAs form an integral component of the regulatory

networks essential for fine tuning the innate immune processes. To date large number of miRNAs (listed in Table 1.1) have been implicated to play a role in innate immune processes.

One of the first examples of miRNA regulation in immunity was shown in human monocytes stimulated with lipopolysaccharide (LPS). The study showed that signalling by TLRs induced a rapid up-regulation of miR-146a (among other miRNA changes), which acts as a negative feedback regulator of the signalling cascade, resulting in suppression of the immune response [176]. The same stimulation was later shown to induce another miRNA, miR-21, that suppressed the pro-inflammatory effect of the signalling [177]; it also showed up-regulation of miR-155, a well-established potent pro-inflammatory miRNA. MiR-155 is heavily induced in macrophages stimulated with both viral and bacterial antigens that activate different TLRs [176, 178-180] and exerts its pro-inflammatory effect by repression of negative regulators of inflammation. These include suppressor of cytokine signalling 1 (SOCS1), phosphatidylinositol-3,4,5-trisphosphate 5-phosphatase 1 (SHIP1) and certain anti-inflammatory proteins [178, 181]. Moreover, miR-155 has been shown to increase the stability of TNF-α mRNA, thereby maintaining a pro-inflammatory environment [182]. Interestingly, mice deficient in miR-155 have decreased immune responses, while miR-155 overexpression leads to a myeloproliferative disorder resembling chronic inflammation, and haematopoietic cancers [183-185].

MicroRNAs can also regulate aspects of innate immune responses, either by targeting signal transduction proteins or the downstream transcripts in the inflammatory signalling pathways. TLRs or Toll like receptors are a class of transmembrane proteins that play an important role in innate immune response by recognizing structurally conserved molecules of microbial origin. Once activated (by ligand recognition) they initiate cell signaling cascades downstream. TLR2, 3 and 4 play important roles in propagating inflammation when triggered by their respective ligands of bacterial, parasitic origin. MiR-223, miR-105, miR-19, and let-7 family

members for instance, can directly target TLR2, TLR3 or TLR4 [180, 185-189], thereby inhibiting the ability of immune cells to engage with ligands specific to those receptors. MiR-9 negatively regulates NF-κB-dependent inflammatory responses by suppressing expression of NFKB1 transcripts in LPS-stimulated neutrophils and monocytes [190]. While, miR-147 can act as a negative regulator of excessive inflammatory responses in macrophages [191] post its inducing via activation of TLR2, TLR3, or TLR4.

Table 1. 1

MiRNAs in innate immunity

MiRNA	Targets	Biological effect
miR-9	NF-κB1	Negative regulator of TLR4 signaling
miR-19	TLR2	Decreases TLR2 mediated inflammation
miR-21	PDCD4, IL-12 p35	Negative regulator of TLR4 signaling
miR-27b	PPAR-γ	Enhances response to LPS
miR-105	TLR2	Decreases TLR2 mediated inflammation
miR-106a	IL-10	Decreases IL-10
miR-125b	TNF-α; IRF4	Diminishes inflammation; enhances
		macrophage activation
miR-145	TIRAP	Inhibits TLR signaling
miR-146a	TRAF6, IRAK1, IRAK2	Negative regulator of TLR signaling
miR-155	AID; MyD88; TAB2;	Enhances inflammation;
	Pellino-1; IKKε; SHIP-1;	negative feedback regulation
	SOCS1; C/EBP-β	
miR-223	IKKα; Pknox1	Proinflammatory activation of macrophages
Let-7i, let-7e	TLR4	Downregulate inflammatory signaling

Taken from:

Liu, G., and Abraham, E. **MicroRNAs in immune response and macrophage polarization** (2013). *Arteriosclerosis, thrombosis, and vascular biology*. 33(2):170-177.

Additionally, reduced expression of the miRNAs Let-7i and miR-125b leads to enhanced inflammation in response to LPS and microbial infections [180, 187, 192, 193]. On the other hand, overexpression of miR-125b potentiates macrophage activation and enhances responsiveness to IFN-γ [194]. Taken together, the data suggest that different miRNAs act synergistically to fine tune of the inflammatory response, and that same miRNAs can have opposing effects in different cellular contexts.

1.3.6 MIRNAS MEDIATING INFLAMMATION IN AMD:

Although miRNAs have only recently become the focus of research in AMD, several miRNAs have been shown to contribute directly to pathological processes including angiogenesis, oxidative stress and inflammation. Specifically, miRs -146a, 125b, -155, -9 and -27 appear to show the most promise to date, with regard to managing inflammation in AMD. The key findings to date are as follows:

1. Both **miR-146a and -155 are up-regulated** following stimulation with pro-inflammatory cues such as LPS and cytokines (IL-1β, TNF-α), leading to regulation of both IL-6 and IL-8 expression [176, 179, 195-198]. **MiR-125b is downregulated** in LPS-treated macrophages and capable of targeting TNFα [180].
2. MicroRNAs miR-9, -155, -146a and -125b are up-regulated in aging brain and retinal tissue. Of these miRs, **-146a, -155 and 125b are capable of negatively regulating CFH** expression by direct binding, thereby acting as potent promoters of the alternate complement pathway [199].
3. **MiR-27 is induced** in LPS-treated human macrophages, and may contribute to both inflammation and neovascularisation in advanced ‘wet’ AMD [200, 201].

A recent seminal study implicated the role of noncoding (*Alu*) RNAs in advanced 'dry' AMD [202] showing that selective downregulation of Dicer-1, or anomalies in Dicer-1 expression in the RPE leads to accumulation of toxic double stranded *Alu* RNAs, and subsequent degeneration of the pigment epithelium. Anomalies in Dicer-1 also suggest anomalous processing of pri-miRNA affecting expression of a range of as yet unidentified genes. In addition, a recent study in the rodent light induced model of retinal degeneration identified modulation of a large proportion of ncRNA during degeneration [96].

The field of miRNA therapeutics is rapidly gaining momentum along with the increasing knowledge of miRNA modulation in association with disease. A number miRNA-based therapeutics have already progressed from discovery to development with one currently in Phase 1 clinical trials while another already in Phase 2 [203, 204].

1.4 PHOTOBIOMODULATION

The therapeutic effects of sunlight have been explored for centuries in civilizations as old as the Roman, Greek and Chinese to treat a number of diseases [205, 206]. The first account of use of modern light therapy, however, was reported in the late 1800s when a Danish physician, Niels Finsen used crudely filtered red light to treat small pox and Lupus vulgaris. A pioneering use of the healing properties of light that earned him a Nobel Prize in 1903 [207, 208]. This work led to further exploration of clinical applications of light and the beginning of a new field of research known presently as either phototherapy or photobiomodulation (PBM), red light therapy, low level light therapy or near infrared (NIR) therapy.

A Hungarian physician Endre Mester in the late 1960s showed the positive biostimulatory effects (including anti-inflammation, vasodilation, stimulated blood circulation and anti-edema) in mice as a result of exposure to low level laser emitting near infrared (NR) light [209]

and further supported by studies in experimental animal models of wound healing and hair growth [210-212]. While the outcomes of these primary studies indicated high therapeutic potential, the mainstream clinical community has not accepted the use of 'low level light therapy' (LLLT) due to lack of proper controls and a lack of understanding of the mechanisms at play [213]. Additionally, a number of complicating factors come into play using lasers to produce low level light, including the inherent property of lasers to produce heat, leading to thermal damage to biological tissues, an inability to treat a large wound area while maintaining homogenous mean intensity/energy distribution due to its highly focused nature, inefficiency in producing different wavelengths of light simultaneously, and high setup and operational costs [214].

The development of the light emitting diode (LED) and particularly the National Aeronautics and Space Administration's (NASA) lightweight LED array system has provided an alternative, cost-effective non-coherent source for phototherapy [215]. Although NASA originally developed the LED array to facilitate growth of plants during space exploration missions, LEDs in the red to NIR spectrum were soon realized to possess significant wound healing properties [214, 216]. LED arrays can be manipulated to produce light at optimal intensity at specific wavelengths. In the red to NIR range these wavelengths penetrate skin and tissue to a depth of approximately 23cm without any heat emission, making them perfect candidates for therapeutic applications [216].

1.4.1 670NM RED LIGHT THERAPY

The beneficial effects of monochromatic light in the red and near infrared (NIR) spectrum (Lambda = 600nm-1000nm) has been reported in a number of diseases over the past 30-40 years. More recently, the use of 670nm wavelength light has attracted the interest of the global scientific community, and has been applied to a variety of human conditions, including cardiovascular [217], musculoskeletal [218, 219], and central nervous system (CNS) [220,

221]. Investigations using animal models of CNS disorders have demonstrated the beneficial effects of 670nm light treatment in optic nerve degeneration [222], long term effects of traumatic brain injury [223] and neuronal toxicity [224, 225]. 670nm light therapy is shown to alleviate clinical symptoms in an animal model of Experimental Autoimmune Encephalomyelitis (EAE) [226], and to reduce the incidence of oral mucositis (OM) in a cohort of pediatric bone marrow transplant patients [227]. Recent studies have also suggested that 670nm light therapy reduces the severity of damage in experimental models of Alzheimer's [228] and Parkinson's disease [229].

In the last decade significant interest has accrued with respect to use of 670nm light irradiation in management of retinal injuries/pathologies. Studies have shown that 670nm light attenuates methanol-induced toxicity in rodents, laser-induced injury in primate retina and development of a retinal lesion in models of diabetic retinopathy [230-232]. Recently work from our group and others have demonstrated protective effects of 670nm light treatment on photoreceptor cell death in retinas exposed to bright white light [118, 233-236].

Using microarray analyses in the light damage-induced model of retinal degeneration we have shown that pre-treatment with an optimal dose of 670nm irradiation maintains retinal function, and suppresses inflammation and oxidative stress-related gene expression [96]. Additionally, studies utilising CFH-/- mouse retina, aged rodent retina and light damaged rat retina have shown a reduction of pro-inflammatory processes by 670nm light treatment [236-239].

1.4.1.1 MECHANISM OF ACTION

Despite a growing body of evidence indicating effective clinical application for 670nm light therapy, the precise molecular mechanisms underlying its effect on mammalian cells/tissue remain unclear [240].

Light in the near infrared wavelength spectrum (~600-1000nm) is not absorbed by water, melanin and haemoglobin (Hb), the most abundant light absorbing molecules in biological systems (Figure 1.6) [241]. This allows for deeper penetration into tissues where the wavelengths can be absorbed by endogenous photo-acceptors such as porphyrins, flavoproteins and cytochromes [241-243]. Once absorbed, these wavelengths lead to excitation of the chromophores which then transfer their electrons to the nearby O_2 molecules, generating potent signaling molecules known as reactive oxygen species (ROS) in the process [244, 245].

It has been demonstrated that 670nm light is the optimal wavelength for absorption by cytochrome c oxidase (CCO), Complex IV of the electron transport chain [244, 246] - the rate limiting step in the oxidative phosphorylation pathway [247]. CCO contains 4 metal centres that catalyse the transfer of electrons from cytochrome c to Complex V, the final complex in the electron transport chain which drives production of ATP. Two of these centres are mixed-valence copper components which are thought to be direct targets of 670nm irradiation (Figure 1.7A) [248].

It has been suggested that exposure to 670nm light modulates the redox state of CCO and increases CCO activity, leading to amplified flux across the electron transport chain and more efficient oxidative phosphorylation, and ATP [224]. A recent study has also documented the upregulation of CCO expression in an animal model of retinal degeneration as a result of 670nm light irradiation (Figure 1.7B) [237]. An alternative hypothesis is that 670nm light dissociates NO from cytochrome c oxidase, thereby, releasing the enzyme from its inhibitory effect. Red-to-NIR irradiation is believed to stimulate a conformational change in CCO resulting in the release of NO [249, 250]. Free NO is then available to act as a signalling molecule to stimulate retrograde signalling between mitochondria and the nucleus, as well as increase oxygen consumption and enhance oxidative phosphorylation [251, 252].

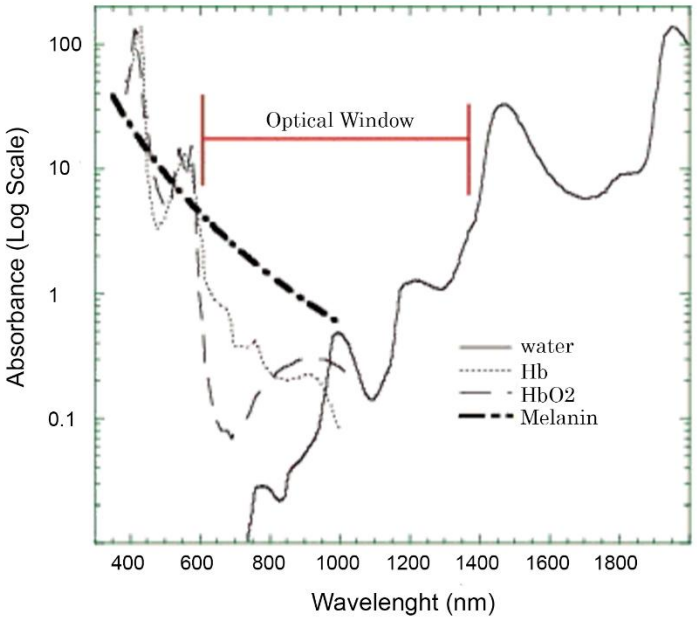

Figure 1. 6 Absorption spectra of biological chromophores

Shows the absorption spectra of abundant tissue chromophores, identifying the maximum tissue penetration window of light in the red and NIR wavelengths. This indicates the so-called "optical window" in biological tissue.

Taken from:

Hamblin, M. R and Demidova, T. N. **Mechanisms of Low Level Light Therapy – an Introduction** (2006). *Proc SPIE*. Vol 6140.

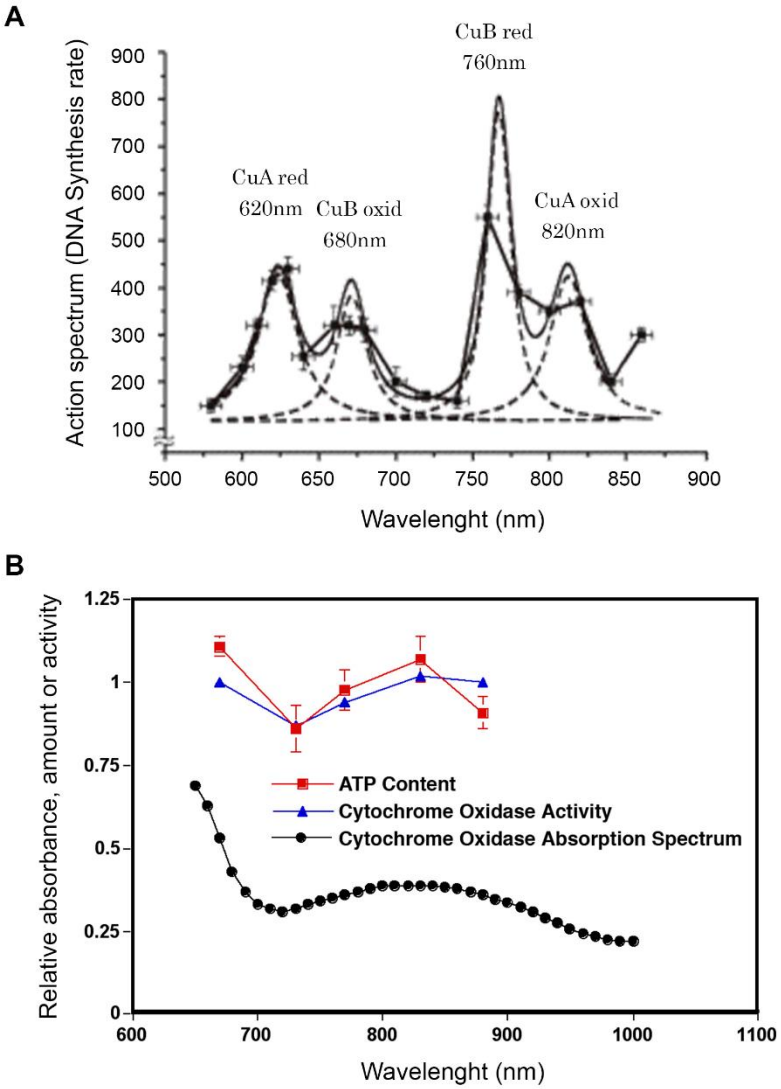

Figure 1. 7 Absorption spectrum of cytochrome c oxidase

Cytochrome c oxidase (COO), a member of complex IV of the mitochondrial electron transport chain, catalyses the final transfer of electron to oxygen molecules thereby driving the production of energy as ATP (adenosine triphosphate) and is suggested to be the primary photoacceptor of 670nm light. (A) Shows the correlation between the absorption spectrum of the multivalent Cu (Copper) centres of COO and the cellular action spectrum in terms of DNA synthesis rate across the red-NIR light spectrum. (B) The overall absorption spectrum of CCO also correlates with its enzymatic activity and amount of cellular ATP.

Images adapted from:

A. Karu, T. *Lasers in Medicine and Dentistry* (2000). Chapter IV, 97-125. *Russian Academy of Science.*

B. Wong-Riley, M.T.T, Liang, H. L, Eells, J. T *et al*. **Photobiomodulation directly benefits primary neurons functionally inactivated by toxins: Role of cytochrome c oxidase** (2004). *The American Society for Biochemistry and Molecular Biology*.

However, if accumulated in extremely high amounts this NO can be cytotoxic to the cells, as mentioned previously [71, 77].

Collectively, all cellular proteins that absorb 670nm light are believed to stimulate a cascade of other proteins or cell signaling molecules which are capable of modulating specific gene transcriptions. Gene expression studies indicate that treatment with 670nm light prior to a damaging stimulus enhances expression of genes associated with antioxidant protection, mitochondrial metabolism and cell proliferation, while suppressing pro-inflammatory, pro-apototic genes [96, 253, 254]. In the retina 670nm light therapy seems to exert a beneficial effect by minimizing oxidative damage and reducing pro-inflammatory events.

1.4.1.2 ROLE OF 670NM LIGHT IN MITIGATING INFLAMMATION

Oxidative stress and inflammation are two interrelated processes identified in almost all degenerative pathologies of the CNS including Alzheimer's disease, Parkinson's disease, Leber's hereditary optic neuropathy (LHON) and AMD. Many studies have shown that 670nm light reduces oxidative damage in animal models of methanol-induced retinal toxicity [231], rotenone-induced neurotoxicity [255], partial optic nerve transection [222], Parkinson's disease model [255, 256] and Multiple sclerosis animal model [226]. However, there is a lack of strong evidence indicating the beneficial effect of 670nm in mitigating inflammation.

Gene expression analysis in wound-healing studies have shown down-regulation of inflammatory factors, such as cytokines and cytokine receptors, following treatment with NIR light [214, 257]. While in the light damage-induced degenerating retina 670nm light irradiation reduces photoreceptor cell death, activation and recruitment of inflammatory cells, and complement propagation [118, 234, 236]. Those studies, however, only investigated changes of gene expression, photoreceptor cell function and histology after prolonged recovery periods.

Hence, further studies are needed to identify the initiating mechanisms by which 670nm light ameliorates the inflammatory processes in retinal degenerations.

1.5 AIMS

In this thesis I aim to explore the global miRNA expression profile of the rat retina in bright light-induced retinal degeneration (Chapter 3), and the role of a particular candidate miRNA (miR-124-3p) in the modulation of inflammatory cytokines (Chapter 4). Building on previous work conducted in our lab suggesting that 670nm light therapy modulates ncRNAs [96], in Chapter 5, I report the impact of 670nm light pre-treatment on the early expression of pro-inflammatory genes and miRNAs that might modulate inflammation. Conclusions drawn from these studies are outlined in Chapter 6.

CHAPTER 2: MATERIALS AND METHODS

2.1 INTRODUCTION

In Chapters 3-5, experiments were performed to understand the role of miRNA in retinal degenerations and developing therapies for treating retinal degenerations. The following chapter provides detailed descriptions of all the methodology used in this study. Any additional techniques/methods used are mentioned in chapters 3-5.

2.2 ANIMAL REARING AND HOUSING CONDITIONS

All procedures were performed in accordance with the Association for Research in Vision and Ophthalmology (ARVO) statement for use of animals and the Australian National University (ANU) ethics protocols outlined by the Animal Experimental Ethics Committee (AEEC). Sprague Dawley (SD) albino rats were obtained from the Australian Phenomics Facility (APF) and housed at the John Curtin school of Medical Research (JCSMR) animal holding facility. Animals were born and raised in dim (5 lux illumination) cyclic light conditions with a 12h light, 12h Dark cycle. Food and water was provided in constant supply and cages changed on a weekly basis. Animals aged between postnatal day (P) 90-120 were used in light damage (LD) experiments. Equal numbers of male and female rats were used throughout the study to avoid any gender biases.

2.3 LIGHT DAMAGE EXPERIMENTS

Adult SD albino rats (P 90 – 120) were placed in individual transparent Perspex chambers and exposed to high intensity (1000 lux) bright white light from an overhead fluorescent source for 24 hours. During the light exposure food was placed on the floor of the chamber and water was provided in transparent bottles to avoid barrier to light. 1000 lux light exposure was started at 9:30AM for all experiments. To encourage increased animal activity during the exposure

period, bird seeds and packaging rice puffs were dispersed throughout the Perspex box floor. After completion of the 24 hour light exposure period, animals were either sacrificed for tissue collection or returned to dim (5 lux) cyclic light conditions to recover for 3 or 7 days.

2.4 LED/NIR 670NM LIGHT TREATMENT

A WARP 75 (Quantum Devices, WI, USA) light emitting diode (LED) device was used to irradiate rat retinas with 670nm light. SD rats were wrapped individually in a cloth and positioned under the LED device such that their eyes were approximately 2-3 cm from the light source and were maintained in this position for 3 minutes at a 60mW/cm^2 output, producing an overall energy rate of 9J/cm^2 at the eye level. Animals were treated with 670nm light for 3 minutes once daily, around 9:00AM for 5 consecutive days to account as one complete treatment. Sham treated animals were also wrapped individually and maintained in the treatment position for 3 minutes daily for 5 days without exposure to 670nm light.

2.5 TISSUE COLLECTION AND FIXATION

Animals were euthanised by administering an intraperitoneal injection of barbiturate overdose (60 mg/kg bodyweight, Valabarb; Virbac, Carros, France). The left eye from each animal was extracted for histological analyses while the right eye was used for RNA extraction. For each left eye, the superior corneal aspect was marked with a black or red permanent marker prior to enucleation using an, forceps and iris scissors. Following enucleation, the eyes were injected with freshly prepared 4% paraformaldehyde using a 1ml syringe and 27 gauge needle. The eyes were then immersed in 4% paraformaldehyde for 3 hours at 4°C. The retina from the right eye of each animal was excised through a corneal incision and placed in RNAlater solution (Ambion Biosystems, Austin, TX, USA), stored at 4°C overnight then transferred to -80°C.

2.6 HISTOLOGICAL PROCESSING

2.6.1 CRYOPRESERVATION, EMBEDDING AND SECTIONING

Following fixation, eyes were rinsed three times with 0.1M PBS for 10 minutes each and cryoprotected via overnight immersion in a 30% sucrose solution, made up with 0.1M PBS. Eyes were then placed into plastic moulds, with the superior marked side being placed parallel to the base of the mould and the cornea facing towards the wall of the mould, filled with Tissue Tek Optimal cutting temperature CT mounting medium (Tissue-Tek®, Sakura Finetechnical, Japan). The mould was then snap frozen in a solution of isopentane (Sigma Chemical Co., St Louis, MI, USA), which was cooled by liquid nitrogen and then placed in -20°C for storage (no longer than 1 month). The embedded eyes were cryosectioned using Leica CM1850 Cryostat at 16µm thickness and mounted directly onto SuperFrost®- Plus slides (Menzel-Glaser) coated in gelatin (Sigma-Aldrich) and poly-L-lysine (Sigma-Aldrich). Sections were cut in the horizontal plane and sections containing the optic nerve head were used in experiments in this study to maintain consistency in location within the tissue. Cut sections were stored at -20°C until required.

Alternatively, following 3 hour fixation in 4% paraformaldehyde the anterior chamber (including lens) was dissected out and the eyes replaced in 4% paraformaldehyde for 24hrs. The eyes were then processed for paraffin coating and embedding before sectioning at 4-6um on the microtome, across the superior-inferior axis. Cut sections were stored at 4°C.

2.7 HISTOLOGICAL TECHNIQUES

2.7.1 TUNEL ASSAY

Cell death was visualised by Terminal deoxynucleotidyl transferase (TdT) dUTP Nick-End Labeling (TUNEL) assay (Roche Inc, NSW, Australia). TUNEL works by incorporating biotinylated UTP to the strand breaks of nicked DNA which is then visualised using streptavidin conjugated flurophore. The technique described below is a modified version of the technique first described by Gavrieli *et al*., 1992.

1. Frozen sections were removed from the -20°C freezer and placed into 70% ethanol for 15 minutes, followed by two 5 minute washes in dH_2O.

2. Sections were immersed in 1x Tdt buffer (3mM Trizma base, 14mM sodium cacodylate and 0.1mM cobalt chloride in dH_2O) for 10 minutes.

3. Sections were then covered in 100-200µl of reaction mixture (1.26 M biotinylated dUTP and 0.5 units/µl terminal transferease (TdT) in 1x TdT Buffer) for 1 hour at 37°C (Roche).

4. Reaction was terminated by a 15 minute wash of 2x SSC (0.3M NaCl, 30mM sodium citrate).

5. 10% normal Goat Serum in 1x PBS was then added to the slides to reduce non-specific binding of the streptavidin conjugated fluorophore, for 10 minutes.

6. Slides were then incubated in a 1:200 dilution of Streptavidin Alexa-594 (Vector - Invitrogen) in 0.1M PBS for 60 minutes at 37°C, followed by two 5 minute washes in 0.1M PBS.

7. Sections were counterstained with a DNA-specific dye Bisbenzamide (Calbiochem) in a 1:10000 dilution for 2 minutes, followed by a final wash in 0.1M PBS for 5 minutes, before being coverslipped with Aqua Poly/Mount (Polysciences).

2.7.2 QUANTITATIVE ANALYSIS OF TUNEL

The TUNEL+ cells were visualised using a LSM5 confocal fluorescence microscopy (Zeiss) and photographed using the Pascal Version 5 software (Zeiss). The TUNEL+ profile counts were performed on LSM5 confocal microscope (Zeiss) using Colibri LED system. Cells were counted across the full length of the retinal sections cut in the vertical meridian, including at the optic nerve head. Cells were counted at 1-mm intervals across retinal sections, the final count from each animal was averaged from at least two sections, with four or five animals analyzed for each experimental condition. All counts were performed in a masked fashion whereby TUNEL labeled slides were de-identified prior to counting.

2.7.3 TOLUIDINE BLUE STAINING AND RETINAL LAYER THICKNESS MEASUREMENT

Toluidine Blue staining was performed to assess the changes in different layers of the retina.

1. Sections were dehydrated by immersing in 70% ethanol for 5 minutes.

2. Slides were rinsed with dH2O for 5 minutes.

3. Sections were then covered with a few drops of 1% Toluidine Blue and stained for 5 minutes, followed by a 5 minute wash in tap H2O.

4. Sections were then coverslipped in Eukitt®.

Sections were visualised using transmitted light on the LSM5 confocal microscope (Zeiss), and photographed using an Axiocam HRc (Zeiss). Measurements of individual retinal layers were obtained using the ProRes® CapturePro 2.5 (JENOPTIK Laser, Optik). Measurements were

obtained at the mid-periphery of the superior retina and collected as absolute values expressed in micro meters (µm). We took 3 measurements per section, 4 sections per animal and the used averaged values for each animal.

2.7.4 BISBENZAMIDE LABELLING AND ONL THICKNESS MEASUREMENTS

Bisbenzamide (BBZ), a DNA binding dye, was used to visualise the different cellular layers of the retina and used to assess the thickness of the ONL. As mentioned previously, cryosections were incubated in BBZ (1:10000; Calbiochem, USA) for 2 minutes, followed by a 5 minute wash in 0.1M PBS and coverslipped with Aqua Poly/Mount (Polysciences).

Sections were visualised using the Leica Axiovert 200 inverted microscope and measurements and images obtained using the ProRes® CapturePro 2.5 (JENOPTIK Laser, Optik). At each retinal location the thickness of the ONL as well as the retina, from the inner limiting membrane to the outer limiting membrane (ILM-OLM) was measured and the ratio of ONL / (ILM-OLM) was used to analyse the change in ONL thickness in the different experimental groups. We took atleast 8-10 measurements per section each approximately 1mm apart along the retina. A minimum of 4 sections per animal were used to perform the measurements and average values were plotted for the whole retina.

2.7.5 IMMUNOHISTOCHEMISTRY

A listing of antibodies used in this study can be found in table 2.1 and 2.2.

1. Retinal cryosections were thawed at room temperature for 5 minutes and washed in 70% alcohol for 10 minutes, followed by a wash in dH_20 for 5 mins and two washes in 0.1M PBS for 5 minutes each.

2. A hydrophobic barrier was then drawn around the sections using a Pap-pen (ProSciTech, Kirwan, QLD) to prevent the loss of aqueous reagents in the subsequent steps.

3. Slides were then incubated in 10% normal goat serum for 30 mins to prevent non-specific binding of the secondary antibody.

4. Primary antibodies were diluted with 0.1M PBS and 1% serum, to optimal dilutions (See table 2.1) and added to the slides, ensuring even coverage. Slides were then incubated overnight at 4°C in a humid chamber.

5. Following the overnight incubation, slides were washed twice in 0.1M PBS for 5 minutes each.

6. Secondary antibodies were diluted in 0.1M PBS as detailed in table 2.2, and incubated at room temperature for about 2-4 hours.

7. Slides were then washed three times in 0.1M PBS for 5 minutes each.

8. Sections were then counterstained using Bizmenzamide incubation (mentioned previoulsy), and coverslipped in Aqua Poly/Mount (Polysciences).

Sections were then visualised using a LSM5 confocal fluorescence (Zeiss), and photographed and analysed using Pascal version 4 software (Zeiss).

2.7.6 MICRORNA IN SITU HYBRIDISATION

In situ hybridization was performed to localize miRNA expression in the retina using commercially available double DIG labelled miR-124-3p miRCURY LNA probe (Exiqon) and miRCURY LNA™ microRNA FFPE ISH detection kit 4, according to manufacturer's protocol; Paraffin was stripped off the rat retinal sections using xylene washes and rehydrated by washing in a decreasing concentration of ethanol. All retinal sections (Human and Rat) were treated with proteinase K (20µg/ml) for 10 minutes. MiR-124-3p probe was hybridized for 1.5 hours at 53°C and then washed in saline sodium citrate at 58°C. Bound probe was visualized with HNPP/Fast-Red (Roche, Basel, Switzerland), which was followed by counter-staining

using immunohistochemistry. HNPP/FastRed is a fluorescent substrate for alkaline phosphatase that enables sensitive detection of alkaline phosphatase (AP) conjugated antibodies. In this study I have used HNPP to detect the AP conjugated anti-DIG antibodies bound to the DIG labeled riboprobe hybridized to mature miR-124-3p. HNPP (in combination with Fast-red) produces an orange (~562nm) signal post catalysis via AP, which is then visualized using fluorescence microscopy.

1. Slides were deparaffinized by immersing in Xylene for 15 minutes, followed by rehydration through washes with decreasing ethanol concentrations:

   100% ethanol (5 minutes)

   100% ethanol (5 minutes)

   90% ethanol (5 minutes)

Table 2. 1

Primary Antibodies used for experiments in this study

Antibody	Source	Species	Optimal Dilution
Iba-1	Wako Chemicals	Rabbit	1:1000
Vimentin	Abcam	Mouse	1:200
Anti-DIG	Sigma	Sheep	1:800

Table 2. 2

Secondary Antibodies used for immunohistochemistry

Antibody	Source	Species	Optimal Dilution
Anti-mouse Alexa 488	Invitrogen	Goat	1:1000
Anti-rabbit Alexa 594	Invitrogen	Goat	1:1000

70% ethanol (5 minutes)

2. Slides were then washed in 0.1M PBS for 5 minutes and the sections circled with liquid blocker – super PAP PEN (Pyramid Innovation) to prevent runoff of solution.
3. Slides were then incubated with 20ug/ml proteinase-K diluted in 1x Prot-K buffer (Prepared according to manufacturer's protocol) for 10 minutes at 37°C.
4. Washed in 0.1M PBS twice (5 minutes each).
5. Slides were then dehydrated by washing with different dilutions of ethanol (freshly prepared):

   70% ethanol (1 minute)

   90% ethanol (1 minute)

   100% ethanol (1 minute)
6. Thereafter, the slides were air dried for approximately 15 minutes inside a class II biosafety cabinet. While the hybridization probes were prepared to required concentrations by heat shocking at 90°C for 4 minutes, followed by diluting in 1x hybridization buffer equilibrated to the hybridization temperature of the ISH probes.
7. 100-140µl of the probe-hyb buffer mix was then applied to the slides, coverslipped and hybridized at 53 °C for 1.5 hours.
8. After the incubation period the coverslip was removed and the slides washed in different grades of Saline Sodium Citrate (SSC) buffer maintained at 4-5°C above the hybridization temperature.

   5x SSC (1 minute)

   1x SSC (5 minutes)

   1x SSC (5 minutes)

   0.2x SSC (5 minutes)

   0.2x SSC (5 minutes)

9. Slides were then washed in 0.1M PBS for 5 minutes. And incubated with blocking solution (including 2% Sheep serum and 1% Bovine serum albumin BSA) for 15 minutes at room temperature in a humid chamber.
10. Following blocking, slides were incubated with sheep-anti-DIG antibody (refer table 2.1) diluted in 0.1% PBS-T (including 1% Sheep serum and 1% BSA) at a 1:800 dilution for 2x 30 minutes (Room temperature).
11. Slides were then washed three times in 0.1% PBS-T for 3 minutes each.
12. Washed in 1x Detection buffer (containing Magnesium ions) for 5 minutes.
13. And incubated with a freshly prepared fluorescent AP substrate (Fast Red) at room temperature until the stain developed.
14. Sections were then double labelled with specific antibodies by following the protocol described in *section 2.7.5* and coverslipped with Aqua Poly/Mount (Polyscience).

2.8 RNA ISOLATION AND ANALYSES

2.8.1 RNA EXTRACTION

RNA isolation was performed using TRIzol reagent (Invitrogen) in conjunction with RNAqueous® kit (Ambion) for rat retina or RNAqueous®-Micro kit (Ambion) for cells. After animals were sacrificed, the retina was dissected out of the eye cup and placed in 1.5ml tube containing 200µl TRIzol. Retinas were homogenised on ice followed by addition of another 400µl TRIzol and 120µl chloroform, vortexed for 20secs and allowed to sit at room temperature for 7 minutes. The tubes were then centrifuged at 13,000g for 10 minutes at 4 °C. The clear supernatant was then carefully removed and placed in a clean 1.5ml tube along with half its volume in 100% ethanol. Following this the tube was vortexed briefly before

commencing the purification and elution steps outlined in Part C of the RNA Isolation protocol provided with the kits (Ambion).

For *in vitro* work, 500µl TRIzol was used to detach and harvest cells from the culture plates followed by addition of 120µl chloroform. Remaining steps were similar to those outlined above and the purification and elution steps were as mentioned in the RNAqueous-Micro kit protocol (Ambion).

2.8.2 RNA ANALYSIS

Purified RNA was quantified on a ND-1000 (Nanodrop Technologies, Wilmington, DE) spectrophotometer. While, the 2100-Bioanalyser (Agilent Technologies, Santa Clara, CA, USA) was used to identified the purity and quality of RNA. Only RNA samples with a A260/A280 ratio above 1.8 and an RNA integrity number (RIN) greater than 8.0 were used for the study. The RNA samples were stored at -80 °C before performing further analyses.

2.9 CDNA SYNTHESIS

Complementary DNA (cDNA) was prepared using the TaqMan® MicroRNA Reverse Transcription kit (Applied Biosystems) – for miRNAs and the Tetro cDNA synthesis kit (Bioline) – for mRNAs, following manufacturer's directions as detailed below:

2.9.1 TAQMAN® MICRORNA RT KIT (MIRNA)

1. Purified RNA was primed in a sterile 0.2ml tube by mixing 0.5-1µg RNA with RNase free H2O up to a total volume of 5µl.
2. The RNA mix was then incubated at 65°C for 5 minutes and placed on ice for 5 minutes.
3. Samples were centrifuged and added to 7µl of the reverse transcription mix containing 1.5µl 10x RT buffer, 0.15µl dNTP mix, 0.19 µl RNase off (20 U/µl), 1µl Multiscribe™ RTase (50 U).

4. Then 3µl of specific miRNA RT primer pool was added to the tubes and mixed by vortexing.
5. The combined 15ul reaction mix was then placed into the VERITI® PCR machine (Applied Biosystems) and run with the following cycling program: 16°C for 30minutes; 42°C for 30minutes and 85°C for 5 minutes. Followed by hold at 4°C.
6. The resulting cDNA was then used for real time qPCR or stored at -20°C.

2.9.2 TETRO CDNA SYNTHESIS KIT (MRNA)

1. Purified RNA was primed in a sterile 0.2ml tube by mixing 1µg RNA with 1µl Oligo (dT)18 primers (500µg/ml), 1µl dNTPs (10mM), made up to 14µl with RNase free H_2O.
2. This mix was incubated at 70°C for 5 minutes and placed on ice for 5 minutes.
3. Samples were then centrifuged and added to 6ul of reverse transcription mix containing 200 U Tetro Reverse Transcriptase, 4 µl 5x RT buffer and 10U Ribosafe RNase Inhibitor.
4. The tubes were then mixed by vortexing and the 20µl reaction mixture centrifuged before placing into the VERITI® PCR machine (Applied Biosystems).
5. The cycling program was run as follows: 30 minutes at 45°C for the reaction to occur, followed by 5 minutes at 85°C to terminate reaction and hold at 4°C.
6. The resulting cDNA was then used for real time qPCR or stored at -20°C.

2.10 QUANTITATIVE REAL TIME POLYMERASE CHAIN REACTION (QRT-PCR)

Changes in expression of genes of interest (both miRNA and mRNA) were determined by qRT-PCR using TaqMan® hydrolysis probes (Applied Biosystems) and Gene Expression Mastermix (Applied Biosystems). All the TaqMan probes used are listed in table 2.3. qPCR was performed on the QuanStudio™ 12K Flex Real-Time PCR System (Applied Biosystems) and results analysed using the QuantStudio 12K Flex Software (Applied Biosystems).

For each comparison, every gene was run as a technical duplicate across a biological triplicate to account for individual sample and animal variability. A 10µl final reaction volume was used in a 384 well clear PCR plate, setup as follows:

1. 0.5-0.9 µl cDNA was added to RNase free water to achieve 4.5µl total volume.
2. This solution was added to 5µl TaqMAn gene expression master mix (Applied Biosystems) and 0.5ul TaqMan primer probe assay.
3. The following program was then run on the QuantStudio 12K Flex qPCR machine:

Step	Temperature (°C)	Duration	Cycles
UDG Incubation	50	2 minutes	1x
AmpliTaq Gold, UP Enzyme activation	95	10 minutes	1x
Denature	95	15 seconds	Cycle 40x
Anneal and Extend*	60	1 minute	

*fluorescence level is measured automatically at the end of each cycle, to establish the critical threshold cycle.

2.10.1 QPCR ANALYSIS

Fold change was determined using the comparative delta-delta Ct method. The QuantStudio 12K Flex Software performs the calculations using the Critical threshold cycle obtained (Ct) and the following equation:

Normalised Target Gene expression level = $2^{(-\Delta\Delta Ct)}$

Where, ΔCt = Ct (Target Gene) – Ct (Endogenous control Gene)

ΔΔCt = ΔCt (Experimental sample) – ΔCt (Control sample)

In this study the reference gene used for the mRNA quantification was GAPDH, while U6 was used as the reference gene for miRNA quantification. All qPCRs in this study were performed and reported in accordance with the Minimum Information for Publication of Quantitative Real-Time PCR Experiments (MIQE) guidelines.

2.11 MICRORNA LOW DENSITY ARRAY

The RNA from dim-reared control retinas, 24-hour light exposed retinas and 670nm treated dim-reared retinas were used for miRNA array card analysis. Total RNA (700 ng) from each animal was reverse transcribed to two different cDNA pools (each containing 350 ng of miRNAspecific cDNA) using the Megaplex RT Primers, Rodent Pool A and B Set v3.0 (Applied Biosystems, Carlsbad, CA, USA) and TaqMan miRNA RT kit (Applied Biosystems) according to manufacturer's protocol; a 7.5μL reaction mixture, including 50 U Multiscribe Reverse Transcriptase and 20 U RNase inhibitor. Card A contains well characterized miRNAs in miRBase v16.0 (available in the public domain at www.mirbase.org), while B contains uncharacterized ones. Both A and B samples then were hybridized to the respective TaqMan Array Rodent MicroRNA Cards v3.0 (A and B), which are preconfigured microfluidic 384-well format plates. Each well in the microfluidic card consists of a TaqMan chemistry-based primer probe set for a unique miRNA or other RNA (control sequences). A total of 20 microRNA cards were run (10 A cards and 10 B cards). The microfluidic cards then were run on the ViiA 7 Real-time PCR machine (Applied Biosystems) to generate the raw expression data. The expression data were compiled and exported into an excel format using the Expression Suite Software. And analyzed using PARTEK Genomic Suite 6.6 software (Partek,

Inc., St. Louis, MO, USA). Amplification data for the target miRNAs were first normalized by subtracting the endogenous control (Y1) values.

Table 2. 3 TaqMan® Hydrolysis probes used

Gene/miRNA Symbol	Name	Accession #	Catalog #
Ccl2	Chemokine (C-C motif) ligand 2	NM_031530.1	Rn01456716_g1
Ccl3	Chemokine (C-C motif) ligand 3	NM_013025.2	Rn00564660_m1
Ccl4	Chemokine (C-C motif) ligand 4	NM_053858.1	Rn00587826_m1
Ccl7	Chemokine (C-C motif) ligand 7	NM_01007612.1	Rn01467286_m1
CxCL1	Chemokine (C-X-C motif) ligand 1	NM_030845.1	Rn00578225_m1
CxCL10	Chemokine (C-X-C motif) ligand 10	NM_139089.1	Rn01413889_g1
CxCL11	Chemokine (C-X-C motif) ligand 11	NM_182952.2	Rn00788262_g1
GAPDH	Glyceraldehyde-3-phosphate dehydrogenase	NM_017008.3	Rn99999916_s1
IL1β	Interleukin 1β	NM_031512.2	Rn00580432_m1
miR-351	mmu-miR-351	MIMAT0000609	001067
miR-155	mmu-miR-155	MIMAT0000165	002571
miR-124-3p	mmu-miR-124-3p	MIMAT0000422	001182
miR-183	has-miR-183	MIMAT0000860	002269
U6	U6 small nuclear RNA	NR_004394	001973
miR-125b-3p	hsa-miR-125b-3p	MIMAT0004592	002378
miR-542-3p	mmu-miR-542-3p	MIMAT0003172	001284
miR-449a	hsa-miR-449a	MIMAT0001541	001030
miR-347	rno-miR-347	MIMAT0000598	001334
miR-207	mmu-miR-207	MIMAT0000240	001198
miR-182	mmu-miR-182	MIMAT0005300	002599
miR-96	mmu-miR-96	MIMAT0000818	000186
miR-467d	mmu-miR-467d	MIMAT0004886	002518

Differential expression was examined using the 1-way ANOVA statistic with a significance cutoff of $P < 0.05$. The statistical robustness of the expression data was visualized with principle component analysis (PCA), provided within the Partek Genomic Suite 6.6 software. MicroRNA expression distribution was visualized using the volcano plot tool embedded within the Partek software. A list of significantly regulated miRNAs was generated from the volcano plot by selecting for miRNAs that changed ‡2-fold and had a P value of <0.05. These highly modulated miRNAs were used for biological functional analyses using PARTEK Genomic Suite 6.6.

2.12 IN-VITRO STUDIES

2.12.1 CELL REARING AND STIMULATION

Cell culture experiments were performed using HeLa cells and low passage (<10) immortalized human Müller cell line (MIO-M1). We also used low passage number 661W photoreceptor cell line, generously provided by Dr. Muayyad Al-Ubaidi (University of Oklahoma), and an immortalized RPE cell line (ARPE19) for this study. Cells were used within 10 passages of authentication and validation from Cell Bank Australia. And were further validated using RT-PCR for expression of cell specific markers including SW opsin, M opsin pigments, SV40 for 661W cells; RPE65, RLBP1 for ARPE19 cells; GFAP, Vimentin for MIO-M1 cells. Cells were cultured in Dulbeco's Modified Eagle's Medium (DMEM; Invitrogen) containing 10% fetal bovine serum, L-glutamine (3 mM), sodium pyruvate (1 mM) and glucose (25 mM) and stored in an incubator at 37°C, 5% CO_2. Human IL-1β protein (10ng/ml) was used as a pro-inflammatory stimulus for MIO-M1 and ARPE19 cell lines. While, 661W photoreceptor cells were stimulated by bright light induced damage. The cell culture plate, containing 80-90% confluent cells, was placed under 15,000 lux light for 5 hours while inside an incubator

maintained at 37°C and 5% CO_2 to ensure even distribution across the plate. The temperature of the setup was monitored vigilantly using a thermometer placed next to the culture plate.

2.12.2 MIO-M1 CELL TRANSFECTION AND STIMULATION

MIO-M1 cells were seeded in clear plastic 6-well tissue culture plates at a density of 80,000 cells per well and the medium was replaced with 2.5 ml low serum (1%) growth medium after sufficient adhering time (24 hours). Cells were then incubated at 37 °C, 5% CO2 for 12h and transfected with miR-124-3p mimic (UAAGGCACGCGGUGAAUGCC) or miR-124a inhibitor (GGCAUUCACCGCGUGCCUUA) or negative control miRNA mimic (Ambion) using Lipofectamine RNAiMAX (Invitrogen) as follows:

1.5µl miRNA stock (10µM) was combined with 300µl Opti-MEM® and 9µl Lipofectamine RNAiMAX®. Vortexed and incubated for 5 minutes at room temperature. Then 250µl of the miRNA:Lipofectamine complex was added to each well, and the plate returned to the incubator.

24hrs post transfection cells were exposed to 10ng/ml IL-1β protein for a duration of 12hrs. The cells were then harvested using TRIzol (Invitrogen) reagent and RNA extracted using the RNAqueous-Micro RNA Isolation Kit (Ambion, Applied Biosystems) [*refer section 2.8.1*].

2.12.3 LUCIFERASE ASSAY

Luciferase assay is used to establish the direct binding between miRNA and their respective target 3'UTRs. In this study it was performed in both HeLa and MIO-M1 cells using a commercially available vector containing the renilla luciferase gene fused to the human CCL2 3'UTR (CCL2 LightSwitch 3'UTR Reporter GoClone; Switchgear Genomics, CA, USA) and the pLightSwitch-3'UTR Luciferase assay system (Switchgear Genomics, CA, USA), following the manufacturer's protocol. Cells were seeded into a white 96 well plate (5000 cells per well) and cultured for 24hrs, similar to cell rearing conditions, in 100µl 10% growth

medium. Once they reached ~90% confluence, the growth media was replaced with fresh media and the cells were transfected with either the vector only or co-transfected with the vector and miR-124-3p mimic (Ambion) or co-transfected with the vector and negative control miRNA mimic (Ambion) following the below mentioned protocol:

1. miRNA mimics and inhibitors were transfected into cells using Lipofectamine® RNAiMAX transfection reagent (Life Technologies). 1µl miRNA mimic or inhibitor stock (10 µM) was added to 50µl Opti-MEM® and 1.5 µl RNAiMAX reagent, mixed by vortexing and incubated at room temperature for 5 minutes.
2. Then 10ul of the miRNA:Lipofectamine complex was added to each well containing 100µl 10% growth medium, resulting in a final miRNA mimic/inhibitor concentration of 20nM in each well.
3. CCL2 3'UTR GoCLone was transfected into the cells simultaneously using ViaFect™ transfection reagent (Promega). 3.33µl of the GoClone stock (30ng/µl) was combined with 0.6µl ViaFect™ and 6.07µl Opti-MEM® medium, mixed by vortexing and incubated at room temperature for 15 minutes.
4. Thereafter, 10µl of Plasmid Vector:ViaFect™ complex was added to each well.
5. The plate was then returned to the incubator for 48 hours before testing for luciferase activity.

Müller cells were transfected with the CCL2 3'UTR GoClone only and placed in the incubator for 36 hours before stimulation with IL1β protein (10ng/ml) for a period of 12 hours.

The luciferase activity for both HeLa and MIO-M1 cells was then analysed using the LightSwitch® Luciferase assay system (SwitchGear Genomics), which was performed according to manufacturer's protocol mentioned in the following document:

https://www.activemotif.com/documents/1946.pdf.

And the luciferase assay reagent bioluminescence was measured by Infinity® 200 plate reader (TECAN, Austria). Statistics were performed using Student's t-test.

STATISTICAL ANALYSES

Varying combinations of different statistical tests were used throughout the thesis to perform statistical analyses of the data presented. Majority of the data were analysed using GraphPad PRISM® statistical software (v5.0, GraphPad Software Inc., San Diego, CA, USA). Parametric One and Two way ANOVA tests along with tukey's and Bonferroni post hoc tests were used for data analyses. In most cases Student's t-tests were also employed on the data to confirm statistical significance. Results are presented as mean values with standard error of the mean (SEM) as error bars. P value of <0.05 was considered significant.

CHAPTER 3: IDENTIFICATION OF MIRNAS IN A MODEL OF RETINAL DEGENERATIONS

This chapter is a reproduction of previously published work:

Saxena K, Rutar MV, Provis JM, Natoli RC. (2015) “Identification of miRNAs in a Model of Retinal Degenerations.” Invest Ophthalmol Vis Sci. Feb 24;56(3):1820-9.

3.1 INTRODUCTION

MicroRNAs (miRNAs) are small evolutionarily conserved non-coding RNA sequences that modulate a range of biological processes [129] including cell death [258, 259] and inflammation [260]. They are ~22-25 nucleotides long and provide a second layer of post-transcriptional gene regulation by targeting messenger RNAs (mRNAs) for degradation or repression of translation [163], and are found in abundance in the CNS [165, 261].

Age-related macular Degeneration (AMD) is a progressive degenerative disease of the retina that causes irreversible vision loss and accounts for up to 50% of central blindness cases worldwide. The involvement of inflammatory processes in the pathogenesis of AMD was documented in the 1980s [63] with gene association studies providing strong statistical support for its involvement in disease pathogenesis [2, 3, 262]. Subsequently a large number of inflammatory factors and co-factors, particularly in the complement pathways, have been implicated in the disease process (for a review see [263]).

The acute retinal light damage (LD) model in rats has features in common with dry AMD [105, 113], including cell death and inflammation [105]. This model has been used to investigate the involvement of chemokines and macrophages in the progression of retinal degeneration [98]. Following light damage (LD) a lesion formed by the death of photoreceptors and atrophy of the RPE presents on the visual axis and enlarges over time, even in the absence of the damaging stimulus [105]. In this model photoreceptor death is associated with expression of chemokines by Müller glia, recruitment of macrophages and deposition of C3 [119], and attenuation of macrophage recruitment, by silencing expression of the chemokine CCL2, reduces photoreceptor cell death [97]. Similar patterns of chemokine expression, macrophage recruitment, C3 deposition and photoreceptor cell death are present in the normally aging rat [264], indicating that the model represents many of the features of normal aging of the retina.

Recent evidence supports the idea that miRNA are involved in inflammation [265, 266]. Many miRNAs are rapidly upregulated in response to inflammatory cues and may either promote the duration and magnitude of inflammation [267] or silence it [176]. In this study we investigated the modulation of miRNAs in the rat LD model of focal retinal degeneration and explored the transcriptional profile of their target genes in the retina following LD, with a focus on identifying miRNA that modulate expression of genes involved in the inflammatory response.

3.2 METHODS

3.2.1 ANIMALS AND LIGHT DAMAGE

Animal handling and treatment protocols were carried out in accordance with the ARVO statement describing the ethical use of animals in vision research, and were approved by the ANU Animal Ethics Committee. Sprague Dawley (SD) rats aged 90-140 post-natal days raised in dim (5 lux) cyclic light ('dim-reared') were used for the study. Light damage was induced by exposure to bright light (1000 lux) from an overhead white fluorescent source (COLDF2 2x36W IHF, THORN lighting, Australia) for a period of 24 hours. Food was provided *ad libitum*. At the end of the exposure period animals were either euthanized immediately by intraperitoneal injection of barbiturate overdose (60mg/kg bodyweight, Valabarb; Virbac), or were returned to dim light (5 lux) conditions for 3 or 7 days prior to euthanasia. Retinal tissue was collected immediately for analysis. Age-matched, dim-reared animals were used as controls. All experimental groups were n=5, unless otherwise stated.

3.2.2 TISSUE COLLECTION

The retina from the right eye of each animal was excised through a corneal incision and placed in RNA*later* solution (Ambion Biosystems, Austin, TX), stored at 4°C overnight then transferred to -80°C. The left eye from each animal was enucleated, the superior margin

marked, then immersed in 4% paraformaldehyde for 3h at 4°C. The anterior segment was removed then the eye cups replaced in fresh 4% paraformaldehyde overnight at 4°C, and subsequently prepared for paraffin embedding. Eyes were sectioned at 6 µm on a microtome on the vertical axis. Only sections containing the optic nerve were used for analysis.

3.2.3 RNA EXTRACTED FROM RAT RETINA

Total RNA was extracted from retinal samples using the *mirVana* miRNA isolation kit (Ambion, Austin, TX), according to manufacturer's protocol. The concentration of the RNA was determined by ND-1000 spectrophotometer (Nanodrop Technologies, Wilmington, DE) and quality using the 2100-Bioanalyser (Agilent Technologies, Santa Clara, CA). Only RNA samples with a A260/A280 ratio above 1.9 and a RNA integrity number (RIN) greater than 8.0 were used for the study. RNA samples were stored at -80°C before performing Taqman miRNA array studies.

3.2.4 TAQMAN MIRNA ARRAY AND ANALYSIS

RNA from dim-reared control retinas and 24hr light-exposed retinas were used for miRNA array card analysis. 700ng of total RNA from each animal was reverse transcribed to two different cDNA pools (each containing 350ng of miRNAs-specific cDNA) using the Megaplex™ RT Primers, Rodent Pool A and B Set v3.0 (Applied Biosystems) and TaqMan miRNA RT kit (Applied Biosystems) according to manufacturer's protocol; a 7.5µl reaction mixture including 50U Multiscribe™ Reverse Transcriptase and 20U RNase inhibitor. Card A, contains well characterized miRNAs in miRBase v16.0 (www.mirbase.org), while B contains uncharacterized ones. Both A and B samples were then hybridized to the respective TaqMan® Array Rodent MicroRNA Cards v3.0 (A and B), which are pre-configured microfluidic 384 well format plates. Each well in the microfluidic card consists of TaqMan® chemistry based primer probe set for a unique miRNA or other RNA (control sequences). 20 microRNA cards were run in total (10 A cards and 10 B cards). The microfluidic cards were then run on the

ViiA™ 7 Real-time PCR machine (Applied Biosystems) to generate the raw expression data. The expression data was compiled and analysed using PARTEK® Genomic Suite™ 6.6 software (Partek Inc., St.Louis, MO, USA). Amplification data for the target miRNAs was first normalized by subtracting the endogenous control (Y1) values. Differential expression was examined using the 1way-ANOVA statistic with a significance cutoff of $p<0.05$. The statistical robustness of the expression data was visualized with principle component analysis (PCA), provided within the Partek® Genomic Suite™ 6.6 software. MicroRNA expression distribution was visualized using the volcano plot tool embedded within the Partek® software. A list of significantly regulated miRNAs was generated from the volcano plot by selecting for miRNAs that changed $\geq$ 2-fold and had a p-value<0.05. These highly modulated miRNAs were used for biological functional analyses using PARTEK® Genomic Suite™ 6.6.

3.2.5 BIOLOGIC FUNCTIONAL ANALYSES

We used data from a previous microarray analysis [96] (accessible through gene expression omnibus (GEO) Series accession number GSE22818) identifying genes modulated by light damage in this same LD model, to identify potential target genes for our differentially expressed miRNAs. To achieve this, the relevant gene expression microarray data (and their accompanying Affymetrix CEL files) was imported into PARTEK® Genomic Suite™ 6.6 software (Partek Inc., St.Louis, MO, USA) along with the current miRNA expression data to compare the two expression profiles. Predicted gene targets were determined using the TargetScan v6.2 algorithm via the PARTEK® software. Which were then subjected to functional analysis via Gene Ontology (GO) enrichment within PARTEK® and clustered according to their respective biological processes.

Table 3. 1

Taqman® small RNA probes used

miRNA ID	Accession #	Product Number
mmu-miR-155	MIMAT0000165	002571
hsa-miR-125b-3p	MIMAT0004592	002378
mmu-miR-351	MIMAT0000609	001067
mmu-miR-542-3p	MIMAT0003172	001284
hsa-miR-449a	MIMAT0001541	001030
rno-miR-347	MIMAT0000598	001334
mmu-miR-207	MIMAT0000240	001198
U6 snRNA	NR_004394	001973
mmu-miR-182	MIMAT0005300	002599
hsa-miR-183	MIMAT0000860	002269
mmu-miR-96	MIMAT0000818	000186
mmu-miR-467d	MIMAT0004886	002518

3.2.6 QUANTITATIVE REAL-TIME PCR

cDNA was synthesized using the TaqMan® MicroRNA RT kit (Applied Biosystems, Life technologies) according to manufacturer's protocol; a 15µl reaction mixture including 500ng-1µg RNA, 50U Multiscribe™ Reverse transcriptase, 3µl 5X miRNA specific RT primer and 3.8U RNase Inhibitor. MiRNA amplification was measured using commercially available miRNA specific TaqMan® hydrolysis probes (Applied Biosystems) detailed in Table 3.1. The hydrolysis probes were utilized according to the manufacturer's directions in a 10µl reaction mix along with TaqMan® Gene Expression Mastermix and the cDNA. Fluorescence was measured by the FAM 510nm channel in the 7900HT Real-time PCR machine (Applied Biosystems), ROX™ passive reference dye present in the Gene Expression Mastermix was used to normalise samples in individual wells. Each biological sample was amplified in a technical replicate and the average C_t (Critical threshold cycle) value was used to determine the change in expression. Fold change was calculated using the $\Delta\Delta C_t$ method where target miRNAs were normalized to the expression of small nuclear RNA U6 (reference RNA), which showed no differential expression in this study. Gel electrophoresis was used to access amplification specificity and statistical analysis was performed using 1-way ANOVA and Student t test, using Prism (GraphPad Software V5).

3.2.7 ANALYSIS OF CELL DEATH

TdT-mediated dUTP nick end labeling (TUNEL) technique was used to quantify cell death over the LD timecourse, in retinal cryosections using a previously published protocol[96]. TUNEL positive cells in the outer nuclear layer (ONL) were counted across the full length of the retinal sections cut in the vertical meridian, including at the optic nerve head. Cells were counted at 1mm intervals across retinal sections, the final count from each animal was averaged from at least two sections, with four or five animals analysed for each experimental condition.

Statistical analysis was performed using 1-way ANOVA and Student t test, using Prism (GraphPad Software v5).

3.3 RESULTS

3.3.1 TUNEL ANALYSIS

There was an evident increase in the number of photoreceptor cells undergoing apoptosis following exposure to 24hrs bright light, consistent with our previous reports (Figure 3.1). This increase was more prominent in the superior retina approximately 2mm superior temporal to the optic disc, shown in the representative image panels (Figure 3.1A-D). We observed a peak in the number of TUNEL+ cells in the ONL after 24hrs bright light exposure followed by a significant decrease during the post exposure periods, 3 and 7 days, as well as a progressive thinning of the ONL/photoreceptor layer as described previously [98].

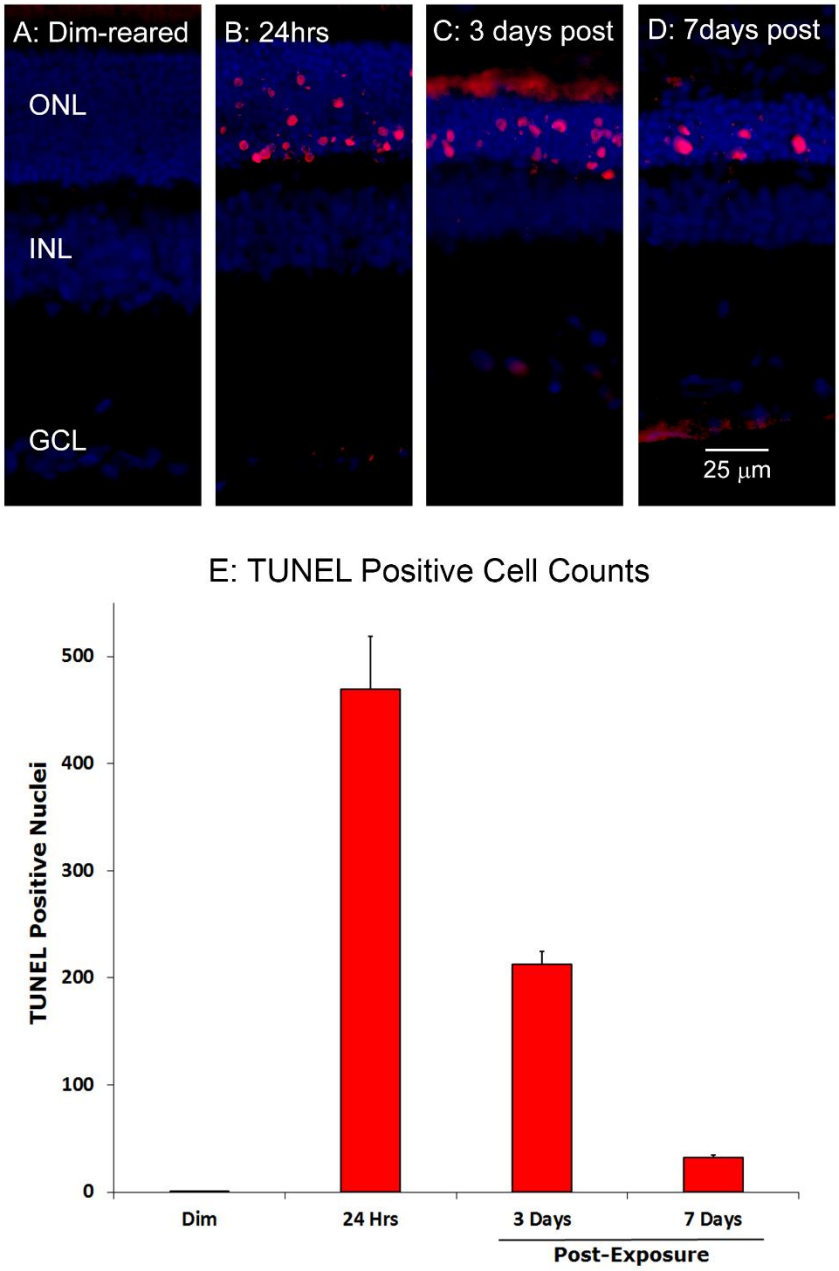

Figure 3. 1 Photoreceptor cell death across protracted LD timecourse

The number of TUNEL positive photoreceptor nuclei in the ONL was used to estimate progression of retinal degeneration at 3 time points. Representative TUNEL staining images are documented in **A-D**, while total number of TUNEL positive cells (across the entire retinas) is quantified in **E**. n=5; error bars represent SEM.

3.3.2 MICRORNA PROFILING

The PCA plot (Figure 3.2) shows that the biological replicates are clustered close together and that majority of variation between the Control and LD groups (50.3%) is due to LD, rather than inherent variability within the groups. The volcano plot (Figure 3.3) shows that a large number of miRNAs were modulated up or down by LD. A list of candidate miRNAs (Table 3.2) was compiled by selecting those with a fold-change ≥ 2 or ≤ -2, and $p<0.05$. A total of 37 miRNAs of the 750 tested showed strong statistical significance and were selected for further analysis. The most highly upregulated miRNA was mmu-miR-467d (66 fold) while mmu-miR-1224_mat was the most downregulated (-16 fold). Of the 37 miRNAs, 26 were upregulated and 11 downregulated; 17 came from the miRNA array card A, which represents the better characterized miRNAs in miRBase v16.0 (www.mirbase.org), while 20 were from the not-so-well-characterized group on array card B.

3.3.3 FUNCTIONAL ANALYSIS OF MIRNAS

Each miRNA targets multiple mRNAs, therefore the list of predicted gene targets is much larger than the list of significantly regulated miRNAs. The list of gene targets (from the ~2000 genes analysed) of the 37 miRNAs were analysed using PARTEK®, to gain insight into their biological relevance by Gene Ontology (GO) enrichment clustering based on 'biological processes'. Through this process we identified the 10 most highly represented gene ontology clusters (Table 3.3). The 'biological processes' with the highest enrichment scores include *positive regulation of cell proliferation* (22.5502), *inflammatory response* (19.9534), *positive regulation of transcription from RNA polymerase II promoter* (19.7899), and *angiogenesis* (19.3955). Table 3.4 shows the 19 miRNAs associated with 'inflammatory response' and identifies the 30 gene targets of those miRNAs. Functional clustering of those genes using the DAVID® Bioinformatics annotation tool 6.7 identifies 7 out of 30 genes clustering into two families of chemokines; the CCL (3,4,7 and 12) and CXCL (1, 10 and 11) families.

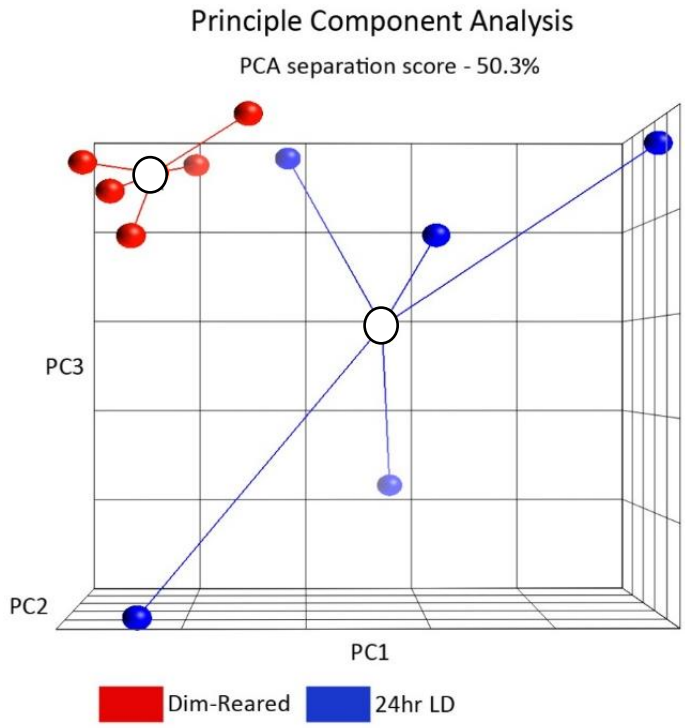

Figure 3. 2 Principle component analysis (PCA) plot

3-D Principle Component Analysis. Each sphere represents a sample and the circle represents the centroid of each distribution. Samples from animals not exposed to LD (red) are more tightly clustered than samples from LD animals (blue), indicating less variability in miRNA expression profiles in control animals compared to animals exposed to LD. The majority of the variance between the 2 different conditions is explained by the PC-1 axis.

Table 3. 2

Candidate microRNAs

miRNA ID	p-value	Fold-Change	F Statistic
mmu-miR-467d	0.00537844	66.934	9.22
mmu-miR-155	0.00502399	55.9242	6.03
mmu-miR-466h	0.0395309	49.8464	2.27
mmu-miR-220	0.0149566	30.91	3.98
mmu-miR-125b-3p	0.0231669	17.3396	2.55
mmu-miR-207	0.00461902	13.4394	5.00
mmu-miR-449a	0.00346565	10.2821	4.97
mmu-miR-467c	0.0121979	9.33694	3.50
mmu-miR-291-5p	0.0149867	7.41014	2.67
mmu-miR-542-3p	0.00820295	7.16889	4.77
mmu-miR-715	0.00948857	6.65874	3.28
rno-miR-347	0.0431166	5.4159	2.71
mmu-miR-494	0.0108949	5.20176	3.94
mmu-miR-351	0.00859523	4.86756	3.45
mmu-miR-1894-3p_mat	0.0145028	4.48047	3.78
mmu-miR-582-3p	0.0339127	4.4609	8.80
hsa-miR-223	0.00343764	4.34528	6.58
mmu-miR-685	0.00584433	4.03733	6.29
mmu-miR-1971_mat	0.000432933	3.9048	8.13
mmu-miR-300	0.0460522	3.78183	3.94
mmu-miR-1195	0.0273212	3.43057	2.89

mmu-miR-2183_mat	0.000281241	3.15076	13.05
mmu-miR-509-3p	0.0192239	2.9015	2.50
mmu-miR-335-3p	0.00999525	2.76217	5.50
hsa-miR-214	0.0291568	2.42738	2.23
mmu-miR-466k_mat	0.0278496	2.2071	3.32
mmu-miR-720	0.0108249	-2.22245	3.07
mmu-miR-376b#	0.00855768	-2.41404	3.27
hsa-miR-124#	0.0217727	-3.01279	2.69
hsa-miR-411#	0.00789667	-3.08945	3.39
mmu-miR-337	0.00319273	-3.23811	4.88
mmu-miR-466d-5p	0.00911546	-3.27501	425.18
rno-miR-743a	0.0272182	-3.56685	2.28
mmu-miR-1939_mat	0.0208102	-5.05438	3.73
mmu-miR-1306_mat	0.012169	-7.46789	2.87
mmu-miR-742	0.00173378	-12.9825	22.07
mmu-miR-1224_mat	0.0184421	-16.0222	19.46

***** **‘–‘** in front of the Fold-Change value indicates a downregulation

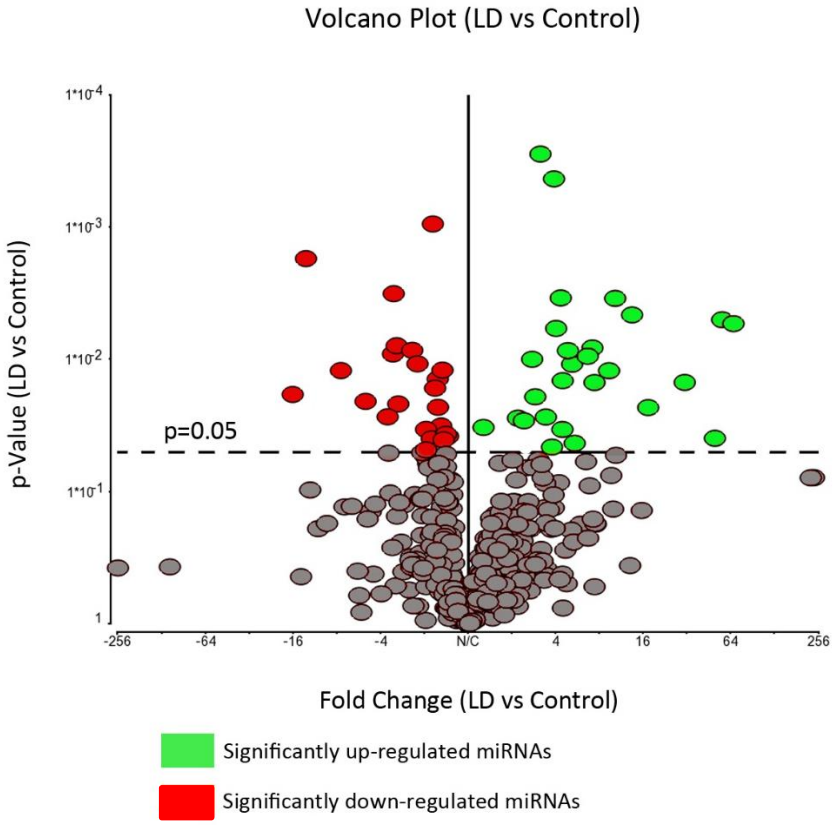

Figure 3. 3 Volcano plot representation of miRNA expression profile

Volcano plot of miRNA expression levels against probability. Only data points lying above the dotted line are significant ($p \leq 0.05$). The solid vertical line indicates zero change in gene expression. Points to the right (green) represent candidates that were up-regulated by LD, while points to the left (red) were down-regulated.

Table 3. 3

Highly represented clusters of biological functions modulated by candidate microRNAs

Biological Process	Enrichment Score	Enrichment p-value	Gene Ontology ID
Positive regulation of cell proliferation	22.5502	1.61E-10	GO: 8284
Inflammatory response	**19.9534**	**2.16E-09**	**GO: 6954**
Positive regulation of transcription from RNA polymerase II promoter	19.7899	2.54E-09	GO: 45944
Angiogenesis	19.3955	3.77E-09	GO: 1525
Negative regulation of cell proliferation	17.4925	2.53E-08	GO: 8285
Cell adhesion	16.9623	4.30E-08	GO: 7155
Cell-cell adhesion	16.9308	4.44E-08	GO: 16337
Negative regulation of transcription, DNA-dependent	16.8136	4.99E-08	GO: 45892
Transcription, DNA-dependent	16.5114	6.75E-08	GO: 6351
Transport	16.0281	1.09E-07	GO: 6810

3.3.4 TEMPORAL EXPRESSION OF INFLAMMATION-ASSOCIATED MIRNAS

Based on the expression signal-to-noise ratio (Critical F value = 2.55), consistency across biological replicates, we selected 8 miRNAs involved in regulating inflammatory responses for validation by qPCR. We tested the expression levels of miR-125-3p, miR-155, miR-207, miR-351, miR-449a, miR-542-3p, miR-467d and rno-miR-347 at three time points - 24hrs light exposure, 3 and 7 days post-exposure (Figure 3.4 A-C). In addition to these, we verified the expression pattern of microRNA cluster miR-183/96/182 at the three timepoints (Figure 3.4D), which has previously been shown to express selectively in photoreceptors, is modulated in rodent models of retinal degenerations and due to environmental light conditions.

Two different expression patterns of the miRNA subset were detected across the time points. Five miRNAs (miR-207, -347, -125b-3p, -155 and -449a) reached peak expression at 3d post exposure (Figure 3.4 B, C); in contrast, two miRNAs, (miR-542-3p and -351) were continuously upregulated over the timecouse (Figure 3.4A). We were unable to generate consistent fold change values for miR-467d across the biological replicates due to very high (end stage) Ct cycle numbers.

MicroRNA cluster miR-183/96/182 exhibited a downward expression trend across the LD time points with all three miRNAs showing significant reduction in expression at the 3 day time point. Only miR-183 and -96 expression reduced significantly at the 24hr mark, while only miR-183 and -182 showed significant reduction at 7 days post LD

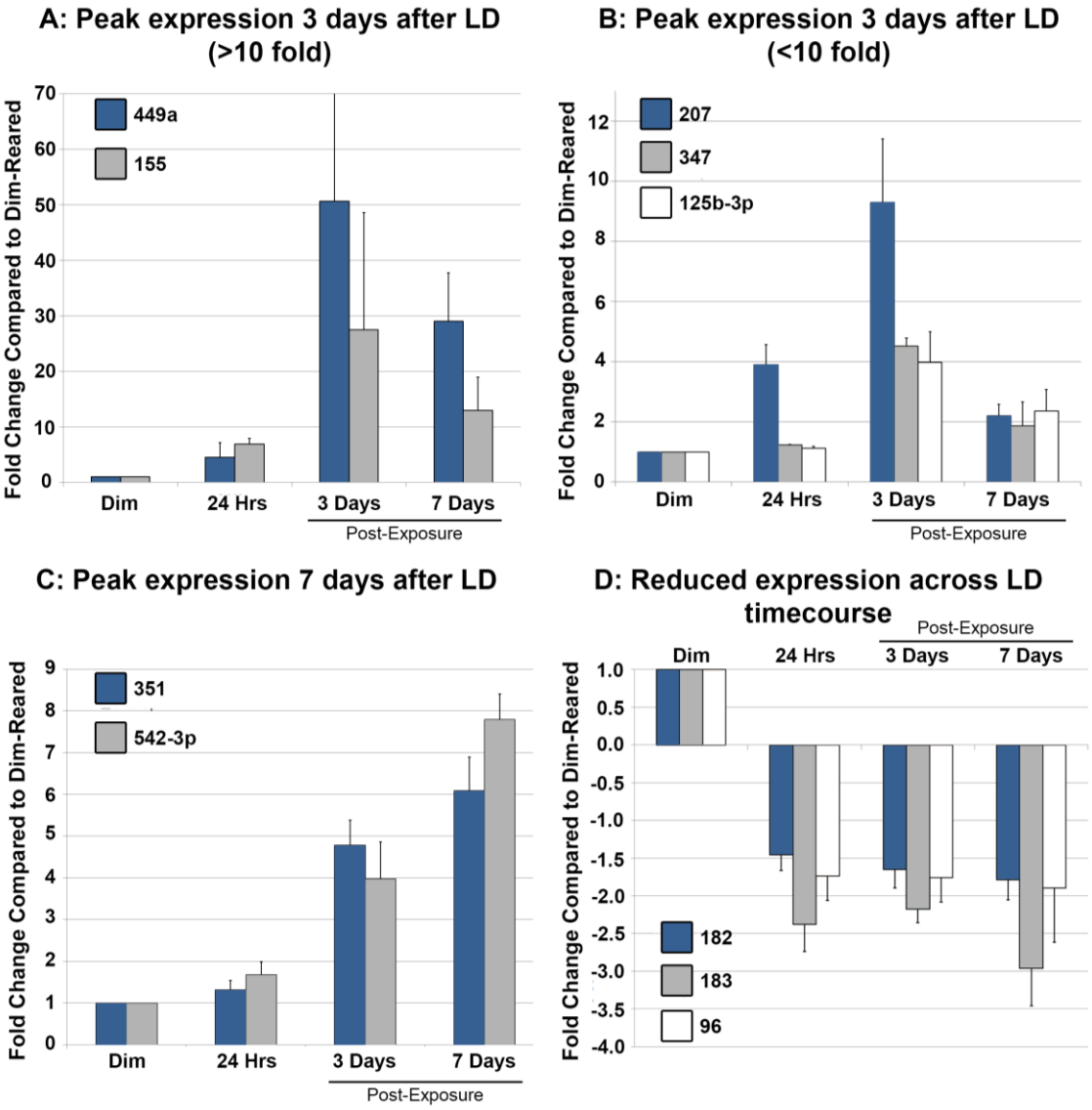

Figure 3. 4 Temporal expression of selected miRNAs

Expression of 10 miRNAs at 24hr, 3 and 7 days post exposure. **A:** miRNAs showing progressive upregulation in the post-exposure period peaking at 7days post exposure. **B&C:** miRNAs showing highest levels of expression at 3 days post exposure. **D:** miRNAs showing downregulation at 24hr and during the post exposure period. The expression trend for all miRNAs was significant based on a one-way ANOVA analysis ($P<0.05$).

Table 3. 4

List of microRNAs and the predicted gene targets implicated in inflammation

miRNA ID	Gene Symbol	Gene Names
mmu-miR-467d	Il20rb	interleukin 20 receptor beta
mmu-miR-467c	Cd14	CD14 antigen
mmu-miR-466h	Myd88	myeloid differentiation factor 88
mmu-miR-466d-5p	Rela	v-rel reticuloendotheliosis viral oncogene homolog A
mmu-miR-125b-3p	Ccl4	chemokine (C-C motif) ligand 4
mmu-miR-155	Chst2	carbohydrate sulfotransferase 2
mmu-miR-207	Il1b	interleukin 1, beta
mmu-miR-351	Tnfrsf1a	tumor necrosis factor receptor superfamily, member 1a
mmu-miR-449a	Il23r	interleukin 23 receptor
mmu-miR-494	Cxcl11	chemokine (C-X-C motif) ligand 11
mmu-miR-509-3p	Gal	galanin prepropeptide
mmu-miR-542-3p	Ccl12	chemokine (C-C motif) ligand 12
mmu-miR-685	Nfkbiz	nuclear factor of kappa light polypeptide gene enhancer in B-cells inhibitor, zeta
rno-miR-347	Ccl7	chemokine (C-C motif) ligand 7
mmu-miR-300	Cxcl10	chemokine (C-X-C motif) ligand 10
mmu-miR-715	Il6	interleukin 6
mmu-miR-720	Tnf	tumor necrosis factor
mmu-miR-220	Ccl3	chemokine (C-C motif) ligand 3
mmu-miR-582-3p	Cxcl1	chemokine (C-X-C motif) ligand 1
	Spn	sialophorin
	Hmox1	heme oxygenase (decycling) 1
	Agt	angiotensinogen
	Jak2	Janus kinase 2
	Sbno2	strawberry notch homolog 2
	Clcf1	cardiotrophin-like cytokine factor 1
	Zfp36	zinc finger protein 36
	Cd276	CD276 antigen
	Ier3	immediate early response 3
	Pla2g4a	phospholipase A2, group IVA
	Alox5ap	arachidonate 5-lipoxygenase activating protein

3.4 DISCUSSION

The results of this study show that miRNAs are modulated in response to LD. Indeed, two of the most highly regulated gene clusters targeted by these miRNAs are 'positive regulation of the transcription from RNA polymerase II promoter' and 'negative regulation of DNA dependent transcription'. This essentially reflects that light damage causes regulation of the retinal transcriptome. The other clusters include genes that regulate cell proliferation, cell adhesion, angiogenesis and our target category, the inflammatory response.

3.4.1 FEATURES OF THE LIGHT DAMAGED RETINA

LD-mediated retinal degeneration has been studied extensively since the landmark study of Noell et al in 1966 [102]. In LD, photoreceptors degenerate in the superiotemporal portion of the rat retina, at the *area centralis*, where there is a peak density of cones, and ganglion cell density is at its highest [268, 269]. In this respect the *area centralis* is homologous to the human macula. Furthermore, the protracted degeneration of photoreceptors and RPE cells triggered by LD in rat retina, and the associated breakdown of the blood retina barrier (BRB) mimic certain histopathological features of dry AMD [105, 109, 113]. Both oxidative damage and inflammation have roles in the pathophysiology of light-induced retinal degeneration.

3.4.2 CELL PROLIFERATION AND ANGIOGENESIS IN LD

A surprising finding of the functional clustering analysis is the high representation of target genes involved in cell proliferation and angiogenesis, since neither of these functions feature prominently in the LD model. There are two possible explanations for this. The first is that, because a single miRNA can regulate translation of multiple genes, the list of 'target genes' introduced into Partek for clustering is not necessarily the actual targets of the miRNAs we have identified. For example, miR-449a is enriched in both 'inflammatory response' and 'angiogenesis' clusters exhibiting putative binding sites for interleukin 23 receptor mRNA,

involved in the immune response, and Angiopoietin-1 receptor mRNA, which facilitates blood vessel formation.

A second possibility is that genes in cell proliferation pathways and/or angiogenic pathways may be upregulated so that the tissues are induced into a 'pro-angiogenesis', or 'pro-proliferation' state, without activating all the genes required for angiogenesis or proliferation to take place. Proliferation of non-neuronal retinal cells (astrocytes, microglia and Müller cells) has been well documented in retinal degenerations including AMD as a response to intense retinal stress [69, 270, 271]. While angiogenesis has not been reported in the LD model previously, it is possible that leukostasis could cause local hypoxia leading to modulation of angiogenic factors, the effects of which might only be detected following much longer survival periods than explored here.

3.4.3 CELL ADHESION AND INFLAMMATION IN LD

Cell adhesion plays a role in a variety of different biological functions, including cell-cell interactions that are part of the immunological response. It is now well established that retinal degeneration that follows LD in this model is mediated by significant inflammatory processes, and the high representation of gene targets in this functional cluster might be expected on this basis. We have previously identified a range of inflammatory genes up-regulated following LD. These include several that encode proteins of the complement system (CFD, C3, C1s, C4b, C5r1) along with several chemokines/cytokines (CCL2, MCP-3, A21a, A6) [97, 119, 120, 272, 273] involved in recruitment of macrophages, monocytes and other leucocytes. Some have also been associated with AMD, including C3, CCL2 and CX3CL1 [94, 274, 275].

3.4.4 EXPRESSION TIMECOURSE OF MIRNAS POST LIGHT EXPOSURE

In this study we find 8 out of 37 miRNAs that are involved in various aspects of regulation of the immune response. Further, our qPCR findings show that 7 out of these are modulated across

the 7 day timecourse of the experiment. MiR-467d showed inconsistent and/or undetectable fold change values across the timecourse potentially due to low target abundance. Hence, its significant upregulation in the miRNA Array analysis could be attributed to a false positive result as a result of the 'Monte Carlo effect' [276].

While all 7 of the 8 selected miRNAs are upregulated post 24hr light damage, in parallel with the TUNEL positive cells in the ONL, only 2 (351 and 542-3p) continue to rise after 3 days post-exposure. Those that reach peak expression at 3d most likely have roles in the acute phase of retinal damage, while 351 and 542-3p are more likely to mediate changes in the retinal environment during the post-acute phase of degeneration in this model. While miR-351 is associated with neuronal and myogenic progenitor cell differentiation [277, 278], and miR-542-3p has been reported to inhibit tumor angiogenesis [279], their roles in retinal remodeling after LD remain to be determined.

The long-term effects of acute bright light exposure are well known [105, 113] and this new data provides insight into genes that may be key players during this phase. The targets of these 2 miRNAs include the chemokines CXCL1 and 10, IL6, TNF, and CD276. CXCL1 and 10 are small molecules belonging to the CXC chemokine family and function as chemoattractants responsible for leukocyte trafficking. While not much is known about their role in AMD or light induced retinal degeneration they have been shown to facilitate the recruitment of lymphocytes to lesion site in atherosclerosis and other inflammatory conditions of the cardiovascular system [280]. Both IL6 and TNF are potent pro-inflammatory cytokines implicated in a wide variety of inflammation-associated disease states. Of these TNF-alpha (one of the most common forms of TNF) has been looked at extensively in AMD and shown to express readily by macrophages present in the choroidal neovascular (CNV) membranes of AMD patients [281]. Additionally, anti-TNF agents are currently being used as a therapeutic strategy for wet AMD [282].

Five miRNA demonstrate peak expression at 3d post-exposure. Of particular interest is the upregulation of miR-155 (increased 55-fold) which facilitates the inflammatory response [283] and targets complement factor H (CFH) [199], a major inhibitor of the alternative complement pathway. The Y402H SNP in the CFH gene is a major risk factor for AMD and multiple variants confer elevated or reduced risk of the disease [2, 3]. MiR-155 binds directly to the 3'-UTR of CFH to facilitate activation of the complement pathway in Alzheimer's Disease [284]. *In vitro,* miR-155 favors the pro-inflammatory (M1) polarisation of immune cells by repressing expression of anti-inflammatory (M2) characteristic proteins [285, 286], and miR-155 deficient mice have a reduced inflammatory macrophages response [267]. Peak expression of miR-155 in this model at 3 days post light-exposure, correlates well with our previous findings showing peak M1 immune cell recruitment at the site of damage at 3d [98].

MiR-207 is upregulated in response to neurotrophins [287], that promote photoreceptor cell survival [288]. Peak expression of mir-207 at 3 days may reflect an attempt by the retina to protect its remaining photoreceptor cell population. In addition, upreguation of miR-207 might sustain the downregulation of one of its predicted targets Carbohydrate (N-Acetylglucosamine-6-O) Sulfotransferase 2 (CHST2), which stimulates the formation of L-selectins on vascular endothelial cell surfaces, to mediate adhesion of lymphocytes around the sites of inflammation [289]. Less is known about MiR-125b-3p, which also had peak expression at 3 days post light exposure, and recently been shown to be a potential biomarker for inflammatory bowel disease [290].

Two other miRNAs reaching peak expression at 3d are miR-347 and miR-449a. Neither has been previously implicated in modulating the inflammatory immune response. MiR-347 promotes neuronal apoptosis [291] and miR-449a is a known tumor suppressor that promotes cell death [292, 293]. Our analysis shows that all 5 miRNAs have putative binding sites in the

3'UTR s of chemokine, cytokine and other inflammatory effector proteins (Table 3.4), indicating that further characterisation of their roles in inflammation is warranted.

It is evident from the above expression profiles that majority of the inflammation related miRNAs show a rapid and sustained increase in expression due to bright light exposure, implying a stricter translational control of their respective targets. However, we know from our previous studies that many cytokines and chemokines (including the ones identified as targets in this study) exhibit increased expression due to bright light exposure [96, 98]. This discrepancy in the expression levels of miRNAs and their target genes could be a facet of the complex regulatory networks, compensatory or otherwise, that are at play inside cells/tissues during ageing, disease and/or damage. Furthermore, there is a growing body of evidence supporting the hypothesis that expression levels of some miRNAs may be directly proportional to the amount of target sites available. A phenomenon known as 'Target Mediated miRNA Protection' (TMMP) [294].

We also analysed the expression pattern of miRNAs of the miR183/96/182 cluster (Figure 4D) which have been shown to occur selectively in the photoreceptor layer. Previous studies have implied the role of this cluster in normal photoreceptor morphogenesis and functioning, maintaining the retinal circadian cycle and playing a protective role in bright light induced retinal degeneration [295, 296]. Unlike Zhu and colleagues who showed an upregulation of these miRNAs due to environmental light conditions (30minute exposure to 10,000 lux light), our model shows a downward expression trend under a more sustained (24hr) exposure of bright (1000 lux) light. This discrepancy could be due to the more chronic degenerative state of the retina in our experimental paradigm inherent in retinal degenerations. Or simply a consequence of the timing differences between the two studies when the miRNA expression was analysed.

While this study gives us a good indication of the different miRNAs that are potentially responsible for modulating retinal inflammation. It is does not give us an exhaustive list of miRNAs being modulated by high intensity light, since the global miRNA screening was conducted only at the 24hr mark. Additionally, since RNA from the whole retina was used for this study, it was not possible to account for the inherent variations between the inferior and superior retina. Which may have contributed to the large variability seen in the 24hr LD data in figure 3.2.

3.4.5 CONCLUSION

In this study we identify 37 miRNA regulated by 24hr LD, including 7 that regulated the inflammatory response, which is a key mediator of retinal degeneration in this model and in AMD. MiRNA are endogenously-occurring molecules that can be safely introduced *in-vivo* without triggering a non-specific immune response. Because these miRNAs regulate multiple genes and pathways simultaneously they provide new potential therapeutic targets with far-reaching biological outcomes suitable for management of complex retinal disorders, like AMD.

CHAPTER 4: MICRORNA-124-3P REGULATION OF A POTENT PRO-INFLAMMATORY CHEMOKINE IN RETINAL DEGENERATIONS

4.1 INTRODUCTION

Recently microRNAs have been shown to be involved in the pathogenesis of AMD [297]. MicroRNAs are a class of small, endogenous, non-coding RNA molecules that are potent negative regulators of gene expression which act by binding to complementary sequences in the 3'UTRs of their messenger RNA (mRNA) targets [131, 132, 135]. Since their discovery just over a decade ago, microRNAs have emerged as critical regulators of gene expression affecting multiple biological processes including development and differentiation, apoptosis and cell proliferation [298]. It has been estimated that miRNAs have the potential to regulate over 60% of protein coding genes in mammals [299]. They have also been identified to have critical roles in a myriad of diseases including various cancers [300], obesity, diabetes, neurological disorders and inflammation [301]. Their therapeutic potential as drug targets is well recognized, with a miRNA-based therapy already in Phase 2 clinical trial (for Hepatitis C) [302].

Activation of the innate immune system and recruitment of inflammatory cells to the retina is a significant factor in progression of AMD [21]. Although the precise mechanisms underlying this targeted recruitment is unclear, a family of chemotactic molecules (chemokines) have been implicated. Recent gene expression studies of AMD donor eyes have shown CCL2 (among other chemokines) to be up-regulated in both the neovascular and atrophic forms of the disease [93]. A light damage model of retinal degeneration, that mimics the inflammatory aspects of 'dry' AMD progression, identified up-regulation of CCL2 [96] by microarray analyses and have shown that silencing CCL2 mRNA using a Ccl2-siRNA attenuates recruitment of inflammatory cells to the site of damage, resulting in reduction of both photoreceptor cell death and RPE atrophy [97]. We reason that because targeted reduction of CCL2 in retinal cells in this model is protective against the progression of retinal degeneration, it may have a similar effect in AMD.

Abundant in the central nervous system, miR-124a was initially believed only to drive neuronal cell differentiation [8]. Recent studies, however, have shown that miR-124 also plays an important role in modulating a number of CNS disorders (reviewed in [303]) including an important role as a driver of the inflammatory immune response in certain cell types [304], including modulation of CCL2 expression [305].

In this study, we demonstrate the modulation of miR-124-3p expression in both light-damaged rat retina (in vivo) and immortalized retinal cell lines. Using *in situ* hybridization we have localized miR-124-3p expression in rat and human retinae to Müller cells, and confirmed *in vitro*, that miR-124-3p directly targets Chemokine (C-C motif) ligand 2 (CCL2) using an immortalized Müller cell line.

4.2 METHODS

4.2.1 ANIMAL HANDLING AND LIGHT DAMAGE

Animals were handled and treated in accordance with the ARVO, ethical use of animal in vision research statement. Sprague Dawley (SD) rats were born and reared in dim cyclic light conditions of approximately 5 lux. The animals were exposed to bright continuous light between post-natal days 100-150 at an intensity of 1000lux for 24hrs starting at 9am. The light source used was white fluorescent light (COLDF2 2 3 36W IHF; Thorn Lighting, Brisbane, Australia) placed overhead with each animal in its own transparent perspex cage to ensure uniform illumination. Rodent food pellets were provided next to the bedding to minimize interference with light exposure and water was provided ad-libitum. After the 24hr light exposure some animals were immediately euthanized by intraperitoneal injection of barbiturate overdose or returned to dim light conditions (5lux). These animals were euthanized 3 or 7 days post return to dim reared conditions. We used age matched dim reared animals as controls.

4.2.2 TISSUE COLLECTION AND PROCESSING

The animals were euthanized by administering an intraperitoneal injection of barbiturate overdose (60mg/kg). The retinas from the right eye of the animals was excises via a corneal incision and stored in cold Trizol solution on ice before proceeding with the RNA extraction. Total RNA, including miRNAs, was extracted using the mirVana miRNA isolation kit (Ambion, Applied Biosystems) and concentration determined with the ND-1000 spectrophotometer (Nanodrop Technologies, Wilmington, DE, USA). The left eye of the animals was enucleated, superior region marked and processed for sectioning. Eyes for cryosectioning were immersed in 4% paraformaldehyde for 3 hours, anterior chamber (including lens) removed and replaced in 4% paraformaldehyde for 24hrs. The eyes were then processed for paraffin coating and embedding before sectioning at 4-6um on the microtome, across the superior-inferior axis. Adult human eyes were obtained through the Lions Sydney Eye Bank. Tissue was processed in accordance with a previously established protocol as described in [44]. Age matched normal and AMD affected human retinal tissue was cryosectioned at 10 μm.

4.2.3 ANALYSIS OF CELL DEATH

TdT-mediated dUTP nick end labelling (TUNEL) labelling technique was used to quantify photoreceptor cell death over the light damage time course, in retinal cryosections using a previously published protocol [96]. TUNEL+ cells were counted in the ONL along the full length of the retinal sections cut the superioinferior plane, including the optic disc, at 1mm intervals across the retinal sections. The final counts for each experimental group is the average of five animals counted at comparable locations. Prism (GraphPad Software V5) was used for statistical analyses by one-way ANOVA and Student's t-test.

4.2.4 MICRORNA QUANTITATIVE REAL-TIME PCR

cDNA was synthesized using TaqMan MicroRNA RT kit (Applied Biosystems) as described previously (Saxena et al 2015). Expression of miR-124-3p was quantified using miRNA specific commercially available TaqMan hydrolysis probes (Applied Biosystems), enlisted in Table 4.1. Fold Change was determined using the ΔΔCt method and expression normalized to endogenous small nuclear U6 RNA. Amplification specificity was assessed using gel electrophoresis and statistical analysis was performed using 1-way ANOVA and Student's t-test.

4.2.5 IN SITU HYBRIDISATION AND IMMUNOHISTOCHEMISTRY

In situ hybridization was performed to localize miRNA expression in the retina using commercially available double DIG labelled miR-124-3p miRCURY LNA probe (Exiqon) and miRCURY LNA™ microRNA FFPE ISH detection kit 4, according to manufacturer's protocol; Paraffin was stripped off the rat retinal sections using xylene washes and rehydrated by washing in a decreasing concentration of ethanol. All retinal sections (Human and Rat) were treated with proteinase K (20µg/ml) for 10 minutes. MiR-124-3p probe was hybridized for 1.5 hours at 53°C and then washed in saline sodium citrate at 58°C. Bound probe was visualized with HNPP/Fast-Red (Roche, Basel, Switzerland), which was followed by counter-staining using immunohistochemistry.

Table 4. 1

TaqMan® probes used

Gene Symbol	Name	Accession #	Catalog #
Ccl2	Chemokine (C-C motif) ligand 2	NM_031530.1	Rn01456716_g1
GAPDH	Glyceraldehyde-3-phosphate dehydrogenase	NM_017008.3	Rn99999916_s1
miR-124-3p	mmu-miR-124a	MIMAT0000422	001182
U6 snRNA	U6 small nuclear RNA	NR_004394	001973

In situ stained sections were incubated with primary antibody overnight at 4°C, raised against Vimentin (1:200; Sigma-Aldrich, St. Louis, MO, USA). Sections were then incubated with secondary antibody, conjugated to Alexa488, raised against mouse IgG's (1:200; Life Technologies, Carlsbad, CA, USA) for 2-4 hrs at room temperature. Slides were then cover slipped with Aqua Poly/Mount (Polysciences, Warrington, PA, USA). Immunoflourescence was viewed using a Zeiss laser scanning microscope, while PASCAL software was used for acquisition.

4.2.6 QUANTITATIVE REAL-TIME PCR

Quantitative PCR was used to measure the expression of CCL2. First-strand cDNA systhesis was performed using Tetro cDNA Synthesis Kit (Bioline, London, UK) according to manufacturer's instruction. A 20-µl reaction mixture, including 500 ng to 1 µg RNA, 200 U Tetro Reverse Transcriptase, 4 µl 5x RT buffer, 500 ng oligo $(dT)_{18}$ primer mix and 10 U RNase Inhibitor. Gene amplification was measured using commercially available TaqMan hydrolysis probes (Table 4.1), in accordance with a previously established qPCR protocol [306]. Fold change was determined using ΔΔCt method where CCL2 expression was normalized to that of reference gene glyceraldehyde-3-phosphate dehydrogenase (GAPDH). Statistical analysis were performed using 1-way ANOVA and Student's t-test.

4.2.7 CELL CULTURE

Cell culture experiments were performed using HeLa cells and low passage (<10) immortalized human Müller cell line (MIO-M1). We also used a low passage 661W photoreceptor cell line, generously provided by Dr. Muayyad Al-Ubaidi (University of Oklahoma), and an immortalized RPE cell line (ARPE19) for this study. Cells were used within 10 passages of authentication and validation from Cell Bank Australia and were further validated using RT-PCR for expression of cell specific markers (SW opsin, M opsin pigments, SV40 for 661W cells; RPE65, RLBP1 for ARPE19 cells; GFAP, Vimentin for MIO-M1 cells). Cells were

cultured in Dulbeco's Modified Eagle's Medium (DMEM; Invitrogen) containing 10% fetal bovine serum, L-glutamine (3 mM), sodium pyruvate (1 mM) and glucose (25 mM) and stored in an incubator at 37°C, 5% CO_2. Human IL-1β protein (Cat#, PHC0811, ThermoFisher) (10ng/ml) was used as a pro-inflammatory stimulus for MIO-M1 and ARPE19 cell lines. While, 661W photoreceptor cells were stimulated by bright light induced damage. The cell culture plate, containing 80-90% confluent cells, was placed under 15,000 lux light for 5 hours while inside an incubator maintained at 37°C and 5% CO_2 to ensure even distribution across the plate. The temperature of the setup was monitored vigilantly using a thermometer placed next to the culture plate.

4.2.8 LUCIFERASE REPORTER ASSAY

Luciferase assay was performed on both HeLa and MIO-M1 cells using a commercially available vector containing the luciferase gene fused to the human CCL2 3'UTR (CCL2 LightSwitch 3'UTR Reporter GoClone; Switchgear Genomics, CA, USA) and pLightSwitch-3'UTR Luciferase assay system (Switchgear Genomics, CA, USA), following the manufacturer's protocol (refer Figure 4.1). HeLa cells were seeded in a 96 well plate (5000 cells per well) and cultured for 24hrs. At ~90% confluence, the cells were transfected with the vector only, co-transfected with the vector plus miR-124-3p mimic (Ambion) or co-transfected with the vector plus negative control miRNA mimic (Ambion) using Viafect (Promega) and/or Lipofectamine RNAiMAX (Invitrogen) for 48hrs. pLightSwitch Luciferase assay system was performed according to manufacturer's protocol and luciferase activity measured by Infinite® 200 plate reader (TECAN, Austria). MIO-M1 cells were seeded in a 96 well plate (3000 cells per well), cultured for 24hrs and transfected with the vector only using viafect (Promega) transfection agent. After 36hrs cells were treated with 10ng/ml IL1ß protein for a duration of 12hrs, following which the luciferase assay was performed and luciferase activity measured. Statistics were performed using Student's t-test.

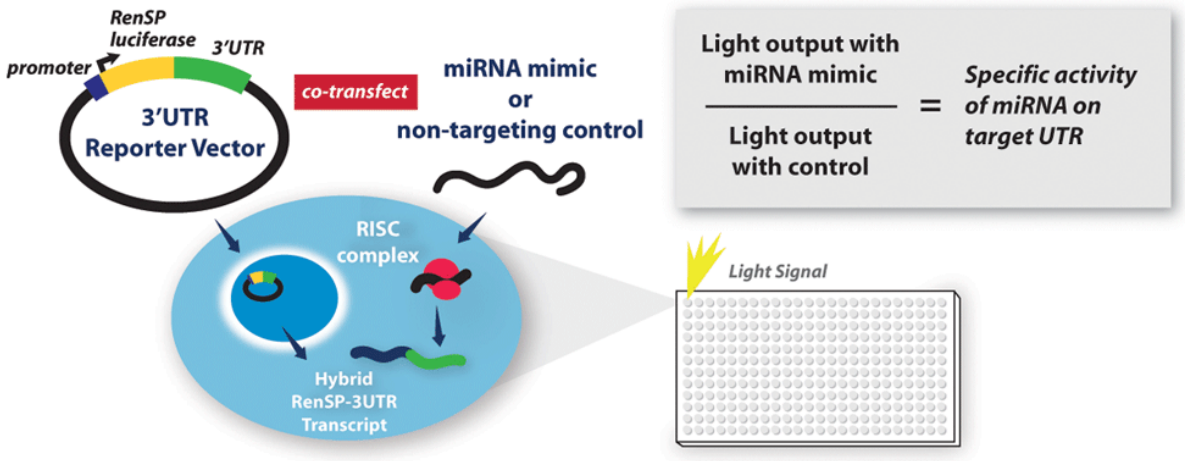

Figure 4. 1 LightSwitch 3'UTR reporter assay

Schematic diagram showing the luciferase assay performed on HeLa and MIO-M1 cells to confirm miR-124-3p and Ccl-3'UTR interaction. A 3'UTR, of a gene of interest, cloned into a LightSwitch 3'UTR reporter vector is co-transfected with miRNA mimics. The relative amount of light (bioluminescence) produced in wells containing candidate miRNA vs control miRNA are used to measure the effect of miRNA-3'UTR interaction on translation of the hybrid RenSP-3'UTR mRNA transcript.

4.2.9 TRANSFECTION OF MIR-124-3P MIMIC AND INHIBITOR INTO MÜLLER CELLS

MIO-M1 cells were seeded in clear plastic 6-well tissue culture plates at a density of 80,000 cells per well and the medium was replaced with low serum (1%) DMEM after sufficient adhering time. Cells were incubated at 37°C in 5% CO2 for 12h and transfected with 10nM miR-124-3p mimic, miR-124-3p inhibitor or negative control miRNA mimic (Ambion), using Lipofectamine RNAiMAX (Invitrogen). After 24hrs cells were exposed to 10ng/ml IL-1b protein for a duration of 12hrs. The cells were then harvested using TRIzol (Invitrogen) reagent and RNA extracted using the RNAqueous-Micro RNA Isolation Kit (Ambion, Applied Biosystems). cDNA was synthesized and qPCR performed using TaqMan hydrolysis probes for CCL2 as described previously. CCL2 expression for the different experimental groups was compared back to that of the non-transfected/treated MIO-M1 cells. Transfection efficiencies in each experimental setup were assessed by co-transfecting a fluorescently tagged negative control oligonucleotide (BLOCK-iT™, Invitrogen) at 10nM concentration.

4.2.10 TRANSFECTION OF MIR-124-3P MIMIC IN VIVO

Both miR-124-3p and negative control miRNA mimic (Ambion) were used for in vivo transfections. Before administration, miRNAs were encapsulated in a cationic lipid based transfection agent (Invivofectamine 2.0, Invitrogen) according to the manufacturer's protocol. Each encapsulated miRNA was formulated to a final concentration of 0.33 µg/µl in 1x PBS solution.

Animals were anaesthetized with an intraperitoneal injection of 30mg ketamine (Troy Laboratories) and 3mg xylazil (Parnell) to perform intravitreal injections. A drop of 1% atropine (Chauvin Pharmaceuticals) was applied to the corneal surface to produce mydriasis, and the injection site (0.5mm posterior to the temporal limbus) was swabbed with 5% povidone iodine (Betadine, Faulding Pharmaceuticals). Intravitreal injections were then performed as described previous by Gao and colleagues [307]. 3µl of either miR-124-3p or negative miRNA

mimic complex was injected into both eyes of each animal, corresponding to 1ug miRNA mimic per eye. As an additional control, 3µl of transfection agent only (processed through the same steps as the miRNA mimic complexes) was injected into both eyes of some animals. Finally, in order to prevent infection at the injection site, 5mg/g neomycin ointment (Amacin, Jurox) was applied after injection. Post injections, all animals were returned to dim (5lux) light conditions for 24hrs prior to initiation of light damage. Transfection efficiencies were assessed by co-transfecting a fluorescently tagged negative control oligonucleotide (BLOCK-iT™, Invitrogen) at 10nM concentration (according to manufacturer's recommendations).

The biological effect of the *in vivo* transfections was assessed by analysing IBA 1 immunoreactivity of the different retinal sections, following immunohistochemistry protocol mentioned in section 4.2.5. IBA 1 or ionizing calcium binding adaptor molecule 1 is a novel protein specifically expressed in microglia and macrophages and is used extensively as a marker for these cells in various tissue types including the retina. Hence immunoreactivity for IBA 1 can identify microglia or macrophages in both their resting and activated forms.

4.3 RESULTS

4.3.1 TIME COURSE OF PHOTORECEPTOR CELL DEATH AND MIR-124-3P EXPRESSION IN VIVO

Following light damage, TUNEL+ nuclei were identified in the ONL/photoreceptor layer, and were more numerous in the superior retina. The average number of TUNEL+ photoreceptor cells reached a peak at 24 hours of bright light exposure ($P < 0.001$, student's t-test) consistent with our previous reports. During the post-exposure period, the number of TUNEL+ nuclei was reduced to ~40% of peak levels at 3 days and to ~33% after 7 days ($P < 0.01$, student's t-test).

We assessed the modulation of miR-124-3p expression across this timecourse, using qPCR (Figure 4.2). Exposure to damaging light led to significant reduction of miR-124-3p expression in the retina, relative to levels of expression in dim-reared animals ($P<0.05$; one-way ANOVA; Figure 4.2). At 24 hours exposure we detected a 287% decrease ($P<0.01$) in miR-124-3p expression compared to the dim-reared animals. This downregulation of expression did not change appreciably at 3 and 7 days post exposure (Figure 4.1B).

4.3.2 LOCALISATION OF MIR-124-3P EXPRESSION IN THE RAT RETINA

Localisation of miR-124-3p in the retina was analysed by *in situ* hybridisation in retinas from dim-reared and light damaged animals (Figure 4.3). In dim-reared retinas mature mir-124-3p was observed in a dense band at the outer extremity of the ONL, suggestive of the External Limiting Membrane (ELM) (Figure 4.3A; arrowheads). In light damaged retinas we detected increased expression of miR-124-3p expression in the INL, with staining visible in cells and radial processes (Figure 4.3B; Arrow heads). Fluorescent markers showed that mature miR-124-3p co-localized with vimentin-immunoreactive Müller cell end feet and processes (Figure 4.3C-D; Arrows) in dim-reared and in light damaged retinas, suggesting that miR-124-3p is expressed by Müller cells.

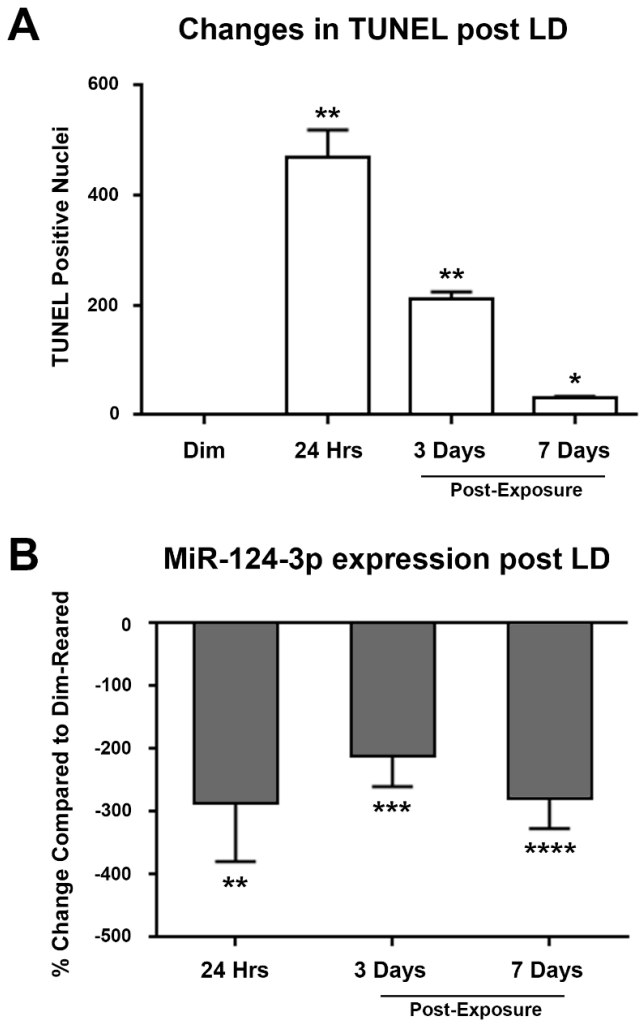

Figure 4. 2 Photoreceptor cell death vs miR-124-3p expression

Quantification of apoptotic photoreceptors and miR-124-3p expression across LD timecourse. Photoreceptor cell death reached a peak of 470 by 24hrs of exposure ($P<0.001$), followed by significant decrease during the post exposure period ($P<0.01$). MiR-124-3p expression showed a significant dowregulation due to light damage (-287%; $P<0.01$). This decrease in expression was sustained up to 7 days post exposure (-277%; $P<0.0001$). TUNEL n=5; miR-124-3p expression n=11; error bars represent SEM. '*' denotes significance based on Student's t-test with $P<0.05$, '**' $P<0.01$, '***' $P<0.001$ and '****' $P<0.0001$.

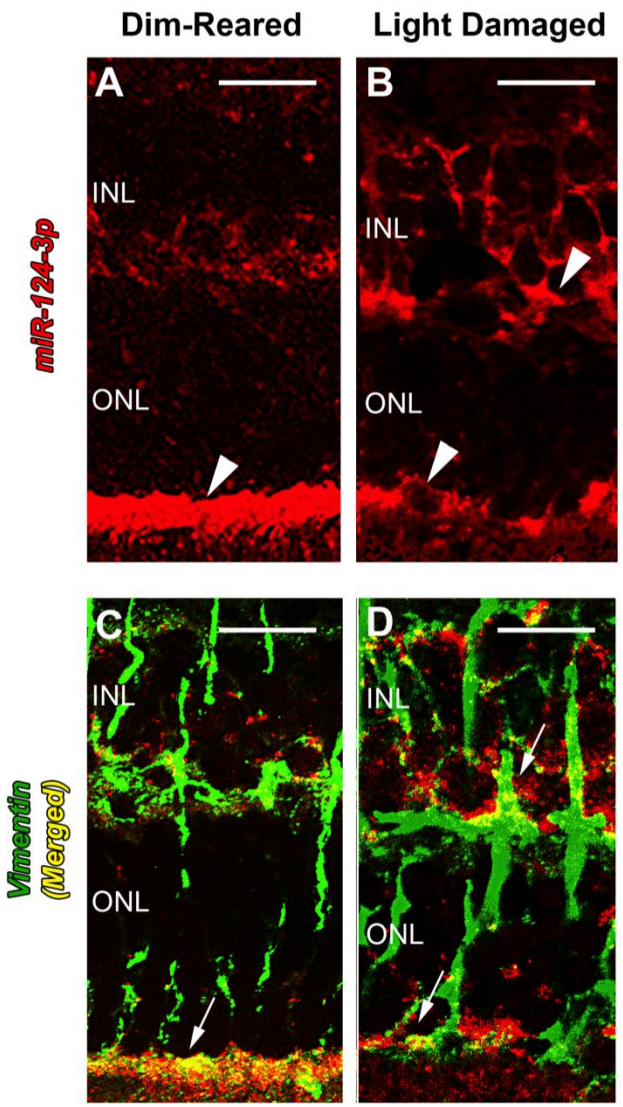

Figure 4. 3 MiR-124-3p *in situ* hybridisation in rat retina

In situ hybridisation for miR-124-3p expression in the light damaged rat retina. **A-D:** Representative images show In situ hybridisation for miR-124-3p (Red) and Müller cells (Vimentin, Green). In dim-reared retinas, expression of miR-124-3p was observed as a strong band at the junction of ONL and photoreceptor inner/outer segments (**A** and **C**; Arrowheads/Arrows). After LD the expression was observed more inwards in radial processes present in the INL (**B** and**D**; Arrowheads/Arrows). The expression in both dim-reared and LD retinas was closely associated with Müller glia labelled with Vimentin (**C** and **D**). INL, inner nuclear layer; ONL, outer nuclear layer; Scale bar (**A-D**) represents 25µm.

4.3.3 EFFECT OF IL1ß ON MIR-124-3P AND CCL2 EXPRESSION IN-VITRO

Using qPCR, we tested three cell lines (MIO-M1, ARPE19 and 661W) for expression of miR-124-3p. Only MIO-M1 cells (Müller cell line) showed significant modulation ($P<0.05$) of miR-124-3p after stimulation with pro-inflammatory IL1β (Figure 4.4A). The effect of prolonged pro-inflammatory stimulation on both miR-124-3p and CCL2 expression indicates that IL1β results a significant downregulation of miR-124-3p ($P<0.05$) expression, and simultaneous upregulation of CCL2 ($P<0.05$) across the exposure timecourse (Figure 4.4B). For the sake of consistency all further experiments utilised 12hours exposure duration.

4.3.4 MIR-124-3P INHIBITS CCL2 THROUGH DIRECT 3'UTR BINDING

To validate a functional interaction between miR-124-3p and CCL2 mRNA in our system, we used a vector containing luciferase gene fused to the human CCL2 3'UTR sequence. When HeLa cells were co-transfected with miR-124-3p mimic the luciferase reporter signal was significantly reduced (by ~50%, $P<0.001$) of levels obtained by co-transfection with scrambled miR (negative control), indicating binding of the miRNA mimic to the vector (Figure 4.5A).

Transfection of the luciferase-CCL2 3'UTR vector into MIO-M1 cells established baseline reporter signal levels (untreated, Figure 4.5B). After challenge with 10ng/ml IL1β protein the luciferase reporter signal in MIO-M1 cells increased by 50-60% above baseline (Figure 4.5B, $P<0.01$) indicating decreased binding of the mimic to the target sequence.

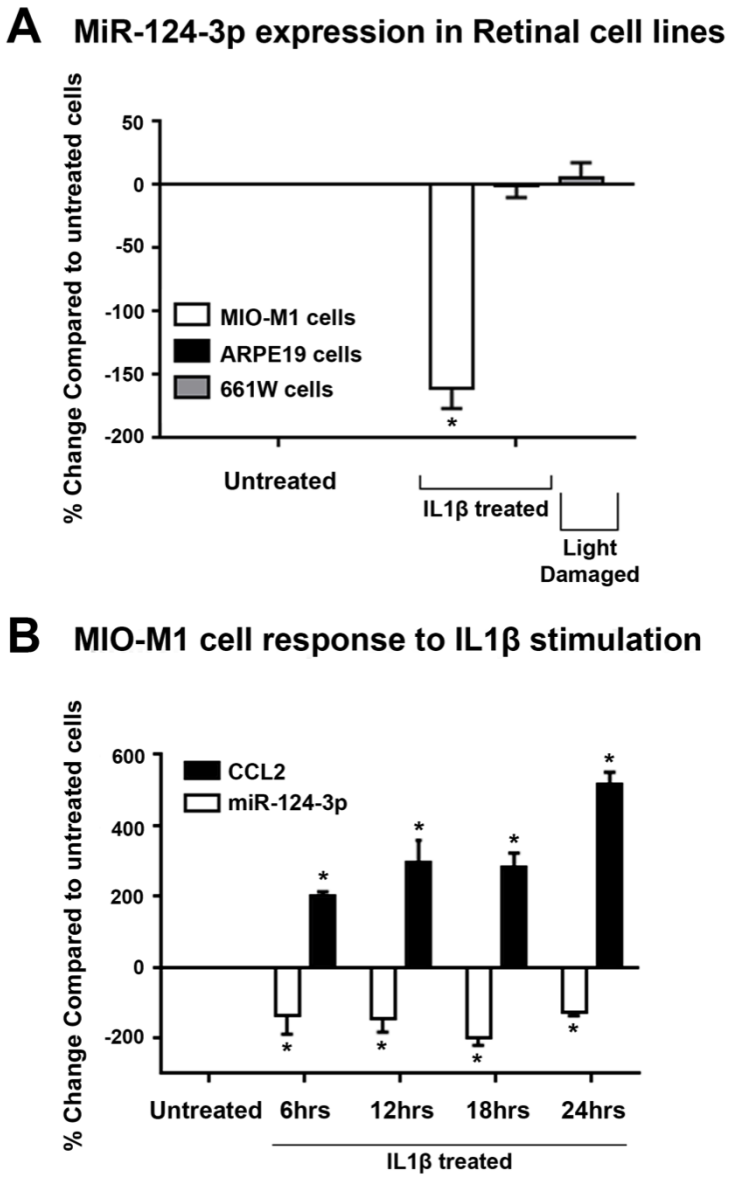

Figure 4. 4 MiR-124-3p and CCL2 expression in retinal cell lines

Expression of miR-124-3p and CCL2 by different retinal cell types under inflammatory or damaging stress in vitro. **A:** MiR-124-3p expression did not change appreciably in ARPE19 cells stimulated with IL1β nor 661W cells damaged by high intensity light, while a significant downregulation was observed in MIO-M1 cells stimulated with IL1β (one-way ANOVA; $P<0.05$). **B:** The expression of CCL2 elevates significantly in MIO-M1 cells stimulated with IL1β across the exposure duration, while miR-124-3p shows significant downregulation simultaneously (one-way ANOVA; $P<0.05$). MIO-M1, 661W, ARPE19 cells n=9 (A); MIO-M1 cells (B) n=8; error bars represent SEM. '*' denotes significance based on Student's t-test with $P<0.05$.

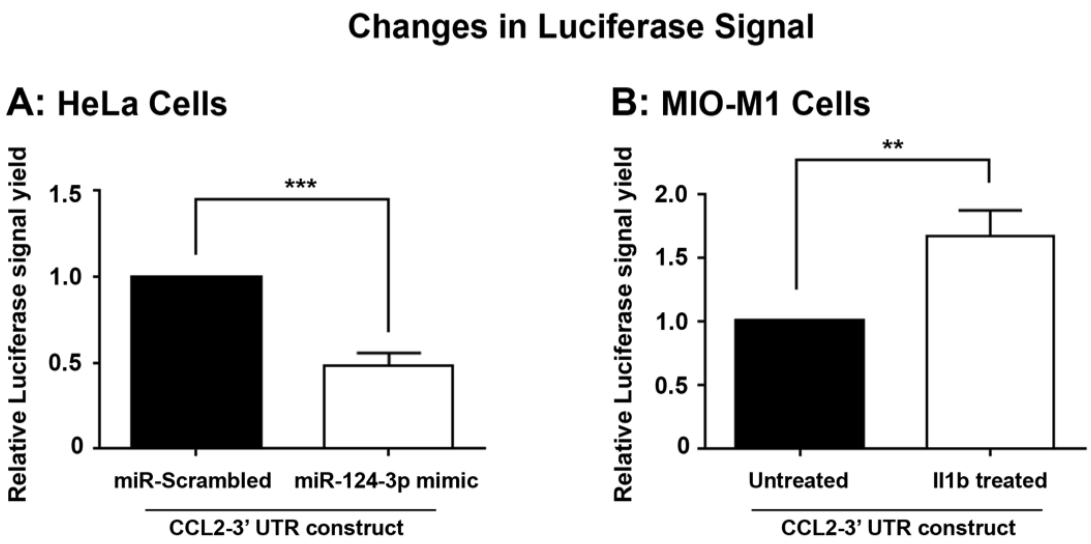

Figure 4. 5 Luciferase assay to confirm miR-124-3p/CCL2 interaction

Luciferase assay to validate miR-124-3p and CCL2 interaction in HeLa cells (A) and MIO-M1 cells (B). **A:** Co-transfection of HeLa cells using a vector containing the human CCL2-3'UTR, fused to luciferase gene, with a miR-124-3p mimic induced a significant reduction in luciferase activity compared to cell co-transfected using the vector with negative control miRNA mimic ($P<0.001$; n=8). **B:** MIO-M1 cells transfected with the CCL2-3'UTR-Luciferase vector show a significant increase in luciferase activity after IL1β protein challenge ($P<0.01$; n=9). Error bars indicate SEM. Significance based on student's t-test.

4.3.5 OVEREXPRESSION OF MIR-124-3P IN MIO-M1 CELLS DOWN-REGULATES INFLAMMATORY CHEMOKINE (CCL2) IN VITRO

To assess the efficiency, specificity and biological impact of the miR-124-3p mimic, we transfected MIO-M1 cells *in vitro* with biomimetic miR-124-3p, a specific inhibitor, or negative control miRNA, then challenged cells with IL1β. Figure 4.6 shows that non-transfected MIO-M1 cells showed an increase in CCL2 expression of ~390% ($P<0.01$) after challenge with IL1β. However, MIO-M1 cells transfected with miR-124-3p mimic showed virtually no change in CCL2 expression, compared to controls. MIO-M1 cells challenged with IL1β, but transfected with miR-124-3p inhibitor or negative control miRNA, showed no significant change in CCL2 expression compared to non-transfected controls.

4.3.6 IN SITU LOCALISATION OF MIR-124-3P

To test the relevance of these experiments to potential modulation of CCL2 expression in the human retina we used *in situ* hybridization for miR-124-3p in human retinal sections from a normal *post mortem* donor, and one with AMD. We detected expression of miR-124-3p in the normal retina in cells in the INL, in radial processes, and at the junction of the ONL and photoreceptor inner segments (Figure 4.7A, arrowheads). This expression pattern is very similar to that seen in the rat retina (Figure 4.3) and is suggestive of miR-124-3p expression in Müller cells. We detected little to no miR-124-3p expression in the foveal region of the AMD affected tissue (Figure 4.6B), consistent with the qPCR data shown in Figure 4.2.

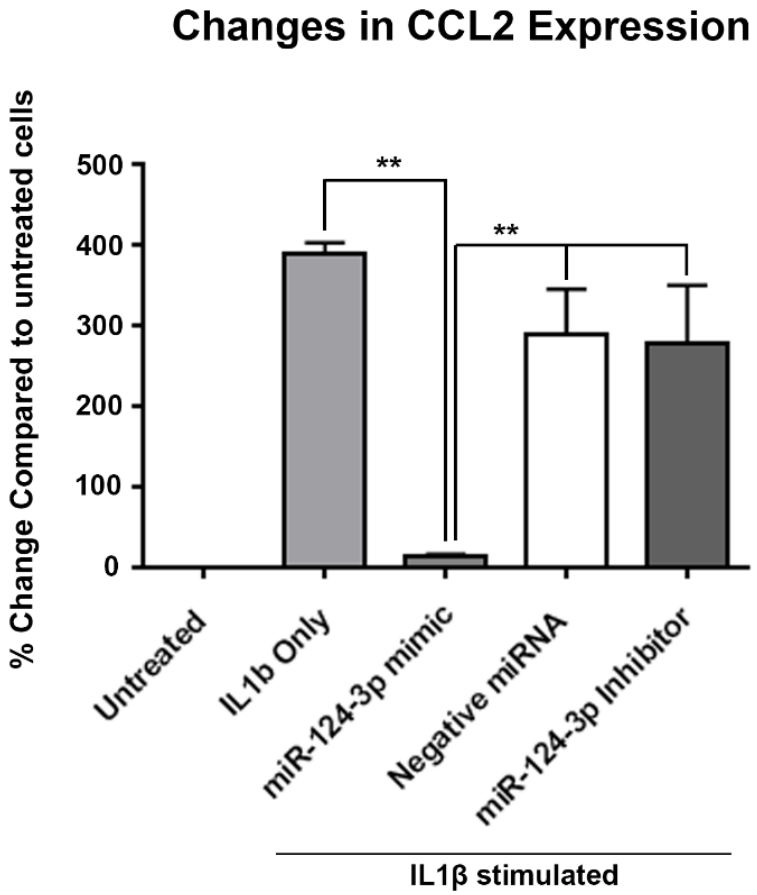

Figure 4. 6 Effect of miR-124-3p knockin on CCL2 expression *in vitro*

Effect of miR-124-3p mimic and inhibitor on CCL2 expression in MIO-M1 cells *in vitro*. The upregulation of CCL2 expression in IL1β stimulated MIO-M1 cells was significantly reduced down to basal expression level by miR-124-3p mimic transfection ($P<0.01$). While, negative control miRNA mimic and miR-124-3p inhibitor transfection had no appreciable effect on the CCL2 upregulation. n=9; error bars represent SEM. 'Untreated' refers to MIO-M1 cells without any transfections or IL1β exposure. Significance based on *Student's t-test*.

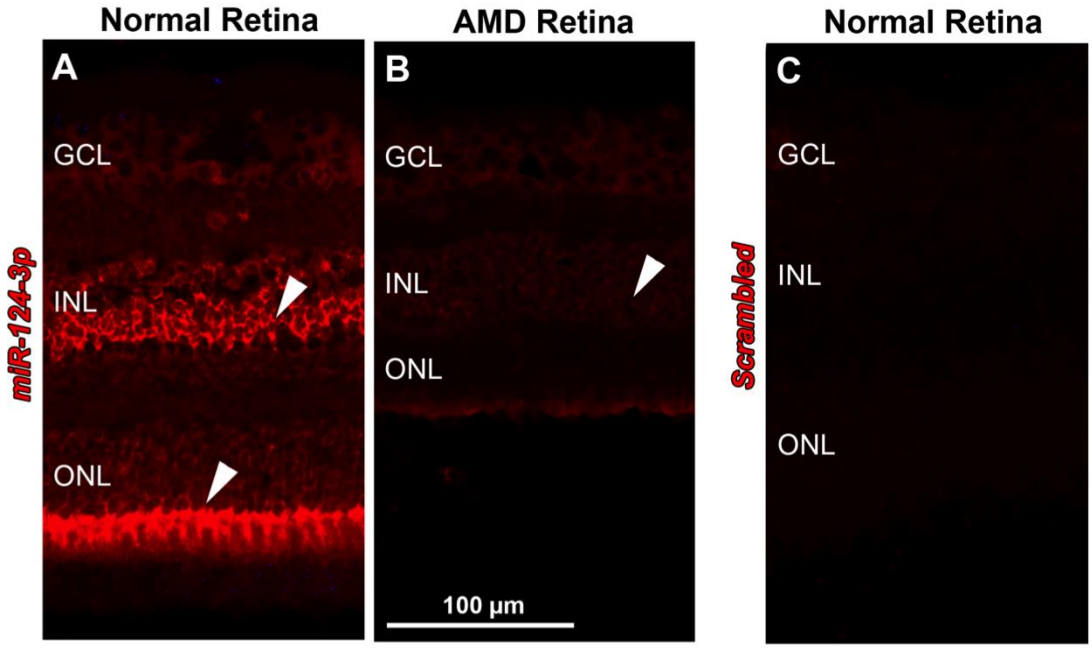

Figure 4. 7 MiR-124-3p in situ hybridisation in human retina

In situ hybridisation for miR-124-3p expression in normal and AMD affected human retina. Representative images demonstrate in situ hybridisation for miR-124-3p at the parafoveal region of normal (A) and AMD affected (B) human retinas. **A:** An abundance of miR-124-3p expression is evident in the normal retinal tissue at the outer edge of the ONL as well as in radial processes distributed across the INL (Arrowheads). **B:** In contrast, much less staining for miR-124-3p expression (Red) was observed in the AMD affected retina. **C:** The negative control miRNA *In situ* probe (Scrambled) was not detectable in the retinal tissue sections. (n=3)

4.3.7 FUNCTIONAL ANALYSIS OF MIR-124-3P OVEREXPRESSION IN VIVO

To investigate the biological impact of miR-124-3p in modulating retinal inflammation in the rat retina, we attempted its overexpression by *in vivo* transfection of synthetic miR-124-3p mimics using intravitreal injections (Figure 4.8). Followed by assessment of IBA1 reactivity in the different experimental rat retinas. We saw a significant difference in the distribution of IBA1 positive cells in the retina between miRNA + Invivofectamine 2.0 or Invivofectamine 2.0 only injected and dim-reared or light damaged only groups. While dim-reared retinas show a uniform distribution of ramified (resting) cells and light damaged retinas show preferential localization in the ONL and OPL layers at the superior region. Light damaged retinas from animals injected with either Invivofectamine 2.0 only or Negative control miRNA mimic or miR-124-3p mimic showed specific localisation of amoeboid (activated) cells at the inner edge throughout the retina.

4.4 DISCUSSION

This study demonstrates a role of miR-124-3p in modulating CCL2 expression in the retina, including its role in the inflammatory response in retinal degeneration. The findings show that miR-124-3p expression is inversely correlated to photoreceptor cell death in the degenerating rat retina, that its expression is predominantly localized to the Müller glia, and that it has a specific function in modulating expression of the chemokine CCL2. We have confirmed the interaction of miR-124-3p and CCL2 mRNA using luciferase reporter assays and used *in vitro* approaches to demonstrate specific suppression of pro-inflammatory CCL2 by miR-124-3p. We also show using *in situ* hybridization that miR-124-3p has a similar expression profile in both human and rat retinas in a pattern that is consistent with Müller cell distribution, and that in the rat retina miR-124-3p undergoes a redistribution from labelling predominantly in the external limiting membrane to the INL.

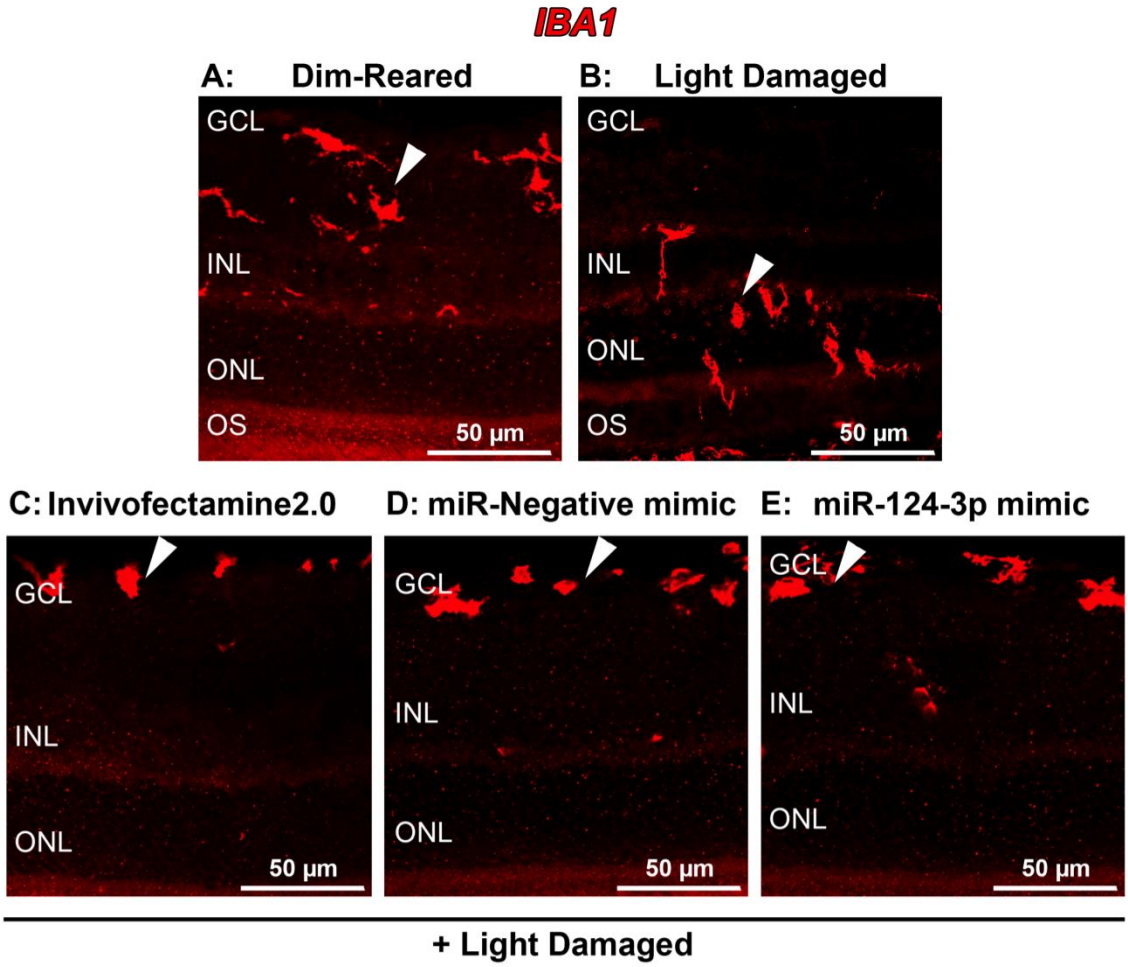

Figure 4. 8 Effect of *in vivo* transfection of miR-124-3p mimic in rat retina

Immunoreactivity for IBA1 (red) in the retina following *in vivo* transfections using Invivofectamine 2.0. Representative images of the superior mid-periphery demonstrate IBA1 positive cell distribution. **A:** Normal distribution of IBA1+ cells localised in the inner retina. **B:** IBA1+ cells are present in the ONL and OS regions after light induced damage. **C-E:** Retinas injected with Invivofectamine2.0® (with or without miR-Negative mimic/miR-124-3p mimic) prior to light damage show a presence of activated IBA1+ cells at the inner edge of the retina (Arrowheads).

MicroRNAs are universal regulators of protein expression that have multiple targets and are expressed in a tissue/cell specific manner at different stages of development and disease [164, 308, 309]. Hence modulation in expression of a single miRNA can contribute significantly to pathology. The miRNA of interest in this study, miR-124-3p, is highly expressed in the CNS and is recognized as a critical regulator of neuronal development and differentiation [310, 311], but is also known to be downregulated in a range of CNS disorders (reviewed in [303]). In an animal model of multiple sclerosis, miR-124-3p is highly expressed in quiescent resident microglia but is reduced in activated cells with the M1/pro-inflammatory phenotype during inflammation [312]. The authors also report that increased miR-124-3p promotes and maintains the M2/anti-inflammatory state of microglia and macrophages by regulating the CEBPα/PU.1 pathway.

Expression of miR-124-3p in the retina has been documented previously using RT-PCR in rodent and human retinas [310, 313-315]. However, no previous studies have looked at changes in miR-124 expression levels during retinal inflammation and degeneration. Here, we demonstrate that this decrease in miR-124 expression due to LD coincides with a dramatic increase in photoreceptor cell death. Previously we have shown that light-induced retinal damage is associated with an increase in CCL2 expression in Müller glial cells [98], and that CCL2 expression is associated with recruitment of complement-bearing macrophages into the retina, and with photoreceptor death. In this study our gene expression analysis shows that miR-124 expression *decreases* as a result of light-induced retinal degeneration consistent with the role of miR-124 reported in other neurodegenerative disorders (reviewed in [303]). Significantly, we also demonstrate that miR-124-3p modulates retinal inflammation specifically by targeting CCL2, which is responsible for recruitment of inflammatory immune cells to the site of photoreceptor degeneration. The inverse relationship between miR-124 expression and CCL2 is consistent with previous findings in rheumatoid arthritis [305, 316].

Our findings also suggest that miR-124-3p may have a number of other targets in the inflamed and degenerating retina, since we find decreased expression as late as 7d post exposure, when CCL2 levels are significantly reduced, and levels of photoreceptor death have dropped significantly [98, 105]. Other targets for miR-124-3p mediated regulation in retinal degeneration therefore, remain to be identified.

4.4.1 MIR-124-3P LOCALIZATION TO RETINAL MÜLLER CELLS

Previous work by Deo, Karali and colleagues [310, 314] showed that miR-124 is expressed throughout adult mouse retina with strong staining observed in the INL, but were unable to identify the specific cell type responsible for its expression. We used immunolabeling combined with *in situ* hybridization to show preferential distribution of mature miR-124-3p in vimentin-positive Müller glial cells. We find that in normal (unstressed) retina, mature miR-124-3p is highly expressed in the outer end-feet of Muller cells, in the region of the ELM where the Müller cell end feet are found, and at lower levels in the Müller cell bodies in the INL and in their radial processes. After light exposure miR-124-3p is redistributed so that higher levels of expression are present in the Müller cell bodies in the INL, but lower levels are present in the outer retina. This post-exposure localization of miR-124-3p in the Müller cell somata is consistent with the localization of the target CCL2 mRNA. We find a similar pattern of expression of miR-124-3p in normal human retinal sections with reduced expression in the degenerated regions of the retina, consistent with a recent gene expression study reporting upregulation of CCL2 in both wet and dry forms of AMD [93].

Our *in vitro* experiments confirm the significance of Müller cells in expression of miR-124-3p. We find in cell lines that MIO-M1 (Müller cells) show significant downregulation of miR-124-3p after IL1β challenge, while there was no change in expression detected in either ARPE19 cells or the 661W photoreceptor cell lines following an appropriate challenge (IL1β and light damage, respectively). IL1β is a potent pro-inflammatory cytokine that induces expression of

both α and β chemokines *in vitro* [317], in arthritis [318] and LPS-induced endotoxemia [319] and is significantly upregulated in our light induced model of retinal degeneration, where it plays broad modulatory roles in chemokine secretion [320]. Photoreceptors, including immortalized 661W cells, do not respond to IL1β but are induced into apoptosis following exposure to bright light; for this reason we chose this as the challenging stimulus in these experiments. As well as showing a significant down-regulation of miR-124-3p after IL1β challenge, we found a concomitant upregulation of CCL2 expression in the MIO-M1 cell line, consistent with our findings *in vivo* [97, 98].

4.4.2 FUNCTIONAL ANALYSES OF MIR-124-3P IN VITRO

Luciferase assays using MIO-M1 and HeLa cells demonstrate a functional relationship between downregulation of miR-124-3p expression and upregulation of CCL2 expression, first by showing a reduction in the luciferase signal in HeLa cells due to co-transfection of the CCL2-3'UTR fused vector along with synthetic miR-124-3p compared with a scrambled miRNA mimic, consistent with a previous report of binding between miR-124 and CCL2 mRNA in E11 cell line [316].

And secondly, by showing an increase in luciferase activity in IL1β stimulated MIO-M1 cells pre-transfected with the CCL2-3'UTR fused vector. As MIO-M1 cells express miR-124-3p endogenously, its downregulation in the presence of IL1β stimulation (as shown in figure 4.3A) would result in reduced translational repression of its target 3'UTR containing mRNAs. Thereby leading to increased translation of the vector derived luciferase gene and hence greater bioluminescent signal.

Third and most importantly, our experiments show that transfection of cells with miR-124-3p mimics prior to IL1β challenge effectively inhibits a subsequent significant increase in CCL2 expression *in vitro* (Figure 4.6).

Our previous work *in vivo* indicates that CCL2 is not expressed in the retina under normal conditions. It is only after photoreceptor cell death that CCL2 expression is upregulated in Müller cells [98] leading to localized recruitment of microglia/monocytes [70, 84, 86]. Because these recruited cells are complement-bearing and also express chemokines (including CCL2), they are part of a process that upregulates the inflammatory cascade. Targeted knockdown of CCL2 with siRNA reduces recruitment and photoreceptor death [97]. In these experiments we attempted to regulate CCL2 expression using a miRNA mimic, but without success due to issues of the transfection agent, which alone promoted an inflammatory response in the retina. Further *in vivo* studies are in progress using a new transfection agent provided by the manufacturer, but which could not be completed within the period of candidature.

Collectively, these experiments indicate that modulation of miR-124-3p has the capacity to control the inflammatory environment of the retina, by modulating expression of CCL2. While CCL2 is not the only chemokine expressed in the degenerating retina [320], our data indicates that CCL2 is a non-redundant factor in retinal inflammation. These findings suggest that miR-124-3p will prove to be a novel therapeutic target in inflammatory disorders of the retina including AMD [78], diabetic retinopathy [79, 80] and glaucoma [81, 82].

CHAPTER 5: EFFECT OF 670NM LIGHT TREATMENT ON EXPRESSION OF INFLAMMATORY REGULATORS AND MIRNA IN THE LIGHT DAMAGED RAT RETINA

5.1 INTRODUCTION

The beneficial effects of light exposure in the red to near infrared (NIR) spectrum have been documented in a number of diseases/maladies over the past few decades [227, 321-325]. Recently, NIR therapies have been useful in treating a number of cardiovascular [326], musculoskeletal [218, 219] and central nervous system (CNS) conditions [220, 221], with studies in animal models showing positive effects in inflammation, neurodegeneration and soft tissue damage [225, 229, 237, 239, 327, 328]. It has been reported that red to NIR light is protective in retinal pathologies with several studies using animal models showing its ability to attenuate light induced retinal degeneration [96, 118, 234, 235], retinal lesion development in diabetic retinopathy [232], methanol toxicity [231] and degeneration during ageing [239]. Investigations using the light induced model of retinal degeneration have shown that 670nm light treatment significantly reduces photoreceptor damage, preserves retinal function, suppresses expression of inflammatory markers and ameliorates oxidative stress in light damaged retinas [118, 233, 234, 236]. However, none of these have looked at the early effects of 670nm light treatment on the retinal transcriptome, which might be key in understanding the molecular mechanisms underlying its anti-inflammatory properties. Although, the exact underlying mechanism of this protective effect is unknown, current evidence suggests the involvement of cytochrome c oxidase (the primary photo-acceptor of 670nm light wavelength) and its downstream effects on mitochondrial membrane potential, cellular ATP production, cell signaling, and transcription [224, 239, 329-333].

Members of our group have shown in the light-induced model of retinal degeneration that 670nm is also able to modulate the noncoding RNA population, which in turn can act as potent regulators of gene expression. Additionally, we have recently shown in our light-induced model that there is significant modulation of microRNAs (a type of endogenous small

noncoding RNA molecule) in the retina. Indicating that these molecules might be able to modulate the inflammatory response during retinal degenerations [306].

Due to the multifactorial and multigenic nature of the disease the pathophysiology of AMD remains to be clearly understood. However, extensive evidence over the years strongly supports the involvement of chronic inflammation in the pathogenesis of AMD, and several studies have documented the upregulation of inflammatory regulators including complement components, cytokines and chemokines in AMD patients [93, 334-338].

In this study we used the light-induced model of retinal degeneration to investigate the early effects of 670nm light irradiation on the inflammatory transcriptome of the retina, both coding and noncoding, to understand the potential molecular interactions at play. We also investigated the histology of the light damaged rat retina to identify any early structural changes occurring due to 670nm light.

5.2 METHODS

All methods are as mentioned in Chapter 2 of this thesis. Additional methods are as follows.

5.2.1 ANIMALS, LIGHT DAMAGE AND 670NM TREATMENT

All procedures conducted were in accordance with the ARVO Statement for the Use of Animals in Ophthalmic and Vision Research. Adult Sprague-Dawley (SD) rats were born and raised in dim cyclic light conditions (5lux; 12hr on, 12hr off).

Before exposure to bright damaging light for 24hrs, some animals were pre-treated with 670nm light using a WARP75 670nm LED array (QBMI Photomedicine, WI, USA) and some sham treated. Animals in the treatment groups were exposed to 9J/cm2 (3 minutes) of 670nm light daily for 5 consecutive days, according to the protocol detailed in chapter 2. Age matched dim

reared animals, either treated or sham treated with 670nm light were used as controls. Animals were culled after their respective treatment/light exposure conditions and retinal tissue obtained for further analyses. In the case of 670nm light treated only group animals were culled straight after the last 670 nm light treatment on the 5th consecutive day.

5.2.2 TISSUE COLLECTION AND PROCESSING

Animals were culled with an overdose of barbiturate injected intraperitoneally at 60mg/kg bodyweight. The left eyes of each animal were marked at the superior aspect and enucleated to be processed for cryosectioning, the retinas from the right eyes were extracted through a corneal incision and used for RNA extraction. Eyes for cryosectioning were immediately fixed in 4% paraformaldehyde for 3 hrs at room temperature and then processed as previously described [105], followed by cryosectioning at 16 µm. Retinas from the right eyes were immediately placed in RNAlater solution (Ambion), and stored according to manufacturer's protocol. Total RNA was extracted from each sample and the concentrations determined using ND-1000 spectrophotometer (NAnodrop Technologies, Wilmington, USA).

5.2.3 CELL DEATH ANALYSIS

Cell death was assessed using the TUNEL technique on retinal cryosections using a previously published protocol [96]. The TUNEL-positive cells were counted across the retina in each of the experimental cohorts, as previously defined [306].

5.2.4 QUANTITATIVE REAL-TIME PCR

First strand cDNA synthesis was performed using TaqMan MicroRNA RT kit (Applied Biosystems) for miRNAs and Tetro cDNA synthesis kit (Bioline) for other genes, according to manufacturer's protocols. Gene and miRNA amplification was measured using commercially available TaqMan hydrolysis probes (Table 5.1), according to a previously established qPCR protocol [306]. Fold change and hence percentage change was determined using the ΔΔCt

method, where miRNAs were normalized to U6 small nuclear RNA (snRNA) expression while chemokine genes were normalized to glyceraldehyde-3-phosphate dehydrogenase (GAPDH).

5.2.5 ONL AND RETINAL LAYER THICKNESS MEASUREMENT

A DNA binding fluorescent dye bisbenzamide (Calbiochem, CA, USA) was used to visualise the cellular layers. ONL thickness was measured in increments of 1mm along the entire length on the retinal cryosection. Thickness was calculated as a ratio of ONL width to the distance between the outer and inner limiting membranes (OLM-ILM).

Toluidine blue staining was used to assess the absolute thickness of all retinal layers. Sections used for staining were carefully selected to ensure that every group was measured at approximately the same retinal axis. Measurements were made at the point of localisation of the 'hotspot' (the part of the superior retina that is extremely susceptible to bright light damage). Multiple sections were measured for each animal and multiple animals were measured for each experimental group. Average values across each group were then plotted. A Two-way ANOVA analysis followed by *bonferroni* post hoc test was used for statistical analyses.

5.2.6 IN SITU HYBRIDIZATION AND QUANTIFICATION OF CCL2-EXPRESSING NUCLEI

To investigate the localisation and quantification of Ccl2 mRNA in the retina following 670nm light treatment and light damage, a DIG labeled riboprobe for Ccl2 (previously designed and used by members of our lab) was applied to retinal cryosections. Frozen retinal sections were thawed for 15-20 minutes at room temperature in a biological safety cabinet (class 2) before being dehydrated in 70% ethanol and rinsed in phosphate buffered saline (PBS).

Table 5. 1

TaqMan® probes used

Gene Symbol	Name	Accession #	Catalog #
Ccl2	Chemokine (C-C motif) ligand 2	NM_031530.1	Rn01456716_g1
Ccl3	Chemokine (C-C motif) ligand 3	NM_013025.2	Rn00564660_m1
Ccl4	Chemokine (C-C motif) ligand 4	NM_053858.1	Rn00587826_m1
Ccl7	Chemokine (C-C motif) ligand 7	NM_01007612.1	Rn01467286_m1
CxCL1	Chemokine (C-X-C motif) ligand 1	NM_030845.1	Rn00578225_m1
CxCL10	Chemokine (C-X-C motif) ligand 10	NM_139089.1	Rn01413889_g1
CxCL11	Chemokine (C-X-C motif) ligand 11	NM_182952.2	Rn00788262_g1
GAPDH	Glyceraldehyde-3-phosphate dehydrogenase	NM_017008.3	Rn99999916_s1
IL1β	Interleukin 1β	NM_031512.2	Rn00580432_m1
miR-351	mmu-miR-351	MIMAT0000609	001067
miR-155	mmu-miR-155	MIMAT0000165	002571
miR-124-3p	mmu-miR-124-3p	MIMAT0000422	001182
miR-183	has-miR-183	MIMAT0000860	002269
U6	U6 small nuclear RNA	NR_004394	001973

Sections were then fixed in 10% neutral buffered formalin (NBF) for 20 minutes, washed in PBS twice for 5 min each and then placed in a 20mg/ml Proteinase K (Roche) solution diluted in TE (50mM Tris-HCL, 5mM EDTA, pH 8) for 7 min at 37 °C. Sections were rinsed in PBS and re-foxed in NBF for 20 min. Slides were placed into a solution of 0.1M Triethanolamine (pH8.0, Sigma) and 2.5% acetic anhydride (Sigma) for 10 min, washed in PBS and then placed in 0.9% NaCl for 5 min. Thereafter, the slides were dehydrated through a series of increasing ethanol concentrations and air dried for 15 min. The prehybridisation solution was preheated to 58 °C on a heat block before being applied to the sections under a coverslip and incubated for 1 h at 55 °C. Following this, the coverslip was removed and preheated hybridization solution (containing the probe) was added to the sections under a new coverslip. Sections were hybridized in 100-300 ng of probe/ml overnight at 55 °C. The following day, coverslips were removed by immersing the slides in 4x saline sodium citrate (SSC, pH 7.4) at 60 °C. The slides were then washed in 2x SSC, 1x SSC, 0.1x SSC at 60 °C for 30 min each and washed in 0.1x SSC at RT for 5 min. Slides were rinsed in washing buffer, placed in blocking solution for 30 min and then incubated with anti-DIG antibody (1:2000) for 1 h at RT. Following antibody incubation, slides were rinsed twice in washing buffer and once in detection buffer for 5 min each. Bound probes were visualised using an alkaline phosphatase conjugated secondary antibody and colorimetric AP substrate 'NBT/BCIP' (Sigma). The AP and substrate reaction was stopped by washing the slides in PBS for MQ Water for 10 min each. Slides were cover slipped using Aqua/Poly mount (Polysciences), sealed with nail varnish and visualised using bright field/light microscopy.

Distinctive punctate labelling was counted as CCL2 positive cells across the retina. Counts were performed in a double blind setup where the individual slides were masked during the counting process. 4 sections were counted for each animal and a total of 5 animals were counted per experimental groups.

5.2.7 TAQMAN MIRNA ARRAY AND BIOLOGICAL FUNCTION ANALYSIS

RNA from retinas of dim-reared, 670nm treated dim-reared animals was used for miRNA array analyses, according to previously described protocols [306]. Differentially expressed miRNAs between dim-reared and 670nm only treated samples were identified using 1-way ANOVA based statistical analysis provided within Partek® Genomic Suite 6.6 software. The biologic functional analysis for miR-351 was performed using DAVID® online functional classification tool. All predicted gene targets for miR-351, extracted from miRWalk™ database were imported into DAVID®s input portal and then the gene ontologies and pathway enrichments analysed for inflammation related processes.

5.3 RESULTS

5.3.1 QUANTIFICATION OF PHOTORECEPTOR DEATH AND CHANGES IN RETINAL THICKNESS:

TUNEL analysis was used to assess the effect of 670nm light pretreatment on photoreceptor survival post light damage. Over a 1000 TUNEL+ photoreceptor cells were observed in the retina after 24hrs bright light exposure. While, pretreatment with 9J/cm^2 670nm light significantly reduced this number of apoptotic photoreceptors to less than half as much ($P<0.05$) (Figure 5.1). However, 670nm light treatment alone had no significant effect on photoreceptor death relative to dim-reared controls. Additionally, ONL and other retinal layer thickness measurements were used to analyse the cumulative effect on photoreceptor death and changes to the retinal architecture following light induced stress (Figure 5.2). The average ONL thickness ratios across the retina did not change significantly between the different experimental groups (Figure 5.2A). Global retinal layer thickness measurements, however, revealed that bright light exposure by itself may be capable of causing expansion of the overall retinal thickness, compared to dim-reared retina (Figure 5.2B). With the ganglion cell layer

(GCL) and inner nuclear layer (INL) showing significant increase in thickness relative to dim-reared control ($P<0.05$). In contrast, animals treated with 670nm light prior to light damage showed preservation of retinal thickness compared to the light damaged ones, and was comparable to the dim-reared animals ($P>0.05$).

5.3.2 MODULATION OF CHEMOKINE-RELATED GENE EXPRESSION:

We used qPCR to examine the effect of 670nm light on the expression of seven chemokines (CCL2, CCL3, CCL4, CCL7, CXCL1, CXCL10 and CXCL11). Expression of all seven chemokines increased significantly following light damage, compared to dim reared control ($P<0.05$, Figure 5.3). Chemokines CCL2 and CCL7 showed the most dramatic increase reaching a peak expression of 2,655- and 1,765-fold respectively, following 24hr light exposure. CCL3, CXCL1 and CXCL10 showed more modest increases of 263, 115 and 250 fold, while CCL4 and CXCL11 only showed a 59 and 22 fold upregulation post light exposure.

In animals treated with 670nm light prior to light damage, the expression of majority of the chemokines analysed was significantly lower than those subjected to light damage only (Figure 5.3). Although, for both CXCL10 and CXCL11 expression appeared to be lower due to the 670nm pre-treatment, the reduction was not statistically insignificant.

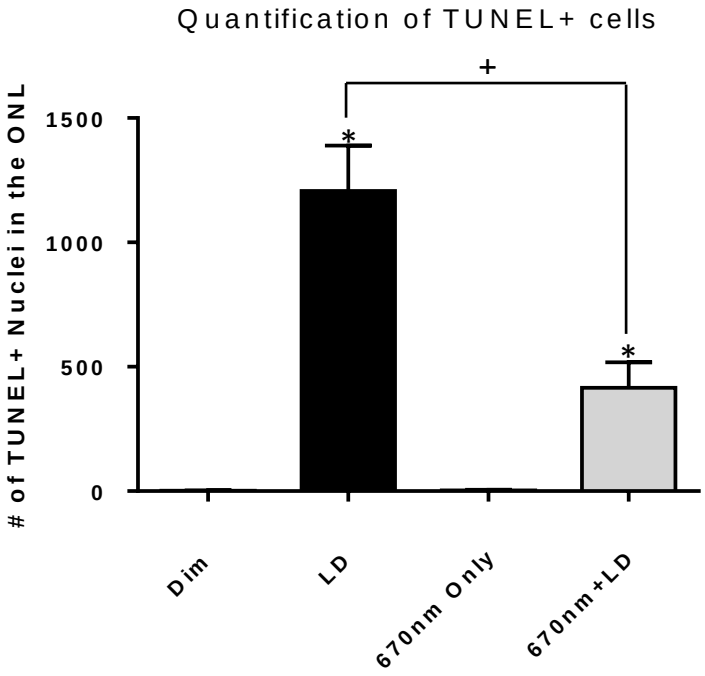

Figure 5. 1 Changes in photoreceptor cell death due to 670nm treatment

Quantification of Photoreceptor cell death by TUNEL following 670nm light treatment and light damage. Increase in TUNEL+ cells in the ONL were observed after LD compared to both dim-reared and 670nm treatment only groups ($P<0.05$). Pre-treatment with 670nm light significantly reduced the number of TUNEL+ photoreceptors post LD. n=4 per experimental group; error bars represent SEM. (*) Indicates significance compared to dim-reared, unless when drawn in conjunction with comparison brackets, where (+) indicates significance between corresponding groups based on *tukey's* post hoc test.

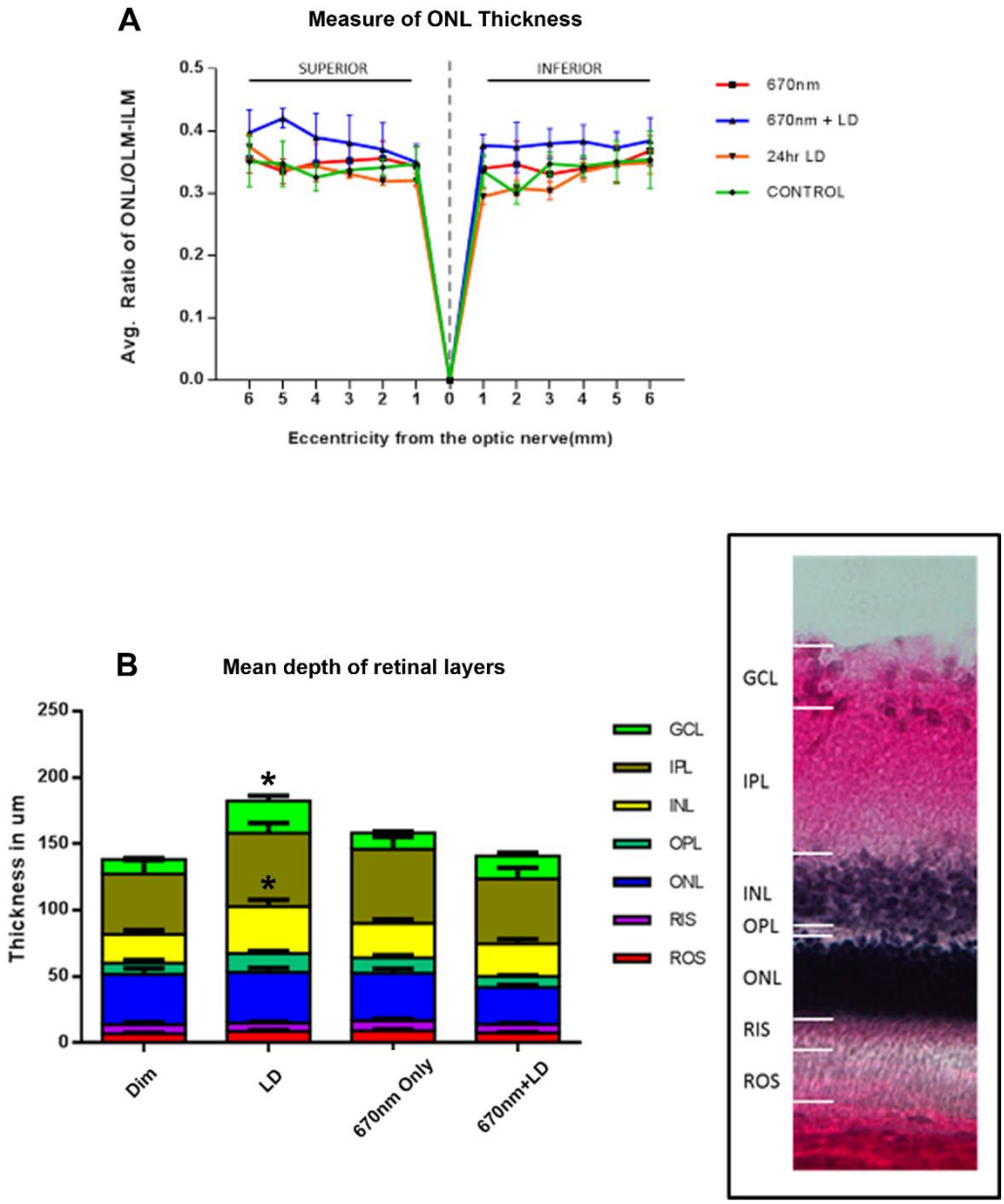

Figure 5. 2 Changes in retinal histology due to 670nm light treatment

Measurements of ONL thickness ratio and individual retinal layer thickness following 670nm light treatment and light damage. (**A**) Graphical representation of ONL thickness ratio across the experimental groups along the length of the retina. No significant changes were observed in the ONL thickness among the different treatment groups across the entire retina. (**B**) *Left*: Graphical representation of the mean retinal depth. Only the GCL and INL show significant increase in thickness after LD compared to dim-reared control group ($P<0.05$), while 670nm light by itself or as a pre-treatment does not result in a significant change. *Right*: Representative image showing the measurement strategy for the retinal layer thickness. White lines indicate approximate boundaries between the retinal layers [the Outer segments (OS), inner segments (IS), outer nuclear layer (ONL), outer plexiform layer (OPL), inner nuclear layer (INL), inner plexiform layer (IPL), and ganglion cell layer (GCL)]. n=5; error bars represent SEM.

Additionally, chemokines CCL2, CCL7 and CXCL1 showed the most substantial reductions in expression, by approximately 50%, due to 670nm pre-treatment prior to light damage ($P<0.05$, Figure 5.3), compared to light damage alone. Of these, CCL7 was statistically indistinguishable from the dim-reared controls ($P>0.05$). No significant change in chemokine expression was observed in retinas treated with 670nm only, compared to the un-treated dim-reared ones ($P>0.05$, Figure 5.3).

5.3.3 LOCALISATION OF CCL2 MRNA IN THE RETINA POST LD AND 670NM LIGHT TREATMENT:

Localisation of CCL2 expression in the retina was assessed using *in situ* hybridisation. CCL2 was expressed in the retina by cells and their radial processes in the INL. In dim-reared animals, miniscule (near zero) amounts of CCL2 mRNA was observed in the retina (Figure 5.4A). Dim-reared retinas treated with 670nm light did not show any significant differences in the number of INL cells expressing CCL2 compared to untreated control retinas (Figure 5.4C, Histogram). However, following 24hr bright light exposure there was a robust increase in the number of INL cells expressing CCL2, specifically in the superior part of the retina (Figure 5.4B). In contrast, in retinas pre-treated with 670nm light there were around 65% fewer INL cells expressing CCL2 compared with light damaged only retinas (Figure 5.4D, Histogram).

5.3.4 MODULATION OF MICRORNA EXPRESSION WITH 670NM LIGHT PRE-TREATMENT:

Global miRNA profiling (of ~750 miRNAs) using low density arrays (LDAs) showed significant modulation of 8 miRNAs in the retina due to 670nm light treatment alone, 4 of which (miR-351, -542-3p, -449a and -467d) were also modulated in light damaged (alone) retinas (refer Chapter 3 Table 3.2).

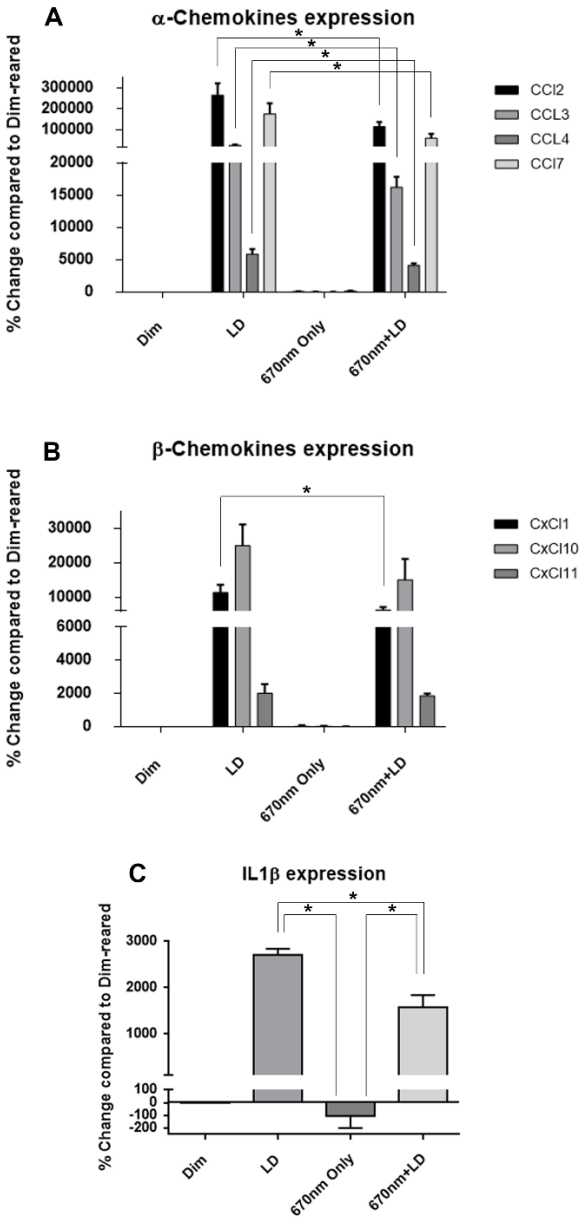

Figure 5. 3 Effect of 670nm light treatment on the expression of α and β chemokines

Comparative expression of α, β chemokines and IL1β in the retina by qPCR following 670nm light treatment and light damage. (**A**) Expression of α chemokines CCL2, 3, 4 and 7. (**B**) Expression of β chemokines CxCL1, 10 and 11. All chemokines increased significantly following light damage relative to dim-reared groups ($P<0.05$). Expression of all chemokines except CxCl10 and 11 were significantly reduced in animals pre-treated with 670nm light, relative to those light damaged only ($P<0.05$). Animals exposed to 670nm light only showed no significant change in chemokine expression compared to dim-reared controls ($P>0.05$). (**C**) IL1β expression increased significantly following light damage relative to dim-reared group. 670nm light pre-treatment significantly reduced this upregulation, however, it still showed a significant upregulation compared to dim-reared ($P<0.05$). 670nm treatment only groups showed a substantial dowregulation of IL1β expression compared to dim-reared, however it did not achieve significance at the current sample size ($P>0.05$). All genes, except in the 670nm only group, were significantly modulated by experimental conditions compared to dim light conditions. n= 10 α-chemokines genes; n=5 β-chemokines genes; n=5 IL1β; error bars represent SEM. Expression trend for all genes was significant based on 1-way ANOVA. (*) Indicates significance between the corresponding groups based on *tukey's* post-test.

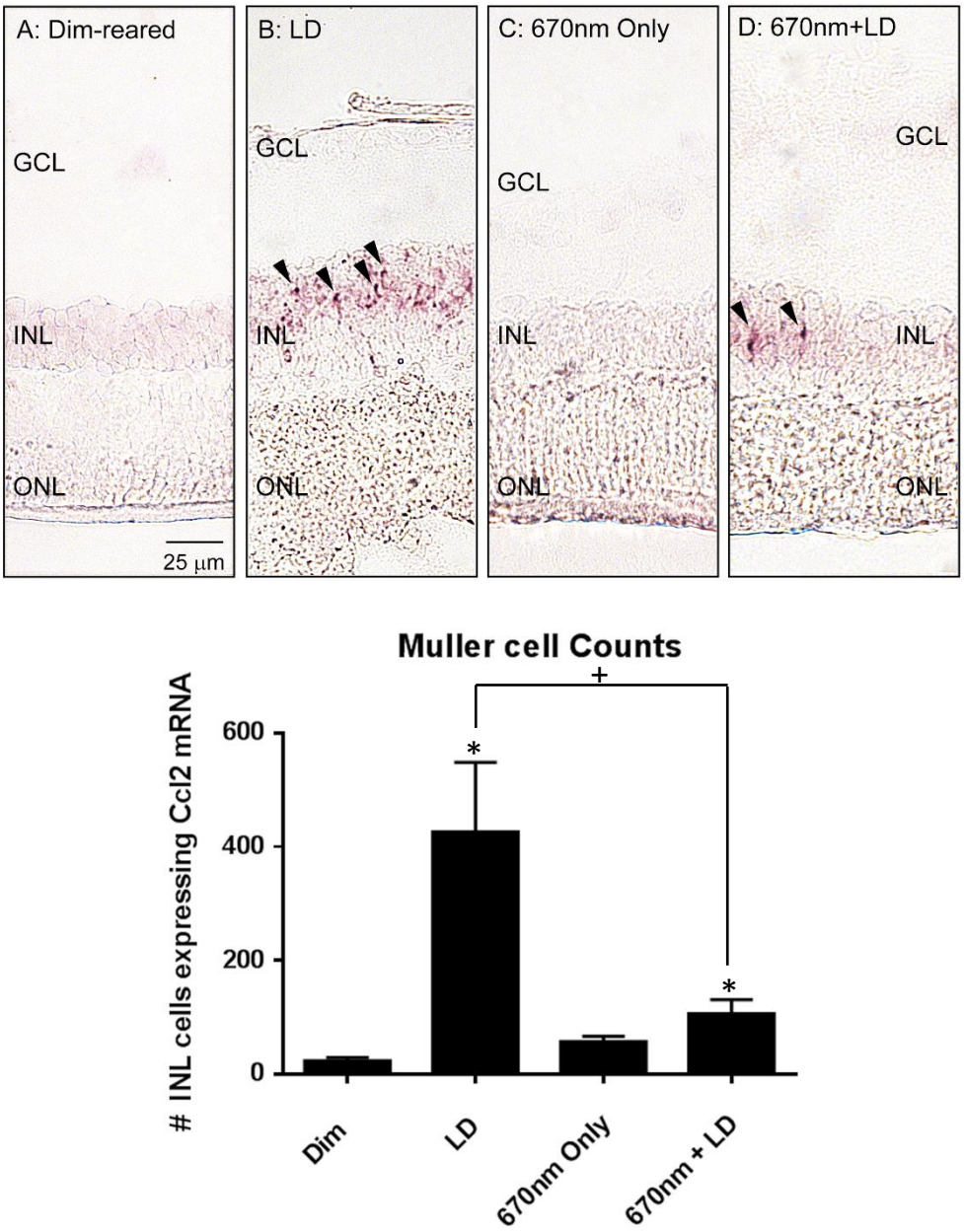

Figure 5. 4 CCL2 *in situ* hybridization and quantification of expression in the retina

In situ hybridization for CCl2 mRNA in the retina following 670nm light treatment and light damage. (**A-D**) Representative images from the superior mid-peripheral region showing *in situ* hybridization for CCl2 mRNA in the retina. CCL2 expression was not detectable in retinas from dim-reared (**A**) and 670nm treated only (**C**) animals. In light damaged animals (**B**) numerous CCL2 expressing cells were observed throughout the inner nuclear layer (INL) (arrowheads), while significantly lower numbers were observed in those treated with 670nm prior to light damage (**D**). (**Histogram**) Quantification of CCL2 mRNA expressing cells per retina showed a drastic increase in LD animals relative to dim-reared and 670nm treated only groups ($P<0.05$). However, this increase was significantly reduced down to control levels in animals pre-treated with 670nm light prior to light damage ($P<0.05$). n=5; error bars represent SEM. (*) Indicates significance compared to dim-reared, unless when drawn in conjunction with comparison brackets, where (+) indicates significance between corresponding groups based in *tukey's* post test.

Table 5. 2

MiRNAs significantly modulated by 670nm treatment only

miRNA ID	P Value	Fold Change
mmu-miR-547	0.0346819	28.563
mmu-miR-501-3p	0.0139051	26.0959
mmu-miR-467d	0.0368586	14.667
mmu-miR-449a	0.00919298	7.37819
mmu-miR-345-3p	0.03215	5.50522
mmu-miR-542-3p	0.0357811	4.36279
mmu-miR-351	0.0283901	3.57415
rno-miR-20b-3p	0.0394982	3.4851

These miRNAs were assessed using qPCR analysis (Figure 5.5 A-D), with only 2 (miR-351 and -155) showing significant modulation due to 670nm light treatment. MiR-351 expression was significantly increased (~65%) in retinas treated with 670nm light alone, relative to the dim-reared and LD samples. MiR-155 was not modulated by 670nm treatment alone but was significantly reduced in light damaged retinas by 670nm pre-treatment, compared to the LD only samples. No other miRNAs were modulated by 670nm light treatment.

Functional classification of the predicted targets for miR-351 was performed using DAVID® online algorithm (Figure 5.6). The analyses included "immune system process" as one of the 8 gene ontology terms and "cytokine-cytokine receptor interactions" as one of the biological pathways involving the predicted gene targets of miR-351. Thirteen (13) genes appeared in both categories.

5.4 DISCUSSION

The results of this study show the efficacy of 670nm light treatment in suppressing early inflammation and chronic photoreceptor cell death following light induced retinal degeneration. First the findings indicate that irradiation with 670nm light reduces early photoreceptor cell death and suppresses the expansion in retinal thickness following bright light damage. Second, gene expression analyses indicate that pre-treatment with 670nm light downregulates a number of pro-inflammatory chemokines - including α-chemokines (CCL2, CCL3, CCL4, CCL7) and β-chemokines (CXCL1, CXCL10, CXCL11) - whose expression coincides strongly with photoreceptor cell death following light damage. Third, the results indicate that 670nm light pre-treatment has an effect on miRNA expression after light damage, with significant modulation of miR-155 and miR-351 detected.

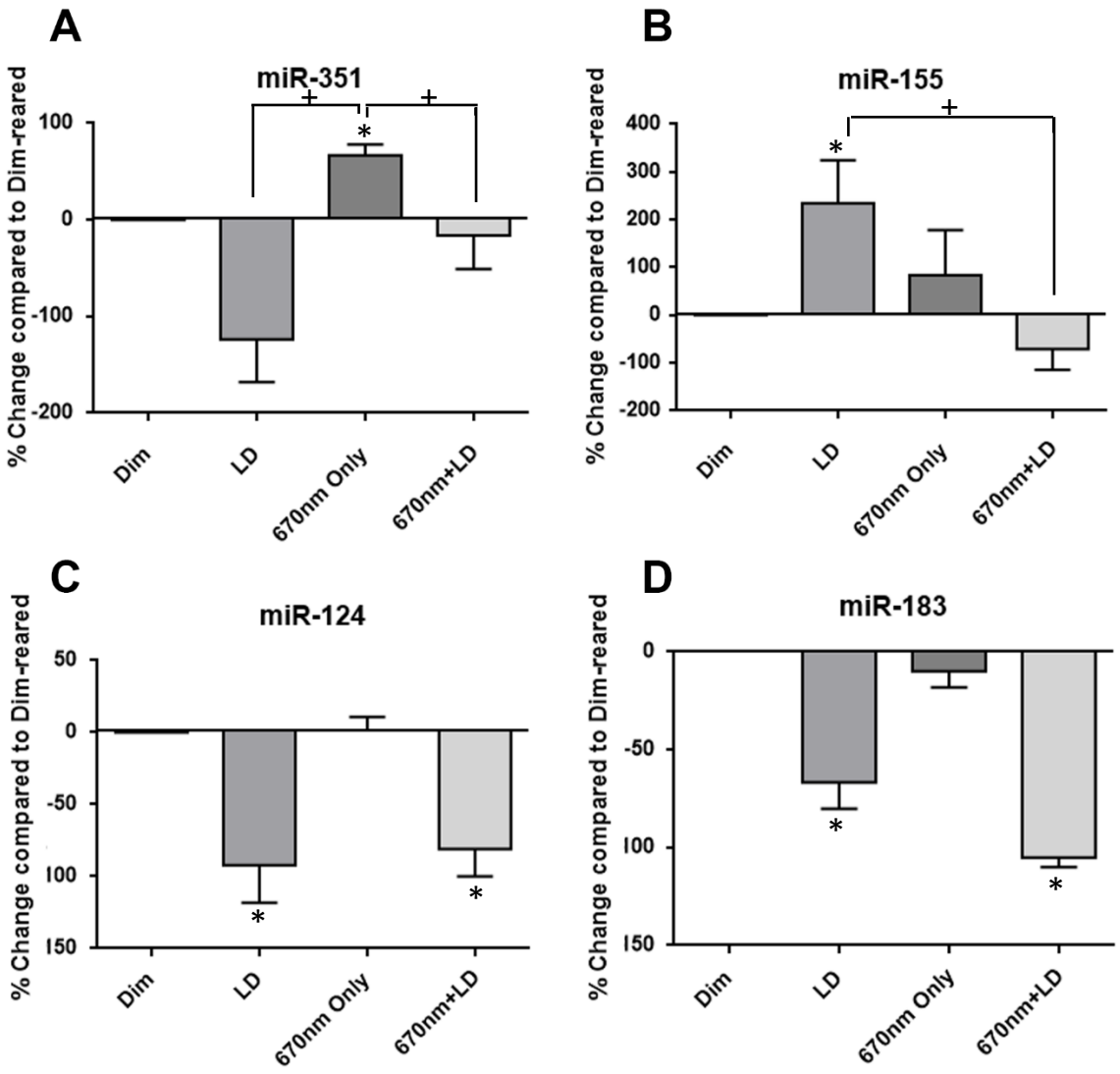

Figure 5. 5 Changes in expression of specific miRNAs due to 670nm light treatment

Expression profile of miRNA in the retina by qPCR following 670nm light treatment and light damage. (**A**) MiRNA showing significant modulation due to 670nm light treatment alone**,** (**B**) Modulation of pro-inflammatory miRNAs due to 670nm pre-treatment, (**C**) Modulation of a CNS specific anti-inflammatory miRNA and (**D**) Modulation of a photoreceptor specific miRNA. MiR-351 was significantly upregulated due to 670nm treatment itself. The increase in pro-inflammatory miRNA, miR-155 was significantly suppressed with 670nm pre-treatment ($P<0.05$). 670nm treatment given alone or as a pre-treatment to LD had no impact on the expression profile of miR-124 or miR-183 ($P>0.05$). n=6; error bars represent SEM. (*) Indicates significance compared to dim-reared, unless when drawn in conjunction with comparison brackets, where (+) indicates significance between corresponding groups based on *tukey's* post test.

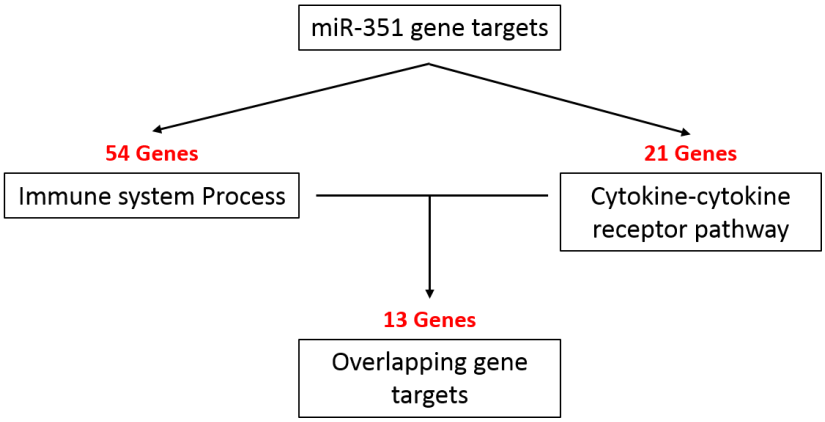

Gene list
Tumor necrosis factor (ligand) superfamily, member 14
Interleukin 1 receptor, type I
Lymphotoxin A
Interleukin 23, alpha subunit p19
Leukemia inhibitory factor
Tumor necrosis factor
Interleukin 13
Kinase insert domain protein receptor
Interleukin 7 receptor
Chemokine (C-X-C motif) ligand 15
Interleukin 1 beta
Tumor necrosis factor (ligand) superfamily, member 4
Colony stimulating factor 3 (granulocyte)

Figure 5. 6 Potential functional impact of miR-351

Functional analyses of miR-351 predicted targets using DAVID® functional annotation database. All predicted gene targets for miR-351 were analysed using an analytical algorithm to identify the functional categories most highly affected by these genes and hence potentially by miR-351. The GO term classification revealed 'immune system process' as one of the major biological processes enriched, while the pathway analyses revealed 'Cytokine-Cytokine receptor interaction' as a highly represented pathway potentially being targeted by miR-351.

Both miR-155 and miR-351 have predicted binding sites for a number of inflammatory molecules, including those that work upstream of chemokine expression, suggesting a possible mechanism by which 670nm influences the retinal immune response.

Previous investigations have shown that irradiation with 670nm light reduces photoreceptor cell death, complement propagation and activated microglial accumulation in the retina during prolonged periods following light-induced damage [118, 233, 236]. In the current study, however, we show some of the early changes in the retinal transcriptome due to 670nm pre-treatment, including inhibition of chemokine genes that have previously been shown to upregulate in the light damaged retina by several PCR and microarray based studies [96, 99, 272, 273, 339].

In the present study we demonstrated using TUNEL analysis that 670nm light irradiation inhibits the early initiation of photoreceptor cell death due the damaging light exposure. While no change is seen in the ONL thickness (a measure of cumulative effect of photoreceptor cell death) across the different experimental groups. Suggesting that photoreceptor death might only have a significant impact on ONL thickness at higher levels or a more sustained period of low level death, as is documented in previous studies focusing on the long term effects of light induced retinal degeneration [105, 118, 236]. Our data indicates that TUNEL analysis is a more robust tool for detecting the neuroprotective effect of 670nm light on photoreceptor cells at the early damage time points such as the one under consideration here. To further characterise the impact on the retinal architecture we used haematoxylin and Eosin stained retinal cross sections to measure the absolute thickness of the different retinal layers. As evident in figure 5.2B we saw a slight increase in the overall retinal thickness, with significant increases in the GCL and INL widths. Suggesting that cells in these layers may be the first to respond to the damaging stimulus. The INL contains the cell bodies of Müller cells, the site of expression of CCL2 post light damage, hence the increase in its width could be attributed to the movement of

inflammatory cells including microglia and monocytes into the INL. While the expansion in GCL width could potentially arise from an increase in infiltration of inflammatory cells from the retinal vasculature. This data, however, is not corrected for the variability in sectioning obliqueness, which can lead to incorrect layer thickness measurements. It would hence be better to flat mount the retina before embedding and cutting to reassess absolute thickness changes.

Chemokines are a well-established family of genes/proteins that possess potent chemoattractant properties and drive targeted recruitment of leukocytes during immune surveillance as well as inflammation [87, 88, 90, 340]. Several studies have shown the upregulation of a number of chemokines following light damage, with a recent study identifying the source of each different chemokine in the light damaged rat retina [99]. Similarly, our data also shows significant upregulation of a subset of these molecules following light damage. Moreover our findings indicate that their expression profile correlates with the pattern of photoreceptor cell death following light damage.

In contrast, retinas pre-treated with 5x 9J/cm2 670nm light show a significant reduction in the respective upregulation post light damage for all chemokines except CXCL10 and CXCL11. Although, their expression trend across the different experimental groups was still significant based on a 1-way ANOVA test. Among the significantly downregulated chemokines were CCL2, CCL3, CCL4, CCL7 and CXCL1, all of which are believed to form a complex network of activity post stimulation by light-induced retinal damage and are expressed by specific cell types of the retina. While the exact roles of most of these molecules in the degenerating retina are still unclear, studies in other diseases/disease models might be useful in highlighting their potential roles.

For instance CCL3 and CCL4, which are specifically expressed by activated microglia in the retina, are capable of monocyte recruitment and Th1 T cell mobilisation via interactions with

Ccr1, Ccr5 receptors [341-345]. CCL7, expressed by Müller cells and activated microglia, acts as an agonist for the well documented Ccr2 receptor, a key player in monocyte chemotaxis [346, 347]. In contrast CXCL1, which is expressed by both Müller cells and RPE, plays a role in neutrophil recruitment from the surrounding vasculature along with its receptor Cxcr2 [348-350]. This is of particular interest as neutrophils have been shown to be involved in the pathophysiology of choroidal neovascularisation [351]. While CCL2, expressed by Müller cells and infiltrating monocytes in the damaged retina, is a well-documented retinal chemokine with potent chemoattractant properties that drive targeted recruitment of macrophages [97, 98, 352, 353].

The CCL2 *in situ* data presented in this study indicate that its downregulation induced by 670nm pre-treatment is due to reduced expression of CCL2 by Müller cells, and not simply a consequence of reduced infiltration of activated CCL2-expressing monocytes from the choroid, which has been shown to occur due to 670nm pre-treatment [118, 236]. Together, the findings suggest that 670 nm light pre-treatment can suppress CCL2-mediated recruitment of blood-borne monocytes as well as the broader leukocyte population into damaged regions of the retina after bright light exposure. This effect mitigates the progressive degenerative state of the retina that promotes photoreceptor cell death.

Mechanistically, this broad spectrum inhibition of inflammatory regulators by 670nm light treatment could be explained by its ability to enhance mitochondrial function which leads to increased ATP production and reduction of oxidative stress [214, 236, 239]. Alternatively, this could potentially be explained by a relatively new hypothesis gaining momentum in the recent past whereby, photobiomodulation is able to increase the bioavailability of nitric oxide (NO), a potent intracellular messenger that could act as a downstream signalling molecule leading to differential effect on the cellular transcriptome [250, 251, 354, 355]. Various *in vitro* and *in vivo* studies suggest that 670nm treatment increases NO availability either by stimulating

inducible nitric oxide synthase (iNOS) expression or by causing the dissociation of NO from cytochrome c oxidase in the mitochondria [210, 356-360].

5.4.1 MIRNA EXPRESSION PROFILE

A previous gene expression study showed that 670nm light irradiation modulates noncoding RNAs as well as protein coding mRNAs [96]. Here, the modulation of miRNAs was assessed to better understand the potential molecular mechanisms by which 670nm light might modulate retinal inflammation.

The present findings indicate that 670nm light on its own may modulate miRNAs in the retina (see Table 5.2) and that some of these are also modulated by light damage (refer Chapter 3). However, the qPCR analysis was not entirely confirmatory in that miR-351 showed a non-significant change in the light damaged retinas compared to the low density array results. This variability could be explained by the biological differences inherent in the light damage model in which some animals respond more severely to others [361, 362].

More importantly, however, there is a consistent and significant upregulation in miR-351 due to 670nm treatment only. While not much is known about its role in inflammation associated with AMD or light-induced retinal degeneration, we found predicted binding sites for miR-351 in the 3'UTR of a number of pro-inflammatory factors including potent chemokine regulators IL1β and TNF. Both have been implicated in AMD and retinal degenerations [281, 363-368]. Both IL1β and TNFα (a common form of TNF) are upregulated as early as 12 hours post bright light exposure in this model, prior to upregulation of a gamut of pro-inflammatory chemokines that reach peak expression at 17-24 hours exposure to bright light [99]. In this study we find that the upregulation of IL1β is significantly reduced by 670nm light pre-treatment consistent with its favourable effects on neuroinflammation. However, because the interaction between

miR-351 and IL1β is only a predicted phenomenon further confirmation using luciferase-based assays are required.

The findings also demonstrate an effect of 670nm light treatment on the modulation of a well-known pro-inflammatory miRNA miR-155, which has previously been shown to upregulate post light-induced damage [306].

MiR-155 is upregulated by light damage, but did not show a significant modulation due to 670nm treatment alone. While it was maintained at control levels in light damaged retinas pre-treated with 670nm light (Figure 5.5B). Since the tissue/cellular localisation of miR-155 in the light damaged albino rat retina is currently unknown, it is difficult to speculate how its expression is being modulated. However, studies in other disease models have shown that both resident microglia and infiltrating monocytes stimulated with pro-inflammatory cues (such as TNFα and IL1β) exhibit an upregulation of miR-155 which in turn supports the activation of their M1 or pro-inflammatory state.

Additionally, previously published work from our group has shown that 670nm pre-treatment significantly reduces the upregulation of various pro-inflammatory factors (cytokines, chemokines) and microglia/monocyte recruitment in the retina post LD. Hence, the lack of miR-155 upregulation (relative to dim reared control) in the 670nm pre-treated light damaged retinas could possibly result from either:

1. Little or no stimulation of microglia/monocytes in the absence of a pro-inflammatory microenvironment, as a result of 670nm pretreatment. OR

2. Reduced recruitment of M1 microglia/monocytes to the retina.

None the less, this result is particularly interesting as miR-155 has recently been shown to target complement factor H (CFH) [199], which is strongly associated with the risk of AMD

[369]. The findings indicate that treatment with 670nm light to reduce levels of miR-155 may result in increased levels of CFH in the retina, leading to down modulation of complement.

In contrast, miR-124 expression was not modulated by 670nm light treatment, even after light damage (Figure 5.5C). Since miR-124 inhibits CCL2 expression by direct binding [305], this observation suggests that anti-inflammatory effects of 670nm light are upstream or independent of CCL2 regulation via miR-124-3p. It is possible that the relatively small inflammatory response elicited in 670nm + LD retinae is still sufficient to exhaust the amount of endogenously expressed miR-124-3p, and that the downregulation of CCL2 seen due to 670nm pre-treatment is a consequence of a secondary mechanism.

The findings for miR-183 were similar in that a downregulation of miR-183 expression was detected post LD, with or without pre-treatment with 670nm light. The data, however, indicate a trend toward 670nm light influencing this downregulation, at marginal levels of significance. MiR-183 cluster is highly specific to the sensory organs and regulates the retinal circadian rhythm [296, 370]. Knockdown and knockout studies in the mouse retina have shown a protective role of the miR-183 cluster against light induced damage [295, 371], while several studies in other disease models have identified disease promoting effects of the miR-183 cluster in neurodegeneration [372, 373] and cancer [374-379]. The effects of miR-183 here may be due to the ability to potentially alter energy metabolism as a result of its affinity for isocitrate dehydrogenase 2 (IDH2), an essential mitochondrial enzyme [378].

5.4.2 CONCLUSIONS

The findings presented in this chapter indicate that 670nm irradiation significantly reduces the early stimulation of chemokine synthesis and photoreceptor cell death in the retina following light-induced damage. The results also indicate that 670nm light treatment may modulate the miRNA transcriptome of the retina. Such modulation is a potential mechanism by which

670nm light modulates inflammatory regulators and inflammation in the retina. However, the data also suggest that the key pro-inflammatory chemokine, CCL2, is not modulated by changes in expression levels of miR-124-3p in the presence of 670nm light. An essential strategy to progress these studies is the use of crosslinking immunoprecipitation in conjunction with high-throughput RNA sequencing, to identify all the functionally active miRNA:mRNA interactions in the retina during both normal and degenerative states.

CHAPTER 6: SUMMARY AND CONCLUSIONS

In this thesis I explore the concept that miRNA play a role in retinal degenerations and that their further study might elucidate potential therapeutic interventions. Firstly, using a LD model of retinal degeneration I show that miRNA are differentially expressed over a protracted time course, and that many of these miRNA regulate inflammatory genes and processes. Secondly, I identified a novel retinal miRNA, miRNA-124-3p, as a potential modulator of the pro-inflammatory state of the retina post light damage, and which may be therapeutically targeted to ameliorate inflammation during retinal degenerations. Finally, I show that some miRNA are modulated by 670nm red light, including two involved in modulating inflammatory genes. This finding reinforces the anti-inflammatory potential of 670nm red light, while also identifying other candidate miRNAs, specifically miR-155 and miRNA-351, as potential therapeutic targets.

In the past decade, studies have shown the modulation of miRNAs (including miR-124-3p) in the developing mammalian retina [314, 370, 380-382] in a strict spatiotemporally distributed profile, suggesting a tight transcriptional control of expression. Many studies have focused on the pathological roles of miRNAs using animal models of retinal disorders including diabetic retinopathy and retinitis pigmentosa [383-387]. In this study significant modulation of miRNAs is identified in a light damage model of focal retinal degeneration. Many of the miRNAs identified regulate the inflammatory response, relevant in AMD. MiRNAs have recently gained momentum with regards to their therapeutic potential in AMD, with a recent study by Lukiw and colleagues [199] showing a direct link between upregulation of 4 miRNAs (miR-9, -125b, -146a and -155) and downregulation of complement factor H (CFH) expression in human post-mortem retinal tissue. Additionally, several other studies have identified a number of miRNAs as potential therapeutic targets for AMD (reviewed in [388]).

Because miRNAs are endogenous, and function as master regulators of gene expression and multiple biological pathways, they are highly attractive therapeutic target for complex diseases.

In other biological systems, some miRNA-based therapies have already entered clinical trials including an anti-miR-122 therapy to efficiently target hepatitis C virus infection, and an miRNA replacement therapy using a miR-34 mimic for its strong anti-tumour activity targeting primary liver cancer / solid tumours / haematological malignancies [203, 204].

Ongoing work investigating the function of miRNAs identified in the present study, and others, is required to better understand their role/s in the onset and progression of retinal degeneration. One approach is through the use of intravitreal injections of specific miRNA mimics or inhibitors to enhance or supress a miRNAs function. A lipid-based transfection method (Invivofectamine ® 1.0) was successfully used in the past in our research group to deliver siRNA [97]. Using a similar approach I attempted transfection of a miR-124-3p mimic into the rat retina, using Invivofectamine ® 2.0. However, the experiments had to be abandoned because our data indicated that the transfection agent was triggering a non-specific immune response, masking any effect of miR-124-3p. Our research group is currently testing a new transfection agent produced by the manufacturers ThermoFisher ™. The mimic / inhibitor experiments will be resumed once we are satisfied that the transfection agent does not induce a biological response. Unfortunately, completion of those experiments will be outside the period of candidature for my PhD.

One of the inherent properties of miRNA biology is that they target many different genes simultaneously. This is a possible hindrance of using miRNAs for therapeutics as it raises questions about potential off-target interactions of mimics and inhibitors. To that end, recent advances in molecular techniques include comprehensive multi-strategy assays to help identify all active miRNA:mRNA interactions occurring inside the cell with high confidence. One such assay is HITS-CLIP, employing high-throughput sequencing of RNA isolated by crosslinking immunoprecipitation, whereby miRNA:mRNA complexes bound to Argonaute 2 (a component of the RNA-induced silencing complex) are crosslinked using ultraviolet light, and pulled down

using anti-AGO2 antibody [389]. This powerful technique can identify all tissue/condition specific miRNA targets, thereby assisting in characterising potential off-target interactions at any given condition. This inherent property of miRNA, however, is also a major benefit when using them to treat complex multifactorial diseases such as AMD that require modification of multiple cellular processes simultaneously.

MiRNAs are potent regulators of the genome and clearly have a role in retinal degenerations through modulation of the local inflammatory response. The results presented in this thesis provide a basis for understanding the potential role of miRNAs in regulating the innate immune response during retinal degeneration. The similarity in the profiles of miRNA modulated in the LD model, and those identified in AMD provides support for the use of the LD model in understanding processes of retinal inflammation relevant to AMD. Further work is warranted to characterise the role/s of these putative candidates in retinal inflammation, including identification of off-target effects and possible synergies, to transform the basic knowledge described here into effective clinical therapies.

6.1 REFERENCES

1. Edwards, A.O., et al., *Complement factor H polymorphism and age-related macular degeneration.* Science, 2005. **308**(5720): p. 421-4.
2. Hageman, G.S., et al., *A common haplotype in the complement regulatory gene factor H (HF1/CFH) predisposes individuals to age-related macular degeneration.* Proc Natl Acad Sci U S A, 2005. **102**(20): p. 7227-32.
3. Haines, J.L., et al., *Complement factor H variant increases the risk of age-related macular degeneration.* Science, 2005. **308**(5720): p. 419-21.
4. Ha, T.Y., *MicroRNAs in Human Diseases: From Lung, Liver and Kidney Diseases to Infectious Disease, Sickle Cell Disease and Endometrium Disease.* Immune Netw, 2011. **11**(6): p. 309-23.
5. Ha, T.Y., *MicroRNAs in Human Diseases: From Autoimmune Diseases to Skin, Psychiatric and Neurodegenerative Diseases.* Immune Netw, 2011. **11**(5): p. 227-44.
6. Ha, T.Y., *MicroRNAs in Human Diseases: From Cancer to Cardiovascular Disease.* Immune Netw, 2011. **11**(3): p. 135-54.
7. Raisch, J., A. Darfeuille-Michaud, and H.T. Nguyen, *Role of microRNAs in the immune system, inflammation and cancer.* World J Gastroenterol, 2013. **19**(20): p. 2985-96.
8. Heavner, W. and L. Pevny, *Eye development and retinogenesis.* Cold Spring Harb Perspect Biol, 2012. **4**(12).
9. Carter-Dawson, L.D. and M.M. LaVail, *Rods and cones in the mouse retina. I. Structural analysis using light and electron microscopy.* J Comp Neurol, 1979. **188**(2): p. 245-62.
10. Steinberg, R.H., S.K. Fisher, and D.H. Anderson, *Disc morphogenesis in vertebrate photoreceptors.* J Comp Neurol, 1980. **190**(3): p. 501-8.
11. Anderson, D.H., S.K. Fisher, and R.H. Steinberg, *Mammalian cones: disc shedding, phagocytosis, and renewal.* Invest Ophthalmol Vis Sci, 1978. **17**(2): p. 117-33.
12. Baylor, D., *How photons start vision.* Proc Natl Acad Sci U S A, 1996. **93**(2): p. 560-5.
13. Nilsson, S.E., *A Globular Substructure of the Retinal Receptor Outer Segment Membranes and Some Other Cell Membranes in the Tadpole.* Nature, 1964. **202**: p. 509-10.
14. Young, R.W., *The organization of vertebrate photoreceptor cells.* UCLA Forum Med Sci, 1969. **8**: p. 177-210.
15. Rodieck, R., *The Vertebrate Retina. Principle of Structure and Function*, 1973, WH Freeman and Co.: San Francisco, CA, USA.
16. Streilein, J.W., *Ocular immune privilege: the eye takes a dim but practical view of immunity and inflammation.* J Leukoc Biol, 2003. **74**(2): p. 179-85.
17. Crane, I.J. and J. Liversidge, *Mechanisms of leukocyte migration across the blood-retina barrier.* Semin Immunopathol, 2008. **30**(2): p. 165-77.
18. Niederkorn, J.Y., *See no evil, hear no evil, do no evil: the lessons of immune privilege.* Nat Immunol, 2006. **7**(4): p. 354-9.
19. Penfold, P.L., et al., *Immunology and age-related macular degeneration*, in *Macular Degeneration*. 2005, Springer. p. 25-44.
20. Cunha-Vaz, J.G., M. Shakib, and N. Ashton, *Studies on the permeability of the blood-retinal barrier. I. On the existence, development, and site of a blood-retinal barrier.* Br J Ophthalmol, 1966. **50**(8): p. 441-53.
21. Penfold, P.L., et al., *Immunological and aetiological aspects of macular degeneration.* Prog Retin Eye Res, 2001. **20**(3): p. 385-414.
22. Shakib, M. and J.G. Cunha-Vaz, *Studies on the permeability of the blood-retinal barrier. IV. Junctional complexes of the retinal vessels and their role in the permeability of the blood-retinal barrier.* Exp Eye Res, 1966. **5**(3): p. 229-34.
23. Prendergast, R.A., et al., *T cell traffic and the inflammatory response in experimental autoimmune uveoretinitis.* Invest Ophthalmol Vis Sci, 1998. **39**(5): p. 754-62.

24. Xu, H., et al., *Requirements for passage of T lymphocytes across non-inflamed retinal microvessels.* J Neuroimmunol, 2003. **142**(1-2): p. 47-57.
25. Kastelan, S., V. Zjacic-Rotkvic, and Z. Kastelan, *Could diabetic retinopathy be an autoimmune disease?* Med Hypotheses, 2007. **68**(5): p. 1016-8.
26. van Best, J.A., et al., *Function and morphology of the retinal pigment epithelium after light-induced damage.* Microsc Res Tech, 1997. **36**(2): p. 77-88.
27. Ambati, J., et al., *Age-related macular degeneration: etiology, pathogenesis, and therapeutic strategies.* Surv Ophthalmol, 2003. **48**(3): p. 257-93.
28. Green, W.R. and C. Enger, *Age-related macular degeneration histopathologic studies. The 1992 Lorenz E. Zimmerman Lecture.* Ophthalmology, 1993. **100**(10): p. 1519-35.
29. Green, W.R. and S.N. Key, 3rd, *Senile macular degeneration: a histopathologic study.* Trans Am Ophthalmol Soc, 1977. **75**: p. 180-254.
30. Bressler, N.M., S.B. Bressler, and E.S. Gragoudas, *Clinical characteristics of choroidal neovascular membranes.* Arch Ophthalmol, 1987. **105**(2): p. 209-13.
31. Lafaut, B.A., et al., *Clinicopathological correlation in exudative age related macular degeneration: histological differentiation between classic and occult choroidal neovascularisation.* Br J Ophthalmol, 2000. **84**(3): p. 239-43.
32. Bressler, N.M., et al., *Clinicopathologic correlation of drusen and retinal pigment epithelial abnormalities in age-related macular degeneration.* Retina, 1994. **14**(2): p. 130-42.
33. Mullins, R.F., et al., *Choriocapillaris vascular dropout related to density of drusen in human eyes with early age-related macular degeneration.* Invest Ophthalmol Vis Sci, 2011. **52**(3): p. 1606-12.
34. Sohn, E.H., et al., *Comparison of drusen and modifying genes in autosomal dominant radial drusen and age-related macular degeneration.* Retina, 2015. **35**(1): p. 48-57.
35. Gass, J.D., *Drusen and disciform macular detachment and degeneration.* Arch Ophthalmol, 1973. **90**(3): p. 206-17.
36. Sarks, S.H., *Ageing and degeneration in the macular region: a clinico-pathological study.* Br J Ophthalmol, 1976. **60**(5): p. 324-41.
37. Klein, R., et al., *The relationship of age-related maculopathy, cataract, and glaucoma to visual acuity.* Invest Ophthalmol Vis Sci, 1995. **36**(1): p. 182-91.
38. Sunness, J.S., et al., *Enlargement of atrophy and visual acuity loss in the geographic atrophy form of age-related macular degeneration.* Ophthalmology, 1999. **106**(9): p. 1768-79.
39. Grunwald, J.E., et al., *Foveolar choroidal blood flow in age-related macular degeneration.* Invest Ophthalmol Vis Sci, 1998. **39**(2): p. 385-90.
40. Dunaief, J.L., et al., *The role of apoptosis in age-related macular degeneration.* Arch Ophthalmol, 2002. **120**(11): p. 1435-42.
41. Fleckenstein, M., et al., *High-resolution spectral domain-OCT imaging in geographic atrophy associated with age-related macular degeneration.* Invest Ophthalmol Vis Sci, 2008. **49**(9): p. 4137-44.
42. Sarks, J.P., S.H. Sarks, and M.C. Killingsworth, *Evolution of geographic atrophy of the retinal pigment epithelium.* Eye (Lond), 1988. **2 (Pt 5)**: p. 552-77.
43. Curcio, C.A., N.E. Medeiros, and C.L. Millican, *Photoreceptor loss in age-related macular degeneration.* Invest Ophthalmol Vis Sci, 1996. **37**(7): p. 1236-49.
44. Shelley, E.J., et al., *Cone degeneration in aging and age-related macular degeneration.* Arch Ophthalmol, 2009. **127**(4): p. 483-92.
45. Wong, W.T., et al., *Treatment of geographic atrophy by the topical administration of OT-551: results of a phase II clinical trial.* Invest Ophthalmol Vis Sci, 2010. **51**(12): p. 6131-9.
46. Young, R.W., *Pathophysiology of age-related macular degeneration.* Surv Ophthalmol, 1987. **31**(5): p. 291-306.

47. Penfold, P., M. Killingsworth, and S. Sarks, *An ultrastructural study of the role of leucocytes and fibroblasts in the breakdown of Bruch's membrane.* Aust J Ophthalmol, 1984. **12**(1): p. 23-31.
48. Penfold, P.L., M.C. Killingsworth, and S.H. Sarks, *Senile macular degeneration: the involvement of immunocompetent cells.* Graefes Arch Clin Exp Ophthalmol, 1985. **223**(2): p. 69-76.
49. Penfold, P.L., J.M. Provis, and F.A. Billson, *Age-related macular degeneration: ultrastructural studies of the relationship of leucocytes to angiogenesis.* Graefes Arch Clin Exp Ophthalmol, 1987. **225**(1): p. 70-6.
50. Penfold, P.L., et al., *Autoantibodies to retinal astrocytes associated with age-related macular degeneration.* Graefes Arch Clin Exp Ophthalmol, 1990. **228**(3): p. 270-4.
51. Hegner, C., *Retinitis exsudativa bei Lymphogranulomatosis.* Klin Monatsbl Augenheilkd, 1916. **57**: p. 27-48.
52. Lopez, P.F., et al., *Pathologic features of surgically excised subretinal neovascular membranes in age-related macular degeneration.* Am J Ophthalmol, 1991. **112**(6): p. 647-56.
53. Seregard, S., P.V. Algvere, and L. Berglin, *Immunohistochemical characterization of surgically removed subfoveal fibrovascular membranes.* Graefes Arch Clin Exp Ophthalmol, 1994. **232**(6): p. 325-9.
54. Cherepanoff, S., et al., *Bruch's membrane and choroidal macrophages in early and advanced age-related macular degeneration.* Br J Ophthalmol, 2010. **94**(7): p. 918-25.
55. Combadiere, C., et al., *CX3CR1-dependent subretinal microglia cell accumulation is associated with cardinal features of age-related macular degeneration.* J Clin Invest, 2007. **117**(10): p. 2920-8.
56. Gupta, N., K.E. Brown, and A.H. Milam, *Activated microglia in human retinitis pigmentosa, late-onset retinal degeneration, and age-related macular degeneration.* Exp Eye Res, 2003. **76**(4): p. 463-71.
57. Espinosa-Heidmann, D.G., et al., *Macrophage depletion diminishes lesion size and severity in experimental choroidal neovascularization.* Invest Ophthalmol Vis Sci, 2003. **44**(8): p. 3586-92.
58. Sakurai, E., et al., *Macrophage depletion inhibits experimental choroidal neovascularization.* Invest Ophthalmol Vis Sci, 2003. **44**(8): p. 3578-85.
59. Tsutsumi, C., et al., *The critical role of ocular-infiltrating macrophages in the development of choroidal neovascularization.* J Leukoc Biol, 2003. **74**(1): p. 25-32.
60. Kim, S.U. and J. de Vellis, *Microglia in health and disease.* J Neurosci Res, 2005. **81**(3): p. 302-13.
61. Wirenfeldt, M., A.A. Babcock, and H.V. Vinters, *Microglia - insights into immune system structure, function, and reactivity in the central nervous system.* Histol Histopathol, 2011. **26**(4): p. 519-30.
62. Ezzat, M.K., et al., *Immune cells in the human choroid.* Br J Ophthalmol, 2008. **92**(7): p. 976-80.
63. Penfold, P.L., M.C. Killingsworth, and S.H. Sarks, *Senile macular degeneration. The involvement of giant cells in atrophy of the retinal pigment epithelium.* Invest Ophthalmol Vis Sci, 1986. **27**(3): p. 364-71.
64. Lewis, G.P., et al., *Microglial cell activation following retinal detachment: a comparison between species.* Mol Vis, 2005. **11**: p. 491-500.
65. Neufeld, A.H., *Microglia in the optic nerve head and the region of parapapillary chorioretinal atrophy in glaucoma.* Arch Ophthalmol, 1999. **117**(8): p. 1050-6.
66. Vrabec, F., *Activated human retinal microglia under pathological conditions.* Albrecht Von Graefes Arch Klin Exp Ophthalmol, 1975. **196**(1): p. 49-60.
67. Yuan, L. and A.H. Neufeld, *Activated microglia in the human glaucomatous optic nerve head.* J Neurosci Res, 2001. **64**(5): p. 523-32.
68. Zeng, H.Y., W.R. Green, and M.O. Tso, *Microglial activation in human diabetic retinopathy.* Arch Ophthalmol, 2008. **126**(2): p. 227-32.

69. Langmann, T., *Microglia activation in retinal degeneration.* J Leukoc Biol, 2007. **81**(6): p. 1345-51.
70. Yang, L.P., X.A. Zhu, and M.O. Tso, *A possible mechanism of microglia-photoreceptor crosstalk.* Mol Vis, 2007. **13**: p. 2048-57.
71. Boje, K.M. and P.K. Arora, *Microglial-produced nitric oxide and reactive nitrogen oxides mediate neuronal cell death.* Brain Res, 1992. **587**(2): p. 250-6.
72. Chao, C.C., et al., *Interleukin-1 and tumor necrosis factor-alpha synergistically mediate neurotoxicity: involvement of nitric oxide and of N-methyl-D-aspartate receptors.* Brain Behav Immun, 1995. **9**(4): p. 355-65.
73. McGuire, S.O., et al., *Tumor necrosis factor alpha is toxic to embryonic mesencephalic dopamine neurons.* Exp Neurol, 2001. **169**(2): p. 219-30.
74. Roque, R.S., et al., *Retina-derived microglial cells induce photoreceptor cell death in vitro.* Brain Res, 1999. **836**(1-2): p. 110-9.
75. Hanisch, U.K., *Microglia as a source and target of cytokines.* Glia, 2002. **40**(2): p. 140-55.
76. Sawada, M., et al., *Production of tumor necrosis factor-alpha by microglia and astrocytes in culture.* Brain Res, 1989. **491**(2): p. 394-7.
77. Garden, G.A. and T. Moller, *Microglia biology in health and disease.* J Neuroimmune Pharmacol, 2006. **1**(2): p. 127-37.
78. Kataoka, K., et al., *The roles of vitreal macrophages and circulating leukocytes in retinal neovascularization.* Invest Ophthalmol Vis Sci, 2011. **52**(3): p. 1431-8.
79. Ibrahim, A.S., et al., *Genistein attenuates retinal inflammation associated with diabetes by targeting of microglial activation.* Mol Vis, 2010. **16**: p. 2033-42.
80. Krady, J.K., et al., *Minocycline reduces proinflammatory cytokine expression, microglial activation, and caspase-3 activation in a rodent model of diabetic retinopathy.* Diabetes, 2005. **54**(5): p. 1559-65.
81. Bosco, A., et al., *Reduced retina microglial activation and improved optic nerve integrity with minocycline treatment in the DBA/2J mouse model of glaucoma.* Invest Ophthalmol Vis Sci, 2008. **49**(4): p. 1437-46.
82. Neufeld, A.H., *Pharmacologic neuroprotection with an inhibitor of nitric oxide synthase for the treatment of glaucoma.* Brain Res Bull, 2004. **62**(6): p. 455-9.
83. Yang, L.P., et al., *Minocycline delayed photoreceptor death in rds mice through iNOS-dependent mechanism.* Mol Vis, 2007. **13**: p. 1073-82.
84. Chang, C.J., et al., *Minocycline partially inhibits caspase-3 activation and photoreceptor degeneration after photic injury.* Ophthalmic Res, 2005. **37**(4): p. 202-13.
85. Hoppeler, T., et al., *Morphology and time-course of defined photochemical lesions in the rabbit retina.* Curr Eye Res, 1988. **7**(9): p. 849-60.
86. Ni, Y.Q., et al., *Neuroprotective effects of naloxone against light-induced photoreceptor degeneration through inhibiting retinal microglial activation.* Invest Ophthalmol Vis Sci, 2008. **49**(6): p. 2589-98.
87. Bajetto, A., et al., *Characterization of chemokines and their receptors in the central nervous system: physiopathological implications.* J Neurochem, 2002. **82**(6): p. 1311-29.
88. Luster, A.D., *Chemokines--chemotactic cytokines that mediate inflammation.* N Engl J Med, 1998. **338**(7): p. 436-45.
89. Oppenheim, J.J., et al., *Properties of the novel proinflammatory supergene "intercrine" cytokine family.* Annu Rev Immunol, 1991. **9**: p. 617-48.
90. Ransohoff, R.M., A. Glabinski, and M. Tani, *Chemokines in immune-mediated inflammation of the central nervous system.* Cytokine Growth Factor Rev, 1996. **7**(1): p. 35-46.
91. Zlotnik, A. and O. Yoshie, *Chemokines: a new classification system and their role in immunity.* Immunity, 2000. **12**(2): p. 121-7.
92. Comerford, I. and S.R. McColl, *Mini-review series: focus on chemokines.* Immunol Cell Biol, 2011. **89**(2): p. 183-4.

93. Newman, A.M., et al., *Systems-level analysis of age-related macular degeneration reveals global biomarkers and phenotype-specific functional networks.* Genome Med, 2012. **4**(2): p. 16.
94. Ambati, J., et al., *An animal model of age-related macular degeneration in senescent Ccl-2- or Ccr-2-deficient mice.* Nat Med, 2003. **9**(11): p. 1390-7.
95. Luhmann, U.F., et al., *The drusenlike phenotype in aging Ccl2-knockout mice is caused by an accelerated accumulation of swollen autofluorescent subretinal macrophages.* Invest Ophthalmol Vis Sci, 2009. **50**(12): p. 5934-43.
96. Natoli, R., et al., *Gene and noncoding RNA regulation underlying photoreceptor protection: microarray study of dietary antioxidant saffron and photobiomodulation in rat retina.* Mol Vis, 2010. **16**: p. 1801-22.
97. Rutar, M., R. Natoli, and J.M. Provis, *Small interfering RNA-mediated suppression of Ccl2 in Muller cells attenuates microglial recruitment and photoreceptor death following retinal degeneration.* J Neuroinflammation, 2012. **9**: p. 221.
98. Rutar, M., et al., *Early focal expression of the chemokine Ccl2 by Muller cells during exposure to damage-inducing bright continuous light.* Invest Ophthalmol Vis Sci, 2011. **52**(5): p. 2379-88.
99. Rutar, M., et al., *Chemokine-mediated inflammation in the degenerating retina is coordinated by Muller cells, activated microglia, and retinal pigment epithelium.* J Neuroinflammation, 2015. **12**: p. 8.
100. Organisciak, D.T. and D.K. Vaughan, *Retinal light damage: mechanisms and protection.* Prog Retin Eye Res, 2010. **29**(2): p. 113-34.
101. Wenzel, A., et al., *Molecular mechanisms of light-induced photoreceptor apoptosis and neuroprotection for retinal degeneration.* Prog Retin Eye Res, 2005. **24**(2): p. 275-306.
102. Noell, W.K., et al., *Retinal damage by light in rats.* Invest Ophthalmol, 1966. **5**(5): p. 450-73.
103. Glickman, R.D., *Phototoxicity to the retina: mechanisms of damage.* Int J Toxicol, 2002. **21**(6): p. 473-90.
104. Wu, J., S. Seregard, and P.V. Algvere, *Photochemical damage of the retina.* Surv Ophthalmol, 2006. **51**(5): p. 461-81.
105. Rutar, M., J.M. Provis, and K. Valter, *Brief exposure to damaging light causes focal recruitment of macrophages, and long-term destabilization of photoreceptors in the albino rat retina.* Curr Eye Res, 2010. **35**(7): p. 631-43.
106. Abler, A.S., et al., *Photic injury triggers apoptosis of photoreceptor cells.* Res Commun Mol Pathol Pharmacol, 1996. **92**(2): p. 177-89.
107. Demontis, G.C., B. Longoni, and P.L. Marchiafava, *Molecular steps involved in light-induced oxidative damage to retinal rods.* Invest Ophthalmol Vis Sci, 2002. **43**(7): p. 2421-7.
108. Organisciak, D.T., et al., *Retinal light damage in rats with altered levels of rod outer segment docosahexaenoate.* Invest Ophthalmol Vis Sci, 1996. **37**(11): p. 2243-57.
109. Marco-Gomariz, M.A., et al., *Phototoxic-induced photoreceptor degeneration causes retinal ganglion cell degeneration in pigmented rats.* J Comp Neurol, 2006. **498**(2): p. 163-79.
110. Noell, W.K., *Possible mechanisms of photoreceptor damage by light in mammalian eyes.* Vision Res, 1980. **20**(12): p. 1163-71.
111. Rapp, L.M., et al., *Predisposing factors to light-induced photoreceptor cell damage: retinal changes in maturing rats.* Exp Eye Res, 1990. **51**(2): p. 177-84.
112. Tanito, M., et al., *Topography of retinal damage in light-exposed albino rats.* Exp Eye Res, 2008. **87**(3): p. 292-5.
113. Marc, R.E., et al., *Extreme retinal remodeling triggered by light damage: implications for age related macular degeneration.* Mol Vis, 2008. **14**: p. 782-806.
114. Rapaport, D.H. and J. Stone, *The area centralis of the retina in the cat and other mammals: focal point for function and development of the visual system.* Neuroscience, 1984. **11**(2): p. 289-301.

115. Sullivan, R., P. Penfold, and D.V. Pow, *Neuronal migration and glial remodeling in degenerating retinas of aged rats and in nonneovascular AMD.* Invest Ophthalmol Vis Sci, 2003. **44**(2): p. 856-65.
116. Hollyfield, J.G., et al., *Oxidative damage-induced inflammation initiates age-related macular degeneration.* Nat Med, 2008. **14**(2): p. 194-8.
117. Wiegand, R.D., et al., *Evidence for rod outer segment lipid peroxidation following constant illumination of the rat retina.* Invest Ophthalmol Vis Sci, 1983. **24**(10): p. 1433-5.
118. Albarracin, R., J. Eells, and K. Valter, *Photobiomodulation protects the retina from light-induced photoreceptor degeneration.* Invest Ophthalmol Vis Sci, 2011. **52**(6): p. 3582-92.
119. Rutar, M., et al., *Analysis of complement expression in light-induced retinal degeneration: synthesis and deposition of C3 by microglia/macrophages is associated with focal photoreceptor degeneration.* Invest Ophthalmol Vis Sci, 2011. **52**(8): p. 5347-58.
120. Rohrer, B., et al., *Eliminating complement factor D reduces photoreceptor susceptibility to light-induced damage.* Invest Ophthalmol Vis Sci, 2007. **48**(11): p. 5282-9.
121. Anderson, D.H., et al., *The pivotal role of the complement system in aging and age-related macular degeneration: hypothesis re-visited.* Prog Retin Eye Res, 2010. **29**(2): p. 95-112.
122. Donoso, L.A., T. Vrabec, and H. Kuivaniemi, *The role of complement Factor H in age-related macular degeneration: a review.* Surv Ophthalmol, 2010. **55**(3): p. 227-46.
123. Jakobsdottir, J., et al., *C2 and CFB genes in age-related maculopathy and joint action with CFH and LOC387715 genes.* PLoS One, 2008. **3**(5): p. e2199.
124. Gold, B., et al., *Variation in factor B (BF) and complement component 2 (C2) genes is associated with age-related macular degeneration.* Nat Genet, 2006. **38**(4): p. 458-62.
125. Yates, J.R., et al., *Complement C3 variant and the risk of age-related macular degeneration.* N Engl J Med, 2007. **357**(6): p. 553-61.
126. Spencer, K.L., et al., *C3 R102G polymorphism increases risk of age-related macular degeneration.* Hum Mol Genet, 2008. **17**(12): p. 1821-4.
127. Donoso, L.A., et al., *The role of inflammation in the pathogenesis of age-related macular degeneration.* Surv Ophthalmol, 2006. **51**(2): p. 137-52.
128. Hageman, G.S., et al., *An integrated hypothesis that considers drusen as biomarkers of immune-mediated processes at the RPE-Bruch's membrane interface in aging and age-related macular degeneration.* Prog Retin Eye Res, 2001. **20**(6): p. 705-32.
129. Ambros, V., et al., *A uniform system for microRNA annotation.* RNA, 2003. **9**(3): p. 277-9.
130. Lee, R.C., R.L. Feinbaum, and V. Ambros, *The C. elegans heterochronic gene lin-4 encodes small RNAs with antisense complementarity to lin-14.* Cell, 1993. **75**(5): p. 843-54.
131. Reinhart, B.J., et al., *The 21-nucleotide let-7 RNA regulates developmental timing in Caenorhabditis elegans.* Nature, 2000. **403**(6772): p. 901-6.
132. Slack, F.J., et al., *The lin-41 RBCC gene acts in the C. elegans heterochronic pathway between the let-7 regulatory RNA and the LIN-29 transcription factor.* Mol Cell, 2000. **5**(4): p. 659-69.
133. Pasquinelli, A.E., et al., *Conservation of the sequence and temporal expression of let-7 heterochronic regulatory RNA.* Nature, 2000. **408**(6808): p. 86-9.
134. Aravin, A.A., et al., *The small RNA profile during Drosophila melanogaster development.* Dev Cell, 2003. **5**(2): p. 337-50.
135. Bartel, D.P., *MicroRNAs: genomics, biogenesis, mechanism, and function.* Cell, 2004. **116**(2): p. 281-97.
136. Cai, X., C.H. Hagedorn, and B.R. Cullen, *Human microRNAs are processed from capped, polyadenylated transcripts that can also function as mRNAs.* RNA, 2004. **10**(12): p. 1957-66.
137. Lagos-Quintana, M., et al., *New microRNAs from mouse and human.* RNA, 2003. **9**(2): p. 175-9.
138. Ying, S.Y. and S.L. Lin, *Intronic microRNAs.* Biochem Biophys Res Commun, 2005. **326**(3): p. 515-20.

139. Lee, Y., et al., *MicroRNA genes are transcribed by RNA polymerase II.* EMBO J, 2004. **23**(20): p. 4051-60.
140. Lee, Y., et al., *The nuclear RNase III Drosha initiates microRNA processing.* Nature, 2003. **425**(6956): p. 415-9.
141. Luciano, D.J., et al., *RNA editing of a miRNA precursor.* RNA, 2004. **10**(8): p. 1174-7.
142. Zeng, Y. and B.R. Cullen, *Sequence requirements for micro RNA processing and function in human cells.* RNA, 2003. **9**(1): p. 112-23.
143. Basyuk, E., et al., *Human let-7 stem-loop precursors harbor features of RNase III cleavage products.* Nucleic Acids Res, 2003. **31**(22): p. 6593-7.
144. Yi, R., et al., *Exportin-5 mediates the nuclear export of pre-microRNAs and short hairpin RNAs.* Genes Dev, 2003. **17**(24): p. 3011-6.
145. Elbashir, S.M., W. Lendeckel, and T. Tuschl, *RNA interference is mediated by 21- and 22-nucleotide RNAs.* Genes Dev, 2001. **15**(2): p. 188-200.
146. Grishok, A. and C.C. Mello, *RNAi (Nematodes: Caenorhabditis elegans).* Adv Genet, 2002. **46**: p. 339-60.
147. Hutvagner, G. and P.D. Zamore, *A microRNA in a multiple-turnover RNAi enzyme complex.* Science, 2002. **297**(5589): p. 2056-60.
148. Khvorova, A., A. Reynolds, and S.D. Jayasena, *Functional siRNAs and miRNAs exhibit strand bias.* Cell, 2003. **115**(2): p. 209-16.
149. Wightman, B., I. Ha, and G. Ruvkun, *Posttranscriptional regulation of the heterochronic gene lin-14 by lin-4 mediates temporal pattern formation in C. elegans.* Cell, 1993. **75**(5): p. 855-62.
150. Zeng, Y., R. Yi, and B.R. Cullen, *MicroRNAs and small interfering RNAs can inhibit mRNA expression by similar mechanisms.* Proc Natl Acad Sci U S A, 2003. **100**(17): p. 9779-84.
151. Doench, J.G., C.P. Petersen, and P.A. Sharp, *siRNAs can function as miRNAs.* Genes Dev, 2003. **17**(4): p. 438-42.
152. Tang, G., et al., *A biochemical framework for RNA silencing in plants.* Genes Dev, 2003. **17**(1): p. 49-63.
153. Brennecke, J., et al., *bantam encodes a developmentally regulated microRNA that controls cell proliferation and regulates the proapoptotic gene hid in Drosophila.* Cell, 2003. **113**(1): p. 25-36.
154. Chen, C.Z., et al., *MicroRNAs modulate hematopoietic lineage differentiation.* Science, 2004. **303**(5654): p. 83-6.
155. Calin, G.A., et al., *Frequent deletions and down-regulation of micro- RNA genes miR15 and miR16 at 13q14 in chronic lymphocytic leukemia.* Proc Natl Acad Sci U S A, 2002. **99**(24): p. 15524-9.
156. van Rooij, E., et al., *A signature pattern of stress-responsive microRNAs that can evoke cardiac hypertrophy and heart failure.* Proc Natl Acad Sci U S A, 2006. **103**(48): p. 18255-60.
157. Bonauer, A., R.A. Boon, and S. Dimmeler, *Vascular microRNAs.* Curr Drug Targets, 2010. **11**(8): p. 943-9.
158. Gascon, E. and F.B. Gao, *Cause or Effect: Misregulation of microRNA Pathways in Neurodegeneration.* Front Neurosci, 2012. **6**: p. 48.
159. Junker, A., R. Hohlfeld, and E. Meinl, *The emerging role of microRNAs in multiple sclerosis.* Nat Rev Neurol, 2011. **7**(1): p. 56-9.
160. Kanwar, J.R., G. Mahidhara, and R.K. Kanwar, *MicroRNA in human cancer and chronic inflammatory diseases.* Front Biosci (Schol Ed), 2010. **2**: p. 1113-26.
161. Thum, T., *MicroRNA therapeutics in cardiovascular medicine.* EMBO Mol Med, 2012. **4**(1): p. 3-14.
162. Bak, M., et al., *MicroRNA expression in the adult mouse central nervous system.* RNA, 2008. **14**(3): p. 432-44.
163. Kosik, K.S., *The neuronal microRNA system.* Nat Rev Neurosci, 2006. **7**(12): p. 911-20.

164. Krichevsky, A.M., et al., *A microRNA array reveals extensive regulation of microRNAs during brain development.* RNA, 2003. **9**(10): p. 1274-81.
165. Rao, P., E. Benito, and A. Fischer, *MicroRNAs as biomarkers for CNS disease.* Front Mol Neurosci, 2013. **6**: p. 39.
166. Krichevsky, A.M., et al., *Specific microRNAs modulate embryonic stem cell-derived neurogenesis.* Stem Cells, 2006. **24**(4): p. 857-64.
167. Zhao, C., et al., *MicroRNA let-7b regulates neural stem cell proliferation and differentiation by targeting nuclear receptor TLX signaling.* Proc Natl Acad Sci U S A, 2010. **107**(5): p. 1876-81.
168. Nakanishi, K., et al., *Responses of microRNAs 124a and 223 following spinal cord injury in mice.* Spinal Cord, 2010. **48**(3): p. 192-6.
169. Hebert, S.S., et al., *Loss of microRNA cluster miR-29a/b-1 in sporadic Alzheimer's disease correlates with increased BACE1/beta-secretase expression.* Proc Natl Acad Sci U S A, 2008. **105**(17): p. 6415-20.
170. Sethi, P. and W.J. Lukiw, *Micro-RNA abundance and stability in human brain: specific alterations in Alzheimer's disease temporal lobe neocortex.* Neurosci Lett, 2009. **459**(2): p. 100-4.
171. Junn, E., et al., *Repression of alpha-synuclein expression and toxicity by microRNA-7.* Proc Natl Acad Sci U S A, 2009. **106**(31): p. 13052-7.
172. Kim, J., et al., *A MicroRNA feedback circuit in midbrain dopamine neurons.* Science, 2007. **317**(5842): p. 1220-4.
173. Johnson, R., et al., *A microRNA-based gene dysregulation pathway in Huntington's disease.* Neurobiol Dis, 2008. **29**(3): p. 438-45.
174. Packer, A.N., et al., *The bifunctional microRNA miR-9/miR-9* regulates REST and CoREST and is downregulated in Huntington's disease.* J Neurosci, 2008. **28**(53): p. 14341-6.
175. Janeway, C.A., et al., *Signaling through immune system receptors.* 2001.
176. Taganov, K.D., et al., *NF-kappaB-dependent induction of microRNA miR-146, an inhibitor targeted to signaling proteins of innate immune responses.* Proc Natl Acad Sci U S A, 2006. **103**(33): p. 12481-6.
177. Sheedy, F.J., et al., *Negative regulation of TLR4 via targeting of the proinflammatory tumor suppressor PDCD4 by the microRNA miR-21.* Nat Immunol, 2010. **11**(2): p. 141-7.
178. Androulidaki, A., et al., *The kinase Akt1 controls macrophage response to lipopolysaccharide by regulating microRNAs.* Immunity, 2009. **31**(2): p. 220-31.
179. O'Connell, R.M., et al., *MicroRNA-155 is induced during the macrophage inflammatory response.* Proc Natl Acad Sci U S A, 2007. **104**(5): p. 1604-9.
180. Tili, E., et al., *Modulation of miR-155 and miR-125b levels following lipopolysaccharide/TNF-alpha stimulation and their possible roles in regulating the response to endotoxin shock.* J Immunol, 2007. **179**(8): p. 5082-9.
181. O'Connell, R.M., et al., *Inositol phosphatase SHIP1 is a primary target of miR-155.* Proc Natl Acad Sci U S A, 2009. **106**(17): p. 7113-8.
182. Bala, S., et al., *Up-regulation of microRNA-155 in macrophages contributes to increased tumor necrosis factor {alpha} (TNF{alpha}) production via increased mRNA half-life in alcoholic liver disease.* J Biol Chem, 2011. **286**(2): p. 1436-44.
183. Costinean, S., et al., *Src homology 2 domain-containing inositol-5-phosphatase and CCAAT enhancer-binding protein beta are targeted by miR-155 in B cells of Emicro-MiR-155 transgenic mice.* Blood, 2009. **114**(7): p. 1374-82.
184. O'Connell, R.M., et al., *MicroRNA-155 promotes autoimmune inflammation by enhancing inflammatory T cell development.* Immunity, 2010. **33**(4): p. 607-19.
185. O'Connell, R.M., et al., *Sustained expression of microRNA-155 in hematopoietic stem cells causes a myeloproliferative disorder.* J Exp Med, 2008. **205**(3): p. 585-94.
186. Benakanakere, M.R., et al., *Modulation of TLR2 protein expression by miR-105 in human oral keratinocytes.* J Biol Chem, 2009. **284**(34): p. 23107-15.

187. Chen, X.M., et al., *A cellular micro-RNA, let-7i, regulates Toll-like receptor 4 expression and contributes to cholangiocyte immune responses against Cryptosporidium parvum infection.* J Biol Chem, 2007. **282**(39): p. 28929-38.
188. McCoy, C.E., et al., *IL-10 inhibits miR-155 induction by toll-like receptors.* J Biol Chem, 2010. **285**(27): p. 20492-8.
189. Philippe, L., et al., *TLR2 expression is regulated by microRNA miR-19 in rheumatoid fibroblast-like synoviocytes.* J Immunol, 2012. **188**(1): p. 454-61.
190. Bazzoni, F., et al., *Induction and regulatory function of miR-9 in human monocytes and neutrophils exposed to proinflammatory signals.* Proc Natl Acad Sci U S A, 2009. **106**(13): p. 5282-7.
191. Liu, G., et al., *miR-147, a microRNA that is induced upon Toll-like receptor stimulation, regulates murine macrophage inflammatory responses.* Proc Natl Acad Sci U S A, 2009. **106**(37): p. 15819-24.
192. Murphy, A.J., P.M. Guyre, and P.A. Pioli, *Estradiol suppresses NF-kappa B activation through coordinated regulation of let-7a and miR-125b in primary human macrophages.* J Immunol, 2010. **184**(9): p. 5029-37.
193. Rajaram, M.V., et al., *Mycobacterium tuberculosis lipomannan blocks TNF biosynthesis by regulating macrophage MAPK-activated protein kinase 2 (MK2) and microRNA miR-125b.* Proc Natl Acad Sci U S A, 2011. **108**(42): p. 17408-13.
194. Chaudhuri, A.A., et al., *MicroRNA-125b potentiates macrophage activation.* J Immunol, 2011. **187**(10): p. 5062-8.
195. Bhaumik, D., et al., *MicroRNAs miR-146a/b negatively modulate the senescence-associated inflammatory mediators IL-6 and IL-8.* Aging (Albany NY), 2009. **1**(4): p. 402-11.
196. Huang, R.S., et al., *MicroRNA-155 silencing enhances inflammatory response and lipid uptake in oxidized low-density lipoprotein-stimulated human THP-1 macrophages.* J Investig Med, 2010. **58**(8): p. 961-7.
197. Moschos, S.A., et al., *Expression profiling in vivo demonstrates rapid changes in lung microRNA levels following lipopolysaccharide-induced inflammation but not in the anti-inflammatory action of glucocorticoids.* BMC Genomics, 2007. **8**: p. 240.
198. Perry, M.M., et al., *Rapid changes in microRNA-146a expression negatively regulate the IL-1beta-induced inflammatory response in human lung alveolar epithelial cells.* J Immunol, 2008. **180**(8): p. 5689-98.
199. Lukiw, W.J., et al., *Common micro RNAs (miRNAs) target complement factor H (CFH) regulation in Alzheimer's disease (AD) and in age-related macular degeneration (AMD).* Int J Biochem Mol Biol, 2012. **3**(1): p. 105-16.
200. Jennewein, C., et al., *MicroRNA-27b contributes to lipopolysaccharide-mediated peroxisome proliferator-activated receptor gamma (PPARgamma) mRNA destabilization.* J Biol Chem, 2010. **285**(16): p. 11846-53.
201. Zhou, Q., et al., *Regulation of angiogenesis and choroidal neovascularization by members of microRNA-23~27~24 clusters.* Proc Natl Acad Sci U S A, 2011. **108**(20): p. 8287-92.
202. Kaneko, H., et al., *DICER1 deficit induces Alu RNA toxicity in age-related macular degeneration.* Nature, 2011. **471**(7338): p. 325-30.
203. Bouchie, A., *First microRNA mimic enters clinic.* Nat Biotechnol, 2013. **31**(7): p. 577.
204. Janssen, H.L., et al., *Treatment of HCV infection by targeting microRNA.* N Engl J Med, 2013. **368**(18): p. 1685-94.
205. McDonagh, A.F., *Phototherapy: from ancient Egypt to the new millennium.* J Perinatol, 2001. **21 Suppl 1**: p. S7-S12.
206. Coulter, A.H., *Let there be light-and healing.* Alternative & Complementary Therapies, 2003. **9**(6): p. 322-326.
207. Finsen, N.R., *The Red Light Treatment of Small-Pox.* Br Med J, 1895. **2**(1823): p. 1412-4.

208. Moller, K.I., et al., *How Finsen's light cured lupus vulgaris.* Photodermatol Photoimmunol Photomed, 2005. **21**(3): p. 118-24.
209. Mester, E., B. Szende, and P. Gartner, *[The effect of laser beams on the growth of hair in mice].* Radiobiol Radiother (Berl), 1968. **9**(5): p. 621-6.
210. Ball, K.A., P.R. Castello, and R.O. Poyton, *Low intensity light stimulates nitrite-dependent nitric oxide synthesis but not oxygen consumption by cytochrome c oxidase: Implications for phototherapy.* J Photochem Photobiol B, 2011. **102**(3): p. 182-91.
211. Bisht, D., et al., *Effect of low intensity laser radiation on healing of open skin wounds in rats.* Indian J Med Res, 1994. **100**: p. 43-6.
212. Bisht, D., et al., *Effect of helium-neon laser on wound healing.* Indian J Exp Biol, 1999. **37**(2): p. 187-9.
213. Basford, J.R., *Low-energy laser therapy: controversies and new research findings.* Lasers Surg Med, 1989. **9**(1): p. 1-5.
214. Desmet, K.D., et al., *Clinical and experimental applications of NIR-LED photobiomodulation.* Photomed Laser Surg, 2006. **24**(2): p. 121-8.
215. Sommer, A.P., et al., *Biostimulatory windows in low-intensity laser activation: lasers, scanners, and NASA's light-emitting diode array system.* J Clin Laser Med Surg, 2001. **19**(1): p. 29-33.
216. Whelan, H.T., et al., *Effect of NASA light-emitting diode irradiation on wound healing.* J Clin Laser Med Surg, 2001. **19**(6): p. 305-14.
217. Oron, U., et al., *Low-energy laser irradiation reduces formation of scar tissue after myocardial infarction in rats and dogs.* Circulation, 2001. **103**(2): p. 296-301.
218. Avni, D., et al., *Protection of skeletal muscles from ischemic injury: low-level laser therapy increases antioxidant activity.* Photomed Laser Surg, 2005. **23**(3): p. 273-7.
219. Lakyova, L., et al., *Low-level laser therapy for protection against skeletal muscle damage after ischemia-reperfusion injury in rat hindlimbs.* Lasers Surg Med, 2010. **42**(9): p. 665-72.
220. Quirk, B.J., et al., *Therapeutic effect of near infrared (NIR) light on Parkinson's disease models.* Front Biosci (Elite Ed), 2012. **4**: p. 818-23.
221. Rojas, J.C., A.K. Bruchey, and F. Gonzalez-Lima, *Low-level light therapy improves cortical metabolic capacity and memory retention.* J Alzheimers Dis, 2012. **32**(3): p. 741-52.
222. Fitzgerald, M., et al., *Near infrared light reduces oxidative stress and preserves function in CNS tissue vulnerable to secondary degeneration following partial transection of the optic nerve.* J Neurotrauma, 2010. **27**(11): p. 2107-19.
223. Quirk, B.J., et al., *Near-infrared photobiomodulation in an animal model of traumatic brain injury: improvements at the behavioral and biochemical levels.* Photomed Laser Surg, 2012. **30**(9): p. 523-9.
224. Wong-Riley, M.T., et al., *Photobiomodulation directly benefits primary neurons functionally inactivated by toxins: role of cytochrome c oxidase.* J Biol Chem, 2005. **280**(6): p. 4761-71.
225. Ying, R., et al., *Pretreatment with near-infrared light via light-emitting diode provides added benefit against rotenone- and MPP+-induced neurotoxicity.* Brain Res, 2008. **1243**: p. 167-73.
226. Muili, K.A., et al., *Amelioration of experimental autoimmune encephalomyelitis in C57BL/6 mice by photobiomodulation induced by 670 nm light.* PLoS One, 2012. **7**(1): p. e30655.
227. Whelan, H.T., et al., *NASA light-emitting diodes for the prevention of oral mucositis in pediatric bone marrow transplant patients.* J Clin Laser Med Surg, 2002. **20**(6): p. 319-24.
228. Sommer, A.P., *A novel approach for addressing Alzheimer's disease: the chemo-optical synergism.* J Neurosci Res, 2012. **90**(7): p. 1297-8.
229. Shaw, V.E., et al., *Neuroprotection of midbrain dopaminergic cells in MPTP-treated mice after near-infrared light treatment.* J Comp Neurol, 2010. **518**(1): p. 25-40.
230. Eells, J.T., et al. *Photobiomodulation for the treatment of retinal injury and retinal degenerative diseases*. in *Proceedings of Light-Activated Tissue Regeneration and Therapy Conference*. 2008. Springer.

231. Eells, J.T., et al., *Therapeutic photobiomodulation for methanol-induced retinal toxicity.* Proc Natl Acad Sci U S A, 2003. **100**(6): p. 3439-44.
232. Tang, J., et al., *Low-intensity far-red light inhibits early lesions that contribute to diabetic retinopathy: in vivo and in vitro.* Invest Ophthalmol Vis Sci, 2013. **54**(5): p. 3681-90.
233. Albarracin, R. and K. Valter, *670 nm red light preconditioning supports Muller cell function: evidence from the white light-induced damage model in the rat retina.* Photochem Photobiol, 2012. **88**(6): p. 1418-27.
234. Albarracin, R.S. and K. Valter, *Treatment with 670-nm light protects the cone photoreceptors from white light-induced degeneration.* Adv Exp Med Biol, 2012. **723**: p. 121-8.
235. Qu, C., et al., *Near-infrared light protect the photoreceptor from light-induced damage in rats.* Adv Exp Med Biol, 2010. **664**: p. 365-74.
236. Rutar, M., et al., *670-nm light treatment reduces complement propagation following retinal degeneration.* J Neuroinflammation, 2012. **9**: p. 257.
237. Begum, R., et al., *Treatment with 670 nm light up regulates cytochrome C oxidase expression and reduces inflammation in an age-related macular degeneration model.* PLoS One, 2013. **8**(2): p. e57828.
238. Kokkinopoulos, I., *670 nm LED ameliorates inflammation in the CFH(-/-) mouse neural retina.* J Photochem Photobiol B, 2013. **122**: p. 24-31.
239. Kokkinopoulos, I., et al., *Age-related retinal inflammation is reduced by 670 nm light via increased mitochondrial membrane potential.* Neurobiol Aging, 2013. **34**(2): p. 602-9.
240. Fitzgerald, M., et al., *Red/near-infrared irradiation therapy for treatment of central nervous system injuries and disorders.* Rev Neurosci, 2013. **24**(2): p. 205-26.
241. Hamblin, M.R. and T.N. Demidova. *Mechanisms of low level light therapy*. in *Biomedical Optics 2006*. 2006. International Society for Optics and Photonics.
242. Ankri, R., R. Lubart, and H. Taitelbaum, *Estimation of the optimal wavelengths for laser-induced wound healing.* Lasers Surg Med, 2010. **42**(8): p. 760-4.
243. Parrish, J.A., *New concepts in therapeutic photomedicine: photochemistry, optical targeting and the therapeutic window.* J Invest Dermatol, 1981. **77**(1): p. 45-50.
244. Karu, T., *Primary and secondary mechanisms of action of visible to near-IR radiation on cells.* J Photochem Photobiol B, 1999. **49**(1): p. 1-17.
245. Rhee, S.G., *Redox signaling: hydrogen peroxide as intracellular messenger.* Exp Mol Med, 1999. **31**(2): p. 53-9.
246. Karu, T.I. and S.F. Kolyakov, *Exact action spectra for cellular responses relevant to phototherapy.* Photomed Laser Surg, 2005. **23**(4): p. 355-61.
247. Fontanesi, F., et al., *Assembly of mitochondrial cytochrome c-oxidase, a complicated and highly regulated cellular process.* Am J Physiol Cell Physiol, 2006. **291**(6): p. C1129-47.
248. Šimunovic, Z. and E.M.L. Association, *Lasers in Medicine and Dentistry: Basic Science and Up-to-date Clinical Application of Low Energy-level Laser Therapy LLLT*. 2000: European Medical Laser Association.
249. Huang, Y.Y., et al., *Biphasic dose response in low level light therapy.* Dose Response, 2009. **7**(4): p. 358-83.
250. Karu, T.I., L.V. Pyatibrat, and N.I. Afanasyeva, *Cellular effects of low power laser therapy can be mediated by nitric oxide.* Lasers Surg Med, 2005. **36**(4): p. 307-14.
251. Poyton, R.O. and K.A. Ball, *Therapeutic photobiomodulation: nitric oxide and a novel function of mitochondrial cytochrome c oxidase.* Discov Med, 2011. **11**(57): p. 154-9.
252. Mason, M.G., et al., *Nitric oxide inhibition of respiration involves both competitive (heme) and noncompetitive (copper) binding to cytochrome c oxidase.* Proc Natl Acad Sci U S A, 2006. **103**(3): p. 708-13.
253. Zhang, Y., et al., *cDNA microarray analysis of gene expression profiles in human fibroblast cells irradiated with red light.* J Invest Dermatol, 2003. **120**(5): p. 849-57.

254. Eells, J.T., et al., *Mitochondrial signal transduction in accelerated wound and retinal healing by near-infrared light therapy.* Mitochondrion, 2004. **4**(5): p. 559-567.
255. Liang, H.L., et al., *Near-infrared light via light-emitting diode treatment is therapeutic against rotenone- and 1-methyl-4-phenylpyridinium ion-induced neurotoxicity.* Neuroscience, 2008. **153**(4): p. 963-74.
256. Peoples, C., et al., *Survival of Dopaminergic Amacrine Cells after Near-Infrared Light Treatment in MPTP-Treated Mice.* ISRN Neurol, 2012. **2012**: p. 850150.
257. Whelan, H.T., et al., *Effect of NASA light-emitting diode irradiation on molecular changes for wound healing in diabetic mice.* J Clin Laser Med Surg, 2003. **21**(2): p. 67-74.
258. Johnson, C.D., et al., *The let-7 microRNA represses cell proliferation pathways in human cells.* Cancer Res, 2007. **67**(16): p. 7713-22.
259. Chang, T.C., et al., *Transactivation of miR-34a by p53 broadly influences gene expression and promotes apoptosis.* Mol Cell, 2007. **26**(5): p. 745-52.
260. O'Connell, R.M., D.S. Rao, and D. Baltimore, *microRNA regulation of inflammatory responses.* Annu Rev Immunol, 2012. **30**: p. 295-312.
261. Pogue, A.I., J.M. Hill, and W.J. Lukiw, *MicroRNA (miRNA): Sequence and stability, viroid-like properties, and disease association in the CNS.* Brain Res, 2014.
262. Klein, R.J., et al., *Complement factor H polymorphism in age-related macular degeneration.* Science, 2005. **308**(5720): p. 385-9.
263. Fritsche, L.G., et al., *Age-Related Macular Degeneration: Genetics and Biology Coming Together.* Annu Rev Genomics Hum Genet, 2014.
264. Rutar, M., et al., *Synthesis and propagation of complement C3 by microglia/monocytes in the aging retina.* PLoS One, 2014. **9**(4): p. e93343.
265. Sonkoly, E., M. Stahle, and A. Pivarcsi, *MicroRNAs and immunity: novel players in the regulation of normal immune function and inflammation.* Semin Cancer Biol, 2008. **18**(2): p. 131-40.
266. O'Neill, L.A., F.J. Sheedy, and C.E. McCoy, *MicroRNAs: the fine-tuners of Toll-like receptor signalling.* Nat Rev Immunol, 2011. **11**(3): p. 163-75.
267. Du, F., et al., *MicroRNA-155 Deficiency Results in Decreased Macrophage Inflammation and Attenuated Atherogenesis in Apolipoprotein E-Deficient Mice.* Arterioscler Thromb Vasc Biol, 2014. **34**(4): p. 759-67.
268. Battelle, B.A. and M.M. LaVail, *Rhodopsin content and rod outer segment length in albino rat eyes: modification by dark adaptation.* Exp Eye Res, 1978. **26**(4): p. 487-97.
269. Ortin-Martinez, A., et al., *Automated quantification and topographical distribution of the whole population of S- and L-cones in adult albino and pigmented rats.* Invest Ophthalmol Vis Sci, 2010. **51**(6): p. 3171-83.
270. Tezel, G., et al., *Mechanisms of immune system activation in glaucoma: oxidative stress-stimulated antigen presentation by the retina and optic nerve head glia.* Invest Ophthalmol Vis Sci, 2007. **48**(2): p. 705-14.
271. Bringmann, A., et al., *Cellular signaling and factors involved in Muller cell gliosis: neuroprotective and detrimental effects.* Prog Retin Eye Res, 2009. **28**(6): p. 423-51.
272. Zhang, C., et al., *Activation of microglia and chemokines in light-induced retinal degeneration.* Mol Vis, 2005. **11**: p. 887-95.
273. Chen, L., et al., *Light damage induced changes in mouse retinal gene expression.* Exp Eye Res, 2004. **79**(2): p. 239-47.
274. Jonas, J.B., et al., *Monocyte chemoattractant protein 1, intercellular adhesion molecule 1, and vascular cell adhesion molecule 1 in exudative age-related macular degeneration.* Arch Ophthalmol, 2010. **128**(10): p. 1281-6.
275. Raoul, W., et al., *CCL2/CCR2 and CX3CL1/CX3CR1 chemokine axes and their possible involvement in age-related macular degeneration.* J Neuroinflammation, 2010. **7**: p. 87.

276. Bustin, S.A. and T. Nolan, *Pitfalls of quantitative real-time reverse-transcription polymerase chain reaction.* J Biomol Tech, 2004. **15**(3): p. 155-66.
277. Li, X., et al., *MicroRNA-351 regulates TMEM 59 (DCF1) expression and mediates neural stem cell morphogenesis.* RNA Biol, 2012. **9**(3): p. 292-301.
278. Chen, Y., et al., *MiR-351 transiently increases during muscle regeneration and promotes progenitor cell proliferation and survival upon differentiation.* Physiol Genomics, 2012. **44**(21): p. 1042-51.
279. He, T., et al., *MicroRNA-542-3p inhibits tumour angiogenesis by targeting angiopoietin-2.* J Pathol, 2014. **232**(5): p. 499-508.
280. van den Borne, P., et al., *The multifaceted functions of CXCL10 in cardiovascular disease.* Biomed Res Int, 2014. **2014**: p. 893106.
281. Oh, H., et al., *The potential angiogenic role of macrophages in the formation of choroidal neovascular membranes.* Invest Ophthalmol Vis Sci, 1999. **40**(9): p. 1891-8.
282. Theodossiadis, P.G., et al., *Intravitreal administration of the anti-tumor necrosis factor agent infliximab for neovascular age-related macular degeneration.* Am J Ophthalmol, 2009. **147**(5): p. 825-30, 830 e1.
283. Kutty, R.K., et al., *Inflammatory cytokines regulate microRNA-155 expression in human retinal pigment epithelial cells by activating JAK/STAT pathway.* Biochem Biophys Res Commun, 2010. **402**(2): p. 390-5.
284. Lukiw, W.J. and P.N. Alexandrov, *Regulation of complement factor H (CFH) by multiple miRNAs in Alzheimer's disease (AD) brain.* Mol Neurobiol, 2012. **46**(1): p. 11-9.
285. Ponomarev, E.D., T. Veremeyko, and H.L. Weiner, *MicroRNAs are universal regulators of differentiation, activation, and polarization of microglia and macrophages in normal and diseased CNS.* Glia, 2013. **61**(1): p. 91-103.
286. Elton, T.S., et al., *Regulation of the MIR155 host gene in physiological and pathological processes.* Gene, 2013. **532**(1): p. 1-12.
287. Montalban, E., et al., *MiR-21 is an Ngf-Modulated MicroRNA That Supports Ngf Signaling and Regulates Neuronal Degeneration in PC12 Cells.* Neuromolecular Med, 2014.
288. LaVail, M.M., et al., *Multiple growth factors, cytokines, and neurotrophins rescue photoreceptors from the damaging effects of constant light.* Proc Natl Acad Sci U S A, 1992. **89**(23): p. 11249-53.
289. Li, X., et al., *CHST1 and CHST2 sulfotransferase expression by vascular endothelial cells regulates shear-resistant leukocyte rolling via L-selectin.* J Leukoc Biol, 2001. **69**(4): p. 565-74.
290. Coskun, M., et al., *miR-20b, miR-98, miR-125b-1*, and let-7e* as new potential diagnostic biomarkers in ulcerative colitis.* World J Gastroenterol, 2013. **19**(27): p. 4289-99.
291. Gubern, C., et al., *miRNA expression is modulated over time after focal ischaemia: up-regulation of miR-347 promotes neuronal apoptosis.* FEBS J, 2013. **280**(23): p. 6233-46.
292. Ren, X.S., et al., *Tumor-suppressive microRNA-449a induces growth arrest and senescence by targeting E2F3 in human lung cancer cells.* Cancer Lett, 2014. **344**(2): p. 195-203.
293. Wei, B., et al., *microRNA-449a functions as a tumor-suppressor in gastric adenocarcinoma by targeting Bcl-2.* Oncol Lett, 2013. **6**(6): p. 1713-1718.
294. Chatterjee, S., et al., *Target-mediated protection of endogenous microRNAs in C. elegans.* Dev Cell, 2011. **20**(3): p. 388-96.
295. Lumayag, S., et al., *Inactivation of the microRNA-183/96/182 cluster results in syndromic retinal degeneration.* Proc Natl Acad Sci U S A, 2013. **110**(6): p. E507-16.
296. Krol, J., et al., *Characterizing light-regulated retinal microRNAs reveals rapid turnover as a common property of neuronal microRNAs.* Cell, 2010. **141**(4): p. 618-31.
297. Wang, S., et al., *miRNAs as potential therapeutic targets for age-related macular degeneration.* Future Med Chem, 2012. **4**(3): p. 277-87.
298. Bartel, D.P. and C.Z. Chen, *Micromanagers of gene expression: the potentially widespread influence of metazoan microRNAs.* Nat Rev Genet, 2004. **5**(5): p. 396-400.

299. Ebert, M.S. and P.A. Sharp, *Roles for microRNAs in conferring robustness to biological processes.* Cell, 2012. **149**(3): p. 515-24.
300. Naidu, S., P. Magee, and M. Garofalo, *MiRNA-based therapeutic intervention of cancer.* J Hematol Oncol, 2015. **8**(1): p. 68.
301. Marques-Rocha, J.L., et al., *Noncoding RNAs, cytokines, and inflammation-related diseases.* FASEB J, 2015.
302. Bader, A.G. and P. Lammers, *The therapeutic potential of microRNAs.* Innovations in Pharmaceutical Technology, 2011: p. 52-55.
303. Sun, Y., et al., *An updated role of microRNA-124 in central nervous system disorders: a review.* Front Cell Neurosci, 2015. **9**: p. 193.
304. Wang, D., et al., *MicroRNA-124 controls the proliferative, migratory, and inflammatory phenotype of pulmonary vascular fibroblasts.* Circ Res, 2014. **114**(1): p. 67-78.
305. Kawano, S. and Y. Nakamachi, *miR-124a as a key regulator of proliferation and MCP-1 secretion in synoviocytes from patients with rheumatoid arthritis.* Ann Rheum Dis, 2011. **70 Suppl 1**: p. i88-91.
306. Saxena, K., et al., *Identification of miRNAs in a Model of Retinal Degenerations.* Invest Ophthalmol Vis Sci, 2015. **56**(3): p. 1820-9.
307. Gao, H., et al., *Safety of intravitreal voriconazole: electroretinographic and histopathologic studies.* Trans Am Ophthalmol Soc, 2003. **101**: p. 183-9; discussion 189.
308. Abdellatif, M., *Differential expression of microRNAs in different disease states.* Circ Res, 2012. **110**(4): p. 638-50.
309. Ardekani, A.M. and M.M. Naeini, *The Role of MicroRNAs in Human Diseases.* Avicenna J Med Biotechnol, 2010. **2**(4): p. 161-79.
310. Deo, M., et al., *Detection of mammalian microRNA expression by in situ hybridization with RNA oligonucleotides.* Dev Dyn, 2006. **235**(9): p. 2538-48.
311. Smirnova, L., et al., *Regulation of miRNA expression during neural cell specification.* Eur J Neurosci, 2005. **21**(6): p. 1469-77.
312. Ponomarev, E.D., et al., *MicroRNA-124 promotes microglia quiescence and suppresses EAE by deactivating macrophages via the C/EBP-alpha-PU.1 pathway.* Nat Med, 2011. **17**(1): p. 64-70.
313. Arora, A., G.J. McKay, and D.A. Simpson, *Prediction and verification of miRNA expression in human and rat retinas.* Invest Ophthalmol Vis Sci, 2007. **48**(9): p. 3962-7.
314. Karali, M., et al., *Identification and characterization of microRNAs expressed in the mouse eye.* Invest Ophthalmol Vis Sci, 2007. **48**(2): p. 509-15.
315. Takada, S., et al., *Mouse microRNA profiles determined with a new and sensitive cloning method.* Nucleic Acids Res, 2006. **34**(17): p. e115.
316. Nakamachi, Y., et al., *MicroRNA-124a is a key regulator of proliferation and monocyte chemoattractant protein 1 secretion in fibroblast-like synoviocytes from patients with rheumatoid arthritis.* Arthritis Rheum, 2009. **60**(5): p. 1294-304.
317. Oh, J.W., L.M. Schwiebert, and E.N. Benveniste, *Cytokine regulation of CC and CXC chemokine expression by human astrocytes.* J Neurovirol, 1999. **5**(1): p. 82-94.
318. Chou, R.C., et al., *Lipid-cytokine-chemokine cascade drives neutrophil recruitment in a murine model of inflammatory arthritis.* Immunity, 2010. **33**(2): p. 266-78.
319. Calkins, C.M., et al., *IL-1 regulates in vivo C-X-C chemokine induction and neutrophil sequestration following endotoxemia.* J Endotoxin Res, 2002. **8**(1): p. 59-67.
320. Rutar, M., et al., *Chemokine-mediated inflammation in the degenerating retina is coordinated by Muller cells, activated microglia, and retinal pigment epithelium.* J Neuroinflammation, 2015. **12**(1): p. 8.
321. Gigo-Benato, D., S. Geuna, and S. Rochkind, *Phototherapy for enhancing peripheral nerve repair: a review of the literature.* Muscle Nerve, 2005. **31**(6): p. 694-701.

322. Irvine, J., et al., *Double-blind randomized controlled trial of low-level laser therapy in carpal tunnel syndrome.* Muscle Nerve, 2004. **30**(2): p. 182-7.
323. Neiburger, E.J., *Rapid healing of gingival incisions by the helium-neon diode laser.* J Mass Dent Soc, 1999. **48**(1): p. 8-13, 40.
324. Papageorgiou, P., A. Katsambas, and A. Chu, *Phototherapy with blue (415 nm) and red (660 nm) light in the treatment of acne vulgaris.* Br J Dermatol, 2000. **142**(5): p. 973-8.
325. Schindl, A., et al., *Low intensity laser irradiation in the treatment of recalcitrant radiation ulcers in patients with breast cancer--long-term results of 3 cases.* Photodermatol Photoimmunol Photomed, 2000. **16**(1): p. 34-7.
326. Oron, U., et al., *Attenuation of infarct size in rats and dogs after myocardial infarction by low-energy laser irradiation.* Lasers Surg Med, 2001. **28**(3): p. 204-11.
327. Sommer, A.P., et al., *670 nm laser light and EGCG complementarily reduce amyloid-beta aggregates in human neuroblastoma cells: basis for treatment of Alzheimer's disease?* Photomed Laser Surg, 2012. **30**(1): p. 54-60.
328. Simunovic, Z., A.D. Ivankovich, and A. Depolo, *Wound healing of animal and human body sport and traffic accident injuries using low-level laser therapy treatment: a randomized clinical study of seventy-four patients with control group.* J Clin Laser Med Surg, 2000. **18**(2): p. 67-73.
329. Chung, H., et al., *The nuts and bolts of low-level laser (light) therapy.* Ann Biomed Eng, 2012. **40**(2): p. 516-33.
330. Hashmi, J.T., et al., *Role of low-level laser therapy in neurorehabilitation.* PM R, 2010. **2**(12 Suppl 2): p. S292-305.
331. Karu, T.I., L.V. Pyatibrat, and G.S. Kalendo, *Photobiological modulation of cell attachment via cytochrome c oxidase.* Photochem Photobiol Sci, 2004. **3**(2): p. 211-6.
332. Lapchak, P.A. and L. De Taboada, *Transcranial near infrared laser treatment (NILT) increases cortical adenosine-5'-triphosphate (ATP) content following embolic strokes in rabbits.* Brain Res, 2010. **1306**: p. 100-5.
333. Wong-Riley, M.T., et al., *Light-emitting diode treatment reverses the effect of TTX on cytochrome oxidase in neurons.* Neuroreport, 2001. **12**(14): p. 3033-7.
334. Hecker, L.A., et al., *Genetic control of the alternative pathway of complement in humans and age-related macular degeneration.* Hum Mol Genet, 2010. **19**(1): p. 209-15.
335. Reynolds, R., et al., *Plasma complement components and activation fragments: associations with age-related macular degeneration genotypes and phenotypes.* Invest Ophthalmol Vis Sci, 2009. **50**(12): p. 5818-27.
336. Scholl, H.P., et al., *Systemic complement activation in age-related macular degeneration.* PLoS One, 2008. **3**(7): p. e2593.
337. Seddon, J.M., G. Gensler, and B. Rosner, *C-reactive protein and CFH, ARMS2/HTRA1 gene variants are independently associated with risk of macular degeneration.* Ophthalmology, 2010. **117**(8): p. 1560-6.
338. Stanton, C.M., et al., *Complement factor D in age-related macular degeneration.* Invest Ophthalmol Vis Sci, 2011. **52**(12): p. 8828-34.
339. Kohno, H., et al., *CCL3 production by microglial cells modulates disease severity in murine models of retinal degeneration.* J Immunol, 2014. **192**(8): p. 3816-27.
340. Taub, D.D. and J.J. Oppenheim, *Chemokines, inflammation and the immune system.* Ther Immunol, 1994. **1**(4): p. 229-46.
341. Amat, M., et al., *Pharmacological blockade of CCR1 ameliorates murine arthritis and alters cytokine networks in vivo.* Br J Pharmacol, 2006. **149**(6): p. 666-75.
342. Braunersreuther, V., et al., *Ccr5 but not Ccr1 deficiency reduces development of diet-induced atherosclerosis in mice.* Arterioscler Thromb Vasc Biol, 2007. **27**(2): p. 373-9.
343. Broxmeyer, H.E., et al., *Dominant myelopoietic effector functions mediated by chemokine receptor CCR1.* J Exp Med, 1999. **189**(12): p. 1987-92.

344. Weber, C., et al., *Specialized roles of the chemokine receptors CCR1 and CCR5 in the recruitment of monocytes and T(H)1-like/CD45RO(+) T cells.* Blood, 2001. **97**(4): p. 1144-6.
345. Zhao, Q., *Dual targeting of CCR2 and CCR5: therapeutic potential for immunologic and cardiovascular diseases.* J Leukoc Biol, 2010. **88**(1): p. 41-55.
346. Jia, T., et al., *Additive roles for MCP-1 and MCP-3 in CCR2-mediated recruitment of inflammatory monocytes during Listeria monocytogenes infection.* J Immunol, 2008. **180**(10): p. 6846-53.
347. Tsou, C.L., et al., *Critical roles for CCR2 and MCP-3 in monocyte mobilization from bone marrow and recruitment to inflammatory sites.* J Clin Invest, 2007. **117**(4): p. 902-9.
348. Burdon, P.C., C. Martin, and S.M. Rankin, *Migration across the sinusoidal endothelium regulates neutrophil mobilization in response to ELR + CXC chemokines.* Br J Haematol, 2008. **142**(1): p. 100-8.
349. Eash, K.J., et al., *CXCR2 and CXCR4 antagonistically regulate neutrophil trafficking from murine bone marrow.* J Clin Invest, 2010. **120**(7): p. 2423-31.
350. Opdenakker, G., W.E. Fibbe, and J. Van Damme, *The molecular basis of leukocytosis.* Immunol Today, 1998. **19**(4): p. 182-9.
351. Zhou, J., et al., *Neutrophils promote experimental choroidal neovascularization.* Mol Vis, 2005. **11**: p. 414-24.
352. Deshmane, S.L., et al., *Monocyte chemoattractant protein-1 (MCP-1): an overview.* J Interferon Cytokine Res, 2009. **29**(6): p. 313-26.
353. Yoshimura, T., et al., *Purification and amino acid analysis of two human glioma-derived monocyte chemoattractants.* J Exp Med, 1989. **169**(4): p. 1449-59.
354. Zhang, R., et al., *Near infrared light protects cardiomyocytes from hypoxia and reoxygenation injury by a nitric oxide dependent mechanism.* J Mol Cell Cardiol, 2009. **46**(1): p. 4-14.
355. Pilz, R.B., et al., *Nitric oxide and cGMP analogs activate transcription from AP-1-responsive promoters in mammalian cells.* FASEB J, 1995. **9**(7): p. 552-8.
356. Cooper, C.E., *Nitric oxide and cytochrome oxidase: substrate, inhibitor or effector?* Trends Biochem Sci, 2002. **27**(1): p. 33-9.
357. Unitt, D.C., et al., *Inactivation of nitric oxide by cytochrome c oxidase under steady-state oxygen conditions.* Biochim Biophys Acta, 2010. **1797**(3): p. 371-7.
358. Moriyama, Y., et al., *In vivo effects of low level laser therapy on inducible nitric oxide synthase.* Lasers Surg Med, 2009. **41**(3): p. 227-31.
359. Moriyama, Y., et al., *In vivo study of the inflammatory modulating effects of low-level laser therapy on iNOS expression using bioluminescence imaging.* Photochem Photobiol, 2005. **81**(6): p. 1351-5.
360. Boelens, R., et al., *EPR studies of the photodissociation reactions of cytochrome c oxidase-nitric oxide complexes.* Biochim Biophys Acta, 1982. **679**(1): p. 84-94.
361. Busskamp, V., et al., *Rapid Turnover Of Light-regulated Retinal MicroRNAs.* Investigative Ophthalmology & Visual Science, 2011. **52**(14): p. 4117-4117.
362. Guo, Y., et al., *Characterization of the mammalian miRNA turnover landscape.* Nucleic acids research, 2015: p. gkv057.
363. Anderson, O.A., A. Finkelstein, and D.T. Shima, *A2E induces IL-1ss production in retinal pigment epithelial cells via the NLRP3 inflammasome.* PLoS One, 2013. **8**(6): p. e67263.
364. de Oliveira Dias, J.R., et al., *Cytokines in neovascular age-related macular degeneration: fundamentals of targeted combination therapy.* Br J Ophthalmol, 2011. **95**(12): p. 1631-7.
365. Nakazawa, T., et al., *Tumor necrosis factor-alpha mediates photoreceptor death in a rodent model of retinal detachment.* Invest Ophthalmol Vis Sci, 2011. **52**(3): p. 1384-91.
366. Tseng, W.A., et al., *NLRP3 inflammasome activation in retinal pigment epithelial cells by lysosomal destabilization: implications for age-related macular degeneration.* Invest Ophthalmol Vis Sci, 2013. **54**(1): p. 110-20.

367. Wan, L., et al., *Tumor necrosis factor-alpha gene polymorphisms in age-related macular degeneration.* Retina, 2010. **30**(10): p. 1595-600.
368. Hu, S.J., et al., *Upregulation of P2RX7 in Cx3cr1-Deficient Mononuclear Phagocytes Leads to Increased Interleukin-1 beta Secretion and Photoreceptor Neurodegeneration.* Journal of Neuroscience, 2015. **35**(18): p. 6987-6996.
369. Magnusson, K.P., et al., *CFH Y402H confers similar risk of soft drusen and both forms of advanced AMD.* PLoS Med, 2006. **3**(1): p. e5.
370. Xu, S., et al., *MicroRNA (miRNA) transcriptome of mouse retina and identification of a sensory organ-specific miRNA cluster.* J Biol Chem, 2007. **282**(34): p. 25053-66.
371. Zhu, Q., et al., *Sponge transgenic mouse model reveals important roles for the microRNA-183 (miR-183)/96/182 cluster in postmitotic photoreceptors of the retina.* J Biol Chem, 2011. **286**(36): p. 31749-60.
372. Ubhi, K., et al., *Widespread microRNA dysregulation in multiple system atrophy - disease-related alteration in miR-96.* Eur J Neurosci, 2014. **39**(6): p. 1026-41.
373. Kye, M.J., et al., *SMN regulates axonal local translation via miR-183/mTOR pathway.* Hum Mol Genet, 2014. **23**(23): p. 6318-31.
374. Jiang, L., et al., *miR-182 as a prognostic marker for glioma progression and patient survival.* Am J Pathol, 2010. **177**(1): p. 29-38.
375. Song, L., et al., *TGF-beta induces miR-182 to sustain NF-kappaB activation in glioma subsets.* J Clin Invest, 2012. **122**(10): p. 3563-78.
376. Weeraratne, S.D., et al., *Pleiotropic effects of miR-183~96~182 converge to regulate cell survival, proliferation and migration in medulloblastoma.* Acta Neuropathol, 2012. **123**(4): p. 539-52.
377. Yan, Z., et al., *miR-96/HBP1/Wnt/beta-catenin regulatory circuitry promotes glioma growth.* FEBS Lett, 2014. **588**(17): p. 3038-46.
378. Tanaka, H., et al., *MicroRNA-183 upregulates HIF-1alpha by targeting isocitrate dehydrogenase 2 (IDH2) in glioma cells.* J Neurooncol, 2013. **111**(3): p. 273-83.
379. Ueno, K., et al., *microRNA-183 is an oncogene targeting Dkk-3 and SMAD4 in prostate cancer.* Br J Cancer, 2013. **108**(8): p. 1659-67.
380. Karali, M., et al., *miRNeye: a microRNA expression atlas of the mouse eye.* BMC Genomics, 2010. **11**: p. 715.
381. Ryan, D.G., M. Oliveira-Fernandes, and R.M. Lavker, *MicroRNAs of the mammalian eye display distinct and overlapping tissue specificity.* Mol Vis, 2006. **12**: p. 1175-84.
382. Hackler, L., Jr., et al., *MicroRNA profile of the developing mouse retina.* Invest Ophthalmol Vis Sci, 2010. **51**(4): p. 1823-31.
383. Kovacs, B., et al., *MicroRNAs in early diabetic retinopathy in streptozotocin-induced diabetic rats.* Invest Ophthalmol Vis Sci, 2011. **52**(7): p. 4402-9.
384. Loscher, C.J., et al., *Altered retinal microRNA expression profile in a mouse model of retinitis pigmentosa.* Genome Biol, 2007. **8**(11): p. R248.
385. Loscher, C.J., et al., *A common microRNA signature in mouse models of retinal degeneration.* Exp Eye Res, 2008. **87**(6): p. 529-34.
386. McArthur, K., et al., *MicroRNA-200b regulates vascular endothelial growth factor-mediated alterations in diabetic retinopathy.* Diabetes, 2011. **60**(4): p. 1314-23.
387. Wu, J.H., et al., *Altered microRNA expression profiles in retinas with diabetic retinopathy.* Ophthalmic Res, 2012. **47**(4): p. 195-201.
388. Wang, S.S., et al., *miRNAs as potential therapeutic targets for age-related macular degeneration.* Future Medicinal Chemistry, 2012. **4**(3): p. 277-287.
389. Zhang, C. and R.B. Darnell, *Mapping in vivo protein-RNA interactions at single-nucleotide resolution from HITS-CLIP data.* Nat Biotechnol, 2011. **29**(7): p. 607-14.

APPENDIX

Table: mRNA targets of the differentially expressed miRNAs

	mmu-miR-125b-3p	**mmu-miR-220**	**mmu-miR-467d**	**mmu-miR-466h**	**rno-miR-347**	**mmu-miR-351**	**mmu-miR-467c**	**mmu-miR-542-3p**	**mmu-miR-207**	**mmu-miR-509-3p**	**mmu-miR-155**	**mmu-miR-685**	**mmu-miR-449a**	**mmu-miR-742**	**mmu-miR-494**	**mmu-miR-582-3p**	**mmu-miR-335-3p**
1	Abhd12	Abhd12	Adpgk	Abhd12	Agtpbp1	Acads	Adfp	Agt	Acbd4	Aldh5a1	Acta1	Acta1	Aldh5a1	Abca4	Adam25	Abca8a	Aass
2	Adk	Abhd5	Agtpbp1	Acbd4	Angptl4	Acss1	Adpgk	Ahcy	Aldob	Alox5ap	Agtpbp1	Adam33	Aldoa	Abhd8	Als2cr4	Aim1	Acta1
3	Aplp1	Acta1	Arg2	Adk	Ap2a1	Adam1a	Agtpbp1	Alcam	Ap2a1	Arhgap24	Arfgef2	Adss	Arfgef2	Adfp	Aqp1	Alox5ap	Als2cr4
4	Atf5	Adam17	Arhgap24	Aifm1	Arhgap10	Agtpbp1	Arg2	Arl5c	Arrb2	C1qb	Arg2	Agt	Atp5b	Ankrd2	Arfgef2	Anxa9	Arg2
5	Brf2	Adam33	Bspry	Anp32a	Arl3	Ankrd35	Arhgap24	Atxn1	Atp7b	Car5b	Arl2bp	Aldoa	Birc3	Bbs12	Asns	Arhgap10	Asns
6	Brsk2	Agt	Cacna2d1	Arrb2	Arl6ip6	Atf5	Atp6ap2	Bad	Bsg	Car6	Arrb2	Atf3	Car14	Caln1	Atp10a	Brf2	Cacna2d1
7	Bsg	Akr1c19	Capzb	Bcl3	Bcl3	Bai1	Bspry	Btg4	C1qtnf4	Casc5	Baiap2l1	Baz1a	Cdk7	Cpne2	Atp1a3	C3ar1	Ccdc104
8	Bspry	Ap2a1	Ccdc89	Capn3	Bsdc1	Bsg	Cacna2d1	Car6	Cby1	Cby1	Ccdc89	C1qtnf3	Cdkn2c	Crot	Ccdc136	Ccl6	Cdk7
9	Ccndbp1	Arhgap29	Ccdc93	Capn7	Car6	Btbd14a	Capzb	Cryzl1	Ccdc104	Ccl7	Ccdc93	Ccdc136	Cryl1	Cyp46a1	Crtac1	Chka	Cenpi
10	Cd14	Atp7b	Cebpb	Ccdc65	Ccl3	Cd276	Ccl12	Cstf3	Ccdc65	Cldn16	Cd46	Ccdc89	Cuedc1	Egfl6	Cryl1	Chodl	Clip4
11	Cd46	Bai2	Cenpi	Ccl6	Chi3l1	Centd3	Cenpi	Cth	Ccl4	Cml5	Cebpb	Ccl4	Dos	Ftsj3	Dmtf1	Cntfr	Cml5
12	Cdh7	Bnip2	Cish	Cebpb	Cldn5	Cfd	Cfd	Cxcl10	Chst2	Cort	Cpne2	Clip4	Gprc5a	Gars	Dnmt3l	Dut	Cp
13	Cdr2	Brd2	Cntfr	Cntn3	Cuedc2	Chst3	Depdc7	Dgcr6	Cryl1	Dhx15	Cyr61	Ctnnbip1	Hes1	Gpr63	Dusp22	Eif5	Csrp2
14	Chi3l1	Cabp4	Cryl1	Ctxn3	Dctn1	Cxcl1	Dll1	Dhx32	Cxcl16	Dnase1l1	Dusp14	Dennd3	Il17rb	Herpud1	Eif5	Emb	Dlg1
15	Clcf1	Capn7	Cyp46a1	Cxcl11	Dennd3	Cxcl16	Dusp8	Dlk2	Cyr61	Emb	Eif2s2	Dnase1l1	Il23r	Hmgn2	Faim	Erbb4	Ecm1
16	Cldn5	Car2	Dad1	Cxcl9	Dok7	Dctn1	Exph5	Ebpl	Dbndd2	Exoc6b	Epn1	Ebpl	Isg20	Homer3	Gpr160	Fgf2	Enox2
17	Cpd	Cd93	Dusp8	Cyp1b1	Egr1	Ebpl	Fhod1	Eef1a1	Dctn1	Fbxl4	Exph5	Eef1a1	Jak2	Id3	H28	Gale	Fbxl4

Cryzl1	Chac1	Exph5	Ecm1	Epn1	Efemp2	G0s2	Egfl8	Ddr1	Fmn1	Fbxl4	Eml2	Jakmip1	Itgb1	Hfe	Gbp5	Hmgn2
Cth	Cml4	F10	Enox2	Ftsj3	Erbb3	Gabrd	Egfr	Fpgs	Hspb1	Fhod1	Gimap9	Kcne1l	Jmjd6	Hmgb2	Gclc	Mcf2
Dhrs3	Diras1	G0s2	Fastkd1	Gal3st4	Etv4	Gabrr1	Emilin1	Gabrd	Ide	Fscn2	Got2	Krt32	Kcnk9	Kif9	Gfap	Mef2d
Dnase1l1	Dot1l	Gabrd	Fat2	Gale	F10	Gfap	Fbxl4	Hbegf	Ifi47	G0s2	Grik4	Kti12	Lars	Klk5	Grik4	Nipsnap1
Dnmt3l	Dpysl5	Gabrr1	Fhod1	Gapdh	Faah	Got1	Fgf2	Igf2bp1	Ifih1	Gars	Herpud1	Ldha	Ltbp3	Krt32	Hfe	Odc1
Dusp14	Esr2	Gdf15	Fmn1	Ggta1	Fen1	Ifit3	Fndc7	Irf2	Il12rb1	Gpr85	Hfe	Lsg1	Map3k8	Lcor	Hs3st2	Opn1mw
Egfr	F10	Gfap	Fndc7	H2-Ea	Fndc7	Il1b	Ghitm	Kcnip3	Itgb1	Hbp1	Hspb1	Lzts2	Mapk8ip2	Map3k8	Mlf1	Pqlc3
Gfap	Fastkd1	Got1	Gal	Hcn2	Hmgb2	Il20rb	Gldc	Klhdc8b	Kcnj14	Hmox1	Hydin	Msln	Mmp25	Mrpl14	Nup153	Qsox2
Gldc	Ftsj3	Gtpbp4	Glmn	Hivep3	Ier3	Jakmip1	Grsf1	Klhl29	Kctd8	Hsd17b12	Icmt	Mx2	Mthfd2	Nfkbiz	Penk1	Rom1
Gpr1	Galnt14	Hmgn2	Gpr88	Hsd3b5	Igtp	Junb	Hes1	L3mbtl	Khdrbs3	Ifi47	Il17rb	Myo1g	Ncdn	Ogfrl1	Plk2	Rpusd4
Heatr1	Ghitm	Hmox1	Ifi47	Irgm	Il12rb1	Kcnip4	Hfe	Lmo1	Kif9	Jun	Incenp	Ncdn	Pdc	Omg	Plk3	Slc25a17
Hmox1	Gosr1	Homer3	Igtp	Krt32	Il1b	Lamc3	Hyal5	Lrrc4b	Kremen1	Lgals8	Itgal	Nfkb2	Pde6d	Pcgf6	Ptn	Tex261
Ide	Gpr45	Hspb1	Il20rb	Lgi3	Impdh2	Lyst	Icam1	Magi1	Lrrc4b	Lims1	Itgax	Omg	Pla1a	Pctk2	Rab40b	Tsen2
Ifi47	Heatr1	Ifit3	Il23r	Lyn	Irf1	Mfap3l	Ik	Mina	Mef2d	Map4k3	Kcnj8	P2ry6	Pqlc3	Penk1	Rcor2	Ush1c
Igtp	Hes1	Il20rb	Irf1	Lzts2	Itfg3	Mlf1	Il6	Mllt6	Myd88	Mcm4	Lenep	Pcsk4	Ptp4a1	Prtg	Samd9l	Usp15
Impdh2	Hpse	Jakmip1	Itgb1	Mcam	Lad1	Mup5	Kcnj8	Myc	Nlgn1	Mdm4	Ltbr	Penk1	Ptpn2	Ptpn12	Scfd2	Wdr36
Inpp5f	Hsd17b12	Kiss1r	Kcng4	Mdm4	Lce1d	Myom2	Kif9	Ncdn	Parp2	Me2	Mboat1	Plcd4	Pus7	Qk	Slc12a6	Znrf4
Irf1	Ifit3	Klc3	Lamc3	Mesp1	Lgi3	Nfe2l2	Lamb3	Nfix	Pbk	Mfsd2	Mcm4	Ppap2a	Rabep2	Rbbp8	Slc4a7	
Itgam	Intu	Lyst	Lmod1	Mpped2	Lrp4	Nostrin	Letmd1	Nfkb2	Pbx1	Mmd2	Mgam	Ptp4a3	Rai14	Rbm41	Spata1	
Klk5	Ipo7	Mamdc2	Lrrc46	Mrps18b	Lrrc36	Nup98	Lrrc57	Pacsin3	Pdc	Mmp21	Msln	Ptpn1	Rfx2	Rom1	Spata5	
Ksr1	Irak4	Mfap3l	Lsg1	Ndrg3	Lsm10	Nxf1	Mak10	Ptn	Pdgfc	Mphosph9	Myl2	Ptpn14	Rnd3	Sardh	Thnsl2	
Ltbp3	Irf1	Mlf1	Lyst	Nkd2	Ltbp3	Otof	Mapkapk3	Ptpn1	Pex1	Nfe2l2	Ncdn	Raly	Ruvbl1	Sec24a	Tmem116	

Ly6e	Itgb1	Mup5	Mxd4	Npr1	Mfhas1	Pbxip1	Mfsd2	Ptpn14	Pi4k2b	Nlgn1	Plp1	Rdh11	Slc4a7	Slc30a7	Tpcn2	
Lypla2	Jmjd6	Nfe2l2	Myd88	Oaf	Ncf4	Pde6d	Mrpl38	Rcvrn	Pkm2	Nme3	Pttg1	Rell2	Sntg2	Surf2	Utp20	
Mfsd2	Jun	Nostrin	Nfix	Odc1	Npr1	Phlda2	Ndufb5	Rell2	Pqlc3	Olfm3	Rab4b	Rhbdf2	Sp140	Taf11	Zbtb1	
Myc	Jup	Nxf1	Ngrn	Pcsk6	Nxph4	Ppp1r1b	Nipa2	Rogdi	Ptprr	Olfml3	Rad51	Rpl41	Surf2	Tap1		
Myd88	Khdrbs3	Pbxip1	Nostrin	Plk3	Pacsin3	Pqlc1	Noc4l	Rpl41	Qsox2	Pde6d	Rai14	Rtn2	Tmem108	Tmem116		
Myo1g	Klk5	Pcsk1n	Otof	Plxnb1	Plk3	Ralgps2	Nxf1	Slc17a7	Rnf213	Prss2	Rarb	Sars	Trip10	Ubp1		
Myom2	Lamb3	Pde6d	Pawr	Ptpn14	Ppef1	Rfx2	Nxn	Slc9a3r2	Rogdi	Ptpn2	Rnf125	Sdcbp2	Utp20	Zfp423		
Nes	Lrrc36	Phlda2	Pdlim3	Ptrh1	Ptpn1	Scfd2	Pank3	Slfn2	Samd9l	Rcvrn	Rtn4	Slc24a1	Wdr78			
Nipsnap1	Magi1	Pla1a	Ptk7	Qser1	Ptpn14	Sds	Penk1	Smarca4	Sh3bp2	Rela	Sigirr	Slc29a1				
Nt5m	Mesp2	Pqlc1	Rbm41	Rad9b	Rabep2	Slc1a5	Pex1	Smcr8	Shmt2	Rfx2	Slc31a2	Slc4a7				
Optn	Mrpl14	Ralgps2	Rcvrn	Rax	Rad9b	Slc22a15	Phf1	Socs3	Slc25a17	Rhbdf2	Surf2	Snw1				
Pacsin3	Msn	Rasa2	Retsat	Rela	Rbp3	Slc24a1	Plat	Srf	Slc4a7	Rogdi	Tdp1	Suox				
Phf1	Myl2	Rfx2	Rhebl1	Rell2	Rhbdf2	Snrk	Ppap2a	Stk22s1	Sox4	Smarca4	Tmem11	Taf5				
Plau	Nap1l1	Rit1	Rnf213	Rhpn1	Rhebl1	Sox4	Prima1	Syngr1	Stc1	Spata1	Tmem138	Tek				
Plk3	Ngrn	Scfd2	Rxrg	Rnf213	Rom1	Spata1	Rab4b	Tekt1	Tm7sf4	Spink2	Trappc3	Tgm1				
Ppap2a	Nrf1	Sds	Sardh	Rnf34	Rps6ka2	Thnsl2	Rad51	Tmem144	Tmem38a	Tmod3	Uck2	Tnnt2				
Ppp4r1	Nup153	Slc1a5	Sec24a	Rogdi	Sbno2	Tmem35	Rpp38	Tmem54	Tmem54	Triml1	Vdac1	Wscd1				
Prkcbp1	Nxn	Slc22a15	Setd2	Sds	Scnn1a	Tnnt2	Sdcbp2	Tnip1	Tnip2	Wwc1	Zcchc17					
Prodh	Plxnb1	Slitrk2	Six6	Sepp1	Sdk2	Tpcn2	Serpinb2	Trim25	Tpcn2	Yars	Zfand1					
Pstpip2	Pola2	Snrk	Slc16a6	Sh2d3c	Sec61a1	Trim21	Speg	Trim47	Trim21	Zdhhc12	Zfp36					
Ptpn1	Ppp4r1	Sox4	Slc46a3	Slc13a5	Slc25a35	Trim25	Stat1	Unc119	Triml1	Zfp217						
Ptpn2	Pqlc1	Stard10	Socs2	Slc14a2	Slc46a3	Trip10	Stmn3	Upp1	Ttbk2							

Rasal2	Rab3b	Thnsl2	Spata1	Slc1a5	Slc9a3r2	Uchl5	Tmem116	Zbtb7b	Vegfc							
Rasgrp2	Rag1ap1	Tmem35	Tap1	Slc25a35	Smcr8	Unc5a	Tmem9	Zc3hav1	Vps26a							
Rax	Rasal2	Tmod1	Tars	Suv39h2	Stmn3	Usp15	Tnf	Zfyve21	Zfp12							
Rbak	Rnf213	Tnnt2	Thnsl2	Tmbim1	Tbc1d1	Utp20	Triml1									
Rhebl1	Rpap1	Trim21	Tmem116	Tmem54	Tmem116	Vldlr	Trip10									
Rilp	Sec61a1	Trim25	Tmem53	Tnfrsf12a	Tmem44	Wdr75	Zfyve21									
Rnd1	Slc1a5	Trip10	Tmod3	Tnfrsf1a	Tmem59l	Yars2										
Rogdi	Slc4a7	Ttbk2	Tubb6	Trip10	Tnfrsf1a	Zfp217										
Rpl41	Sost	Txnip	Uchl5	Trpm2	Ush1c											
Rtbdn	Spata20	Uchl5	Unc5a	Wscd1	Wnt7a											
Sntg2	Speg	Unc5a	Usp18	Zfp217	Zfhx2											
Tbc1d1	Sucla2	Usp15	Usp25	Zfp84												
Tmem116	Susd3	Wdr75	Wnt7a													
Tmem54	Thoc3	Yars2														
Trip10	Tmem132e															
Ttbk2	Utp20															
Ush1c	Wdr36															
Usp15	Ythdf3															